T.C.
YEDİTEPE UNIVERSITY
INSTITUTE OF HEALTH SCIENCES
DEPARTMENT OF HISTOLOGY AND EMBRYOLOGY

DETECTION OF HIPPO SIGNALING PATHWAY IN 7,12-DIMETHYLBENZ(A)ANTHRACENE (DMBA) INDUCED MOUSE OVARY

MASTER OF HISTOLOGY AND EMBRYOLOGY THESIS

SERRA NUR ERSOY

İSTANBUL-2023

T.C.
YEDİTEPE UNIVERSITY
INSTITUTE OF HEALTH SCIENCES
DEPARTMENT OF HISTOLOGY AND EMBRYOLOGY

DETECTION OF HIPPO SIGNALING PATHWAY IN 7,12-DIMETHYLBENZ(A)ANTHRACENE (DMBA) INDUCED MOUSE OVARY

MASTER OF HISTOLOGY AND EMBRYOLOGY THESIS

SERRA NUR ERSOY

SUPERVISOR

PROF. DR. AYLİN YABA UÇAR

İSTANBUL-2023

APPROVAL

Institute : Yeditepe University Institute of Health Sciences

Programme : Master of Histology and Embryology

Title of the Thesis : Detection of Hippo Signaling Pathway in 7,12-Dimethylbenz(a)anthracene (DMBA) Induced Mouse Ovary

Owner of the Thesis : Serra Nur ERSOY

Examination Date : 05.07.2023

The Jury judges that the candidate named above has satisfactorily completed his thesis.

	Title, Name-Surname (Institution)
Supervisor:	Prof. Dr. Aylin YABA UÇAR (Yeditepe University)
Member/Examiner:	Prof. Dr. Fevziye Figen KAYMAZ (İstinye University)
Member/Examiner:	Assoc. Prof. Dr. Alev CUMBUL (Yeditepe University)

APPROVAL

This thesis has been deemed by the jury in accordance with the relevant articles of Yeditepe University Graduate Education and Examinations Regulation and has been approved by Administrative Board of Institute with decision dated ..... and numbered .....

Prof. Dr. Bayram Yılmaz

Director of Institute of Health Sciences

DECLARATION

I hereby declare that this thesis is my own work and that, to the best of my knowledge and belief, it contains no material previously published or written by another person nor material which has been accepted for the award of any other degree except where due acknowledgment has been made in the text.

../../2023

Serra Nur ERSOY

DEDICATION

To my beloved family...

ACKNOWLEDGEMENTS

I owe deepest gratitude to my supervisor Prof. Dr. Aylin YABA UÇAR with whom I am honored to have worked with. Throughout my graduate studies, she has been a great mentor in all aspects of life, developing me academically, and guiding me with her guidance, patience and support. I am grateful for the knowledge she has given me and also for her help in my laboratory experiments and her checks and corrections on my thesis.

I have taken pleasure in working with Dr. Tuğçe Önel, Ecem Yıldırım and Dr. Cihan Süleyman Erdoğan while doing my experiments; I give them endless thanks for their understanding and encouragement. I am also appreciative for their interest and help in conducting the thesis experiments.

I would like to thank Zeynep Alkan Öztürk, our lab technician who helped me in the laboratory during my Master's study, and my dear friends Ezgi Şahin, İlayda Kaya, Elaza Aliyeva and Narmin Asadova for their friendship, support and help.

My greatest thanks are for my family; my mother Figen Ersoy, my father Sedat Ersoy and my grandmother Nezaket Altındağ. Their love and support makes my achievements possible.

TABLE OF CONTENTS

APPROVAL ..... İİ

DECLARATION ..... İİİ

DEDICATION ..... İV

ACKNOWLEDGEMENTS V

TABLE OF CONTENTS ..... Vİ

LIST OF TABLES ..... İX

LIST OF FIGURES X

LIST OF SYMBOLS AND ABBREVIATIONS ..... XVİİ

ABSTRACT ..... XİX

ÖZET XX

1.INTRODUCTION AND PURPOSE 1

2. LITERATURE REVIEW 3

2.1. The Female Reproductive System 3

2.2. The Ovaries 4

2.2.1. Embryonic Development of The Ovary 4

2.2.1.1. Follicle Formation 6

2.2.2. Histology of The Ovary 6

2.2.3. Ovarian Cycle 8

2.2.4. Follicular Growth and Development (Folliculogenesis) 10

2.3. Overview of Endocrine Disruptors 13

2.3.1. General Properties of Polycyclic Aromatic Hydrocarbons (PAHs) 13

2.3.1.1. Overview of 7,12-Dimethylbenz(a)anthracene (DMBA) 15

2.3.1.2. Role of 7,12-Dimethylbenz(a)anthracene (DMBA) in Ovotoxicity 16

2.4. The Hippo Signaling Pathway 18

2.4.1. The Hippo Signaling Pathways in Mammals 19

2.4.2. The Hippo Signaling Pathway in Ovary 22

3. MATERIALS AND METHODS 25

3.1. Animal Groups and Experimental Design 25

3.2. Tissue Processing 26

3.3. Morphological Analysis with Periodic Acid - Schiff (PAS) Staining 26

3.4. Determination of Serum Anti-Müllerian Hormone (AMH) Concentrations by ELISA 26

3.5. Follicle Counting 27

3.6. Immunohistochemistry Staining 28

3.6.1. Immunohistochemistry Staining For MST1/2, LATS1/2, YAP1 and TEAD4 Antibodies 28

3.6.2. Immunohistochemistry Staining For Nitrotyrosine Antibody 29

3.7. Quantitative Real-Time Polymerase Chain Reaction (qRT-PCR) 31

3.7.1. RNA Isolation 31

3.7.2. cDNA Synthesis 32

3.7.3. qRT-PCR 32

3.8. Statistical Analysis 34

4. RESULTS 35

4.1. Morphological Evaluation of Experimental Groups by Periodic Acid-Schiff (PAS) Staining 35

4.2. ELISA Results 38

4.3. Follicle Counting 40

4.4. Localization of Hippo Signaling Pathway Proteins by Immunohistochemistry 40

4.5. Localization of Nitrotyrosine (NTY) by Immunohistochemistry 53

4.5. qRT-PCR Results 56

5. DISCUSSION AND CONCLUSION 58

6. REFERENCES 64

7. APPENDICES 77

7.1. Ethical Approval 77

7.2. CURRICULUM VITAE 78

LIST OF TABLES

Table 1. The 16 PAH compounds recognized as priority pollutants aree shown (43)... 14
Table 2. List of primary antibodies for immunohistochemistry staining. 29
Table 3. List of secondary antibody for immunohistochemistry staining. 29
Table 4. List of antibodies for NTY immunohistochemistry staining. 31
Table 5. cDNA synthesis reaction contents. 32
Table 6. qRT-PCR reaction contents. 33
Table 7. Primer sequences used in qRT-PCR. 33

LIST OF FIGURES

Figure 1. Structures of the female reproductive system (2)…….3

Figure 2. Diagram of a cross-section of the ovary (5)……..4

Figure 3. Illustrating an embryo at the end of the third week with primordial germ cells (PGCs) positioned with in the yolk sac wall (11)……..5

Figure 4. The developmental process of primordial follicles from primordial germ cells in the mouse ovary (13,16) (The figure adapted from the sources)……..6

Figure 5. Hematoxylin-eosin (H&E) staining of the histological section of the mouse ovary. The cortex (C) contains numerous growing follicles (GF) and corpus luteum (CL) at various stages of maturation. Medulla (M) contains lymphatic nerves and numerous blood vessels (18)……...7

Figure 6. Hormonal regulation changes in ovarian and uterine cycles (21)…….8

Figure 7. The concentration of ovarian hormones and anterior pituitary hormones changes (21)…….**.....**9

Figure 8. Schematic representation of folliculogenesis (24)…….**....**11

Figure 9. Hematoxylin-Eosin (H&E) staining of the histological section of the ovary (20)…….. 11

Figure 10. The figure shows the metabolic pathway of DMBA……..16

Figure 11. Functions of Hippo signaling pathway in cells. The Hippo signaling pathway controls cell proliferation, differentiation, death, and growth (80) (The figure adapted from the source)……...19

Figure 12. Comparison of Hippo signaling pathway core components between Drosophila and mammals (82) (The figure adapted from the source)…….20

Figure 13. Schematic representation of the Hippo signaling pathway components in mammals (100)……21

Figure 14. Schematic representation of the major known biological activities regulated by the Hippo signaling pathway (101)…….22

Figure 15. Emerging roles of Hippo signaling in the ovary (104)……23

Figure 16. Schematic representation of animal groups and experimental design…….25

Figure 17. Morphological evaluation of control, vehicle and DMBA groups by Periodic Acid-Schiff (PAS) staining. The structure of cortex and medulla of the ovaries from control (A), vehicle (B) and DMBA (C) groups are shown (Scale bar: 400 μm)……36

Figure 18. Morphological evaluation of control group by PAS staining. In the control group primordial (A), primary (B), secondary (C), antral (D), corpus luteum (E) and atretic (F) follicle structures are shown (Scale bar: 50 μm and 100 μm)…….36

Figure 19. Morphological evaluation of vehicle group by PAS staining. In the vehicle group primordial (A), primary (B), secondary (C), antral (D), corpus luteum (E) and atretic (F) follicle structures are shown (Scale bar: 50 μm and 100 μm)…….37

Figure 20. Morphological evaluation of DMBA group by PAS staining. In the DMBA group primordial (A), primary (B), secondary (C), antral (D), corpus luteum (E) and atretic (F) follicle structures are shown (Scale bar: 50 μm and 100 μm)…….38

Figure 21. Standard concentration curve for AMH……..39

Figure 22. Comparison of serum AMH levels between control, vehicle and DMBA groups…….. 39

Figure 23. Comparison of the number of primordial, primary, secondary, antral, Graafian, atretic follicles and corpus luteum with control, vehicle and DMBA-treated groups (****p<0,0001, ***p<0,001, **p<0,01, *p<0,1)……40

Figure 24. MST1/2 protein localization to primordial, primary and secondary follicles in control, vehicle and DMBA groups demonstrated by immunohistochemistry staining. The yellow circles represent primordial follicles in control (A), vehicle (A') and DMBA (A") groups, primary follicles in control (B), vehicle (B") and DMBA (B") groups and secondary follicles in control (C), vehicle (C') and DMBA (C'') groups. The brown stained areas indicate MST1/2 and blue stained areas indicate the nucleus. The nucleus staining was performed with Hematoxylin. In the additional images shown in the control, vehicle and DMBA group, there is no staining pattern in the negative control (Scale bar: 50 μm). ……... 42

Figure 25. MST1/2 protein localization to antral, atretic follicles and corpus luteum in control, vehicle and DMBA groups demonstrated by immunohistochemistry staining. The yellow circles represent antral follicles in control (D), vehicle (D') and DMBA (D") groups, corpus luteum in control (E), vehicle (E") and DMBA (E") groups and atretic follicles in control (F), vehicle (F') and DMBA (F'') groups. The brown stained areas indicate MST1/2 and blue stained areas indicate the nucleus. The nucleus staining was performed with Hematoxylin. In the additional images shown in the control, vehicle and DMBA group, there is no staining pattern in the negative control (Scale bar: 100 μm and 50 μm)…….. …….. 43

Figure 26. Results of the MST1/2 positive cell intensity in granulosa cells, oocytes and total ovary for control, vehicle and DMBA groups. One-way ANOVA and Tukey's multiple comparison test were applied. A. Representative positive granulosa cell intensity (%). B. Representative oocyte intensity (%). C. Representative total ovary intensity (%) (*p<0.1), (****p<0.0001). …… 44

Figure 27. LATS1/2 protein localization to primordial, primary and secondary follicles in control, vehicle and DMBA groups demonstrated by immunohistochemistry staining. The yellow circles represent primordial follicles in control (A), vehicle (A') and DMBA (A") groups, primary follicles in control (B), vehicle (B") and DMBA (B") groups and

secondary follicles in control (C), vehicle (C') and DMBA (C'') groups. The brown stained areas indicate LATS1/2 and blue stained areas indicate the nucleus. The nucleus staining was performed with Hematoxylin. In the additional images shown in the control, vehicle and DMBA group, there is no staining pattern in the negative control (Scale bar: 50 μm)…….. …….. 45

Figure 28. LATS1/2 protein localization to antral, atretic follicles and corpus luteum in control, vehicle and DMBA groups demonstrated by immunohistochemistry staining. The yellow circles represent antral follicles in control (D), vehicle (D') and DMBA (D") groups, corpus luteum in control (E), vehicle (E") and DMBA (E") groups and atretic follicles in control (F), vehicle (F') and DMBA (F'') groups. The brown stained areas indicate LATS1/2 and blue stained areas indicate the nucleus. The nucleus staining was performed with Hematoxylin. In the additional images shown in the control, vehicle and DMBA group, there is no staining pattern in the negative control (Scale bar: 100 μm and 50 μm). ……46

Figure 29. YAP1 protein localization to primordial, primary and secondary follicles in control, vehicle and DMBA groups demonstrated by immunohistochemistry staining. The yellow circles represent primordial follicles in control (A), vehicle (A') and DMBA (A") groups, primary follicles in control (B), vehicle (B") and DMBA (B") groups and secondary follicles in control (C), vehicle (C') and DMBA (C'') groups. The brown stained areas indicate YAP1 and blue stained areas indicate the nucleus. The nucleus staining was performed with Hematoxylin. In the additional images shown in the control, vehicle and DMBA group, there is no staining pattern in the negative control (Scale bar: 50 μm). ……... 48

Figure 30. YAP1 protein localization to antral, atretic follicles and corpus luteum in control, vehicle and DMBA groups demonstrated by immunohistochemistry staining. The yellow circles represent antral follicles in control (D), vehicle (D') and DMBA (D") groups, corpus luteum in control (E), vehicle (E") and DMBA (E") groups and atretic follicles in control (F), vehicle (F') and DMBA (F'') groups. The brown stained areas indicate YAP1 and blue stained areas indicate the nucleus. The nucleus staining was performed with Hematoxylin. In the additional images shown in the control, vehicle and

DMBA group, there is no staining pattern in the negative control (Scale bar: 100 μm and 50 μm). ……... 49

Figure 31. Results of the YAP1 positive cell intensity in granulosa cells, oocytes and total ovary for control, vehicle and DMBA groups. One-way ANOVA and Tukey's multiple comparison test were applied. A. Representative positive granulosa cell intensity (%). B. Representative oocyte intensity (%). C. Representative total ovary intensity (%) (***p<0.001, **p<0.01, *p<0.1)…… 50

Figure 32. TEAD4 protein localization to primordial, primary and secondary follicles in control, vehicle and DMBA groups demonstrated by immunohistochemistry staining. The yellow circles represent primordial follicles in control (A), vehicle (A') and DMBA (A") groups, primary follicles in control (B), vehicle (B") and DMBA (B") groups and secondary follicles in control (C), vehicle (C') and DMBA (C'') groups. The brown stained areas indicate TEAD4 and blue stained areas indicate the nucleus. The nucleus staining was performed with Hematoxylin. In the additional images shown in the control, vehicle and DMBA group, there is no staining pattern in the negative control (Scale bar: 50 μm). ……51

Figure 33. TEAD4 protein localization to antral, atretic follicles and corpus luteum in control, vehicle and DMBA groups demonstrated by immunohistochemistry staining. The yellow circles represent antral follicles in control (D), vehicle (D') and DMBA (D") groups, corpus luteum in control (E), vehicle (E") and DMBA (E") groups and atretic follicles in control (F), vehicle (F') and DMBA (F'') groups. The brown stained areas indicate TEAD4 and blue stained areas indicate the nucleus. The nucleus staining was performed with Hematoxylin. In the additional images shown in the control, vehicle and DMBA group, there is no staining pattern in the negative control (Scale bar: 100 μm and 50 μm)…… 52

Figure 34. Results of the TEAD4 positive cell intensity in granulosa cells, oocytes and total ovary for control, vehicle and DMBA groups. One-way ANOVA and Tukey's multiple comparison test were applied. A. Representative positive granulosa cell intensity (%). B. Representative oocyte intensity (%). C. Representative total ovary intensity (%) (**p<0.01)……... 53

Figure 35. NTY protein localization to primordial, primary and secondary follicles in control, vehicle and DMBA groups demonstrated by immunohistochemistry staining. The yellow circles represent primordial follicles in control (A), vehicle (A') and DMBA (A") groups, primary follicles in control (B), vehicle (B") and DMBA (B") groups, secondary follicles in control (C), vehicle (C') and DMBA (C'') groups. The brown stained areas indicate NTY and blue stained areas indicate the nucleus. The nucleus staining was performed with Hematoxylin. In the additional images shown in the control, vehicle and DMBA group, there is no staining pattern in the negative control (Scale bar: 50 μm)... 54

Figure 36. NTY protein localization to antral, atretic follicles and corpus luteum in control, vehicle and DMBA groups demonstrated by immunohistochemistry staining. The yellow circles represent antral follicles in control (D), vehicle (D') and DMBA (D") groups, corpus luteum in control (E), vehicle (E") and DMBA (E") groups and atretic follicles in control (F), vehicle (F') and DMBA (F'') groups. The brown stained areas indicate NTY and blue stained areas indicate the nucleus. The nucleus staining was performed with Hematoxylin. In the additional images shown in the control, vehicle and DMBA group, there is no staining pattern in the negative control (Scale bar: 100 μm and 50 μm)……..55

Figure 37. Results of the NTY positive cell intensity in granulosa cells, oocytes and total ovary for control, vehicle and DMBA groups. One-way ANOVA and Tukey's multiple comparison test were applied. A. Representative positive granulosa cell intensity (%). B. Representative oocyte intensity (%). C. Representative total ovary intensity (%). (*p<0.1)……...56

Figure 38. Results of the qRT-PCR experiment. A. MST1, B. MST2, C. LATS1, D. LATS2, E. YAP1 and F. TEAD4 mRNA expression levels……57

Figure 39. The association of DMBA-induced mouse ovotoxicity model with the Hippo signaling pathway has been demonstrated. In conclusion, we demonstrated that DMBA-induced increase in YAP and TEAD expression may play a role in the mechanisms underlying the rapid depletion of follicles through the Hippo signaling pathway by

causing an increase in the number of atretic follicles and a decrease in the number of corpus luteum……...62

LIST OF SYMBOLS AND ABBREVIATIONS

AMH: Anti-Müllerian hormone

BMP15: Bone morphogenetic protein 15

C: Cortex

CL: Corpus luteum

CYP450: Cytochrome P450

CYP1B1: CYP 450 isoform 1B1

7,12-DMBA: 7,12-dimethylbenz(a)anthracene

DPC: Day post coitus

E: Embryonic

ECM: Extracellular matrix

EDs: Endocrine disrupting compounds

ELISA: Enzyme-linked immuno sorbent assay

FSH: Follicle stimulating hormone

GC: Granulosa cell

GDF9: Growth factor 9

GnRH: Gonadotropin releasing hormone

GF: Growing follicle

H&E: Hematoxylin-Eosin

HPO: Hippo

HPO: Hypothalamic-pituitary-ovarian

IP: Intraperitoneal

KL: Kit ligand

LATS1/2: Large tumor suppressor homolog 1/2

LH: Luteinizing hormone

M: Medulla

mEH: Microsomal epoxide hydrolase

MST1/2: Mammalian sterile 20-like 1/2

MOB1a/b: MOB kinase activator 1A/B

NTY: Nitrotyrosine

PAHs: Polycyclic aromatic hydrocarbons

PAS: Periodic acid-schiff

PBS: Phosphate buffer saline

PCOS: Polycystic ovary syndrome

PGC: Primordial germ cell

POF: Premature ovarian failure

SAV: Salvador

SD: Scalloped

TAZ: PDZ binding motif

TAOK1/2/3: TAO kinases

TAZ: Two homologs of *Drosophila* Yki

TEAD: TEA domain transcription factor

US-EPA: United States Environmental Protection Agency

VGLL4: Vestigial like family member 4

YAP: Yes-associated protein

YKI: Yorkie

YUDETAM: Yeditepe University Experimental Research Center

WTS: Warts

q-RT-PCR: Quantitative real time polymerase chain reaction (qRT-PCR)

ABSTRACT

Ersoy,S.N.(2023). Detection of Hippo Signaling Pathway in 7,12-Dimethylbenza(a)nthracene (DMBA) Induced Mouse Ovary, Yeditepe University, Institute of Health Sciences, Department of Histology and Embryology, Master Thesis, İstanbul.

7,12-dimethylbenz(a)anthracene (DMBA) has well known ovotoxicant and present carcinogenic effects on ovarian follicular development in rodents. The Hippo signaling pathway induces cell proliferation, differentiation, apoptosis and regulation of organ size in diverse species. The relationship between follicular development and the Hippo signaling pathway in DMBA-induced mouse ovaries has not been investigated in previous studies. Therefore, in this thesis study, we hypothesized that Hippo signaling pathway proteins may have a role in the ovotoxicity which is induced by DMBA treatment in the mouse ovary. We aimed to demonstrate the Hippo signaling pathway in DMBA-treated ovaries by immunohistochemistry and quantitative real-time PCR (qRT-PCR). In this thesis study, 28 days old 18 BalbC female mice were used and designed 3 groups (n=6): Control (No treatment), Vehicle group (Daily injection of sesame oil), Experimental group (The intraperitoneal injection of DMBA (1 mg/kg in sesame oil) for 14 consecutive days). To demonstrate the morphological difference between DMBA and control group mouse ovary, sections were stained with Periodic-Acid Schiff (PAS) staining. AMH serum levels analyzed by ELISA and follicles were counted to evaluate follicle reserve. Immunohistochemistry was performed in the ovary to determine the localization of Hippo signaling pathway proteins MST1/2, LATS1/2, YAP1, TEAD4 and to show oxidative stress with NTY antibody. The levels of Hippo signaling proteins at the mRNA level were measured by qRT-PCR. According to the results, DMBA-treated ovaries showed decreased follicular reserve, increased oxidative stress and follicular atresia. In our study, we provide evidence for the first time of the relationship between follicular development and the Hippo signaling pathway in DMBA-treated mouse ovaries. We believe that our data will shed new light on the rapid depletion of follicular reserve and the signaling mechanism related to DMBA-induced ovotoxicity on mouse ovaries. Therefore, it is suggested that our results may contribute to the further investigation of ovotoxicity related problems and the development of new strategies.

Key words: Hippo signal pathway, 7,12-DMBA, ovotoxicity, mouse.

ÖZET

Ersoy,S.N.(2023). 7,12-dimetilbenz(a)antrasen (DMBA) ile İndüklenen Fare Ovaryumunda Hippo Sinyal Yolağının Belirlenmesi, Yeditepe Üniversitesi, Sağlık Bilimleri Enstitüsü, Histoloji ve Embriyoloji Anabilim Dalı , Yüksek Lisans Tezi, İstanbul.

7,12-dimetilbenz(a)antrasen (DMBA), kemirgen ovaryumunda foliküler gelişim üzerinde iyi bilinen bir ovotoksik ve karsinojenik etkiye sahiptir. Hippo sinyal yolağı, çeşitli canlı türlerinde hücre proliferasyonunu, farklılaşmasını, apoptozunu ve organ boyutunun düzenlenmesini kontrol eder. DMBA uygulanmış fare ovaryumlarında foliküler gelişim ve Hippo sinyal yolağı arasındaki ilişki daha önceki çalışmalarda araştırılmamıştır. Bu nedenle, bu tez çalışmasında, Hippo sinyal yolağı proteinlerinin fare ovaryumunda DMBA uygulaması ile indüklenen ovotoksisitede bir rolü olabileceğini hipotez etmekteyiz. DMBA uygulanan ovaryumlarda Hippo sinyal yolağını immünohistokimya ve kantitatif gerçek zamanlı PCR (qRT-PCR) yöntemleri ile göstermeyi amaçlamaktayız. Bu tez çalışmasında 28 günlük 18 adet BalbC dişi fare kullanılarak 3 grup oluşturulmuştur (n=6): Kontrol grubu (Herhangi bir tedavinin yapılmadığı grup), Çözgen grubu (Sadece susam yağı verilen grup), Deney grubu (1 mg/kg DMBA'nın susam yağı içinde çözülerek 14 gün boyunca intraperitoneal olarak verildiği grup). DMBA ile kontrol fare ovaryumları arasındaki morfolojik farklılıkları göstermek için kesitler Periyodik Asit-Schiff (PAS) boyası ile boyandı. Ovaryumdaki folikül rezervini belirlemek amacıyla ELISA yöntemi ile AMH serum seviyeleri ve folikül sayımı yapıldı. Hippo sinyal yolağı proteinleri olan MST1/2, LATS1/2, YAP1 ve TEAD4 lokalizasyonlarını belirlemek ve ayrıca ovaryumda oksidatif stresi göstermek amacıyla NTY antikoru ile immünohistokimya yapıldı. Hippo sinyal proteinlerinin mRNA seviyeleri qRT-PCR yöntemi ile belirlendi. Sonuçlara göre, DMBA ile indüklenen fare ovotoksisite modelinde azalmış foliküler rezerv, artmış oksidatif stres ve foliküler atrezi gösterildi. Çalışmamızda ilk kez DMBA uygulanan fare ovaryumlarında foliküler gelişim ile Hippo sinyal yolağı arasındaki ilişki gösterilmiştir. Verilerimizin, foliküler rezervin hızla tükenmesine ve fare ovaryumlarında DMBA ile indüklenen ovotoksisite ile ilgili sinyal mekanizmasına yeni bir ışık tutacağına inanıyoruz. Dolayısıyla, bu çalışma sonucunda elde edilen verilerin ovotoksisite ile ilgili problemlerin daha fazla araştırılmasına ve yeni stratejilerin geliştirilmesine katkıda bulunabileceği ileri sürülmektedir.

Anahtar Kelimeler: Hippo sinyal yolağı, 7,12-DMBA, ovotoksisite, fare.

1.INTRODUCTION AND PURPOSE

In the female reproductive system, the ovary is responsible for the production of oocytes and the secretion of various steroid hormones (1) and the ovarian cortex is composed of follicles at different stages of development (2). In mammals, the oocyte reserve accumulated during prenatal life is continuously depleted throughout postnatal life (3). Induction of ovaries with an environmental toxic chemical agent can lead to ovotoxicity by depleting the primordial follicle reserve (4).

7,12-dimethylbenz(a)anthracene (DMBA) is a polycyclic aromatic hydrocarbon and endocrine disruptor consisting of fused aromatic rings, induces many tumors and has been used as a cancer model in rodents (5,6). Exposure to DMBA in daily life comes from the combustion of organic matter such as charred food, cigarette smoke and fossil fuels (7). DMBA is associated with an acceleration of the onset of ovarian failure in female smokers, which supports its ovotoxicity(8). In addition to its carcinogenic effect, DMBA causes the loss of all ovarian follicle types, disrupting the folliculogenesis and causing a decrease in follicle population (3). For ovotoxicity to occur, DMBA requires bioactivated by microsomal epoxide hydrolase (mEH) and members of the cytochrome P450 oxidase family to DMBA-3,4-diol,1,2-epoxide, an ovotoxic metabolite (4,9). The bioactive metabolite has been reported to bind to both dAdo and dGuo residues in DNA, forming DMBA-DNA adducts and causing follicular atresia (10).

The Hippo signaling pathway, as an evolutionarily conserved pathway contributes to the understanding of many molecular mechanisms, including cell proliferation, differentiation, apoptosis, organ size regulation and tumorigenesis (11–15). Dysregulation of the Hippo signaling pathway contributes to impaired follicular development due to reproductive disorders such as loss of follicular homeostasis and depletion of follicular reserve. The Hippo signaling pathway consists of Mammalian sterile 20-protein kinase 1 and 2 (MST1/2), large tumor suppressor homologues 1 and 2 (LATS1/2), Yes-associated protein (YAP1), and its transcriptional cofactor Two homologs of Drosophila Yki (TAZ)(16). Furthermore, activation of YAP1, a major effector of the Hippo signaling pathway, plays an crucial role in cellular processes such as follicular development, follicle activation and ovarian steroidogenesis (17). When the

Hippo signaling pathway is active, YAP/TAZ is transcriptionally active and phosphorylates YAP/TAZ activity in the cytoplasm. Conversely, when the Hippo pathway is inactive, YAP/TAZ is transcriptionally active and localizes to the nucleus thereby regulating gene expression (18).

The signaling pathway mechanism involved in the effects of DMBA on follicular development have not yet been fully elucidated. In this study, we have shown the expression of Hippo signaling pathway proteins may have a role in the ovotoxicity which is induced by DMBA treatment in the mouse ovary. Besides, by this study, we demonstrated the relationship between follicular development and the Hippo signaling pathway in DMBA-induced mouse ovaries for the first time. Thus, this study may contribute to the further investigation of DMBA-induced ovotoxicity related problems and the development of new strategies.

2. LITERATURE REVIEW

2.1. The Female Reproductive System

The existence of the female reproductive system is essential to the continuation of life and preservation of species. Female reproduction is regarded as one of the most important systems in the body due to its crucial functions. The female reproductive system comprises internal organs, including the ovaries, the oviducts, the uterus, and the vagina located in the pelvis, and external genital organs located in the anterior part of the perineum that functions together to facilitate sexual reproduction (19,20). This system is organized to perform a variety of functions such as the secretion of sex hormones, the formation of the oocytes, transport to the oviducts for fertilization, and as well as the development and growth of the fetus during pregnancy (21,22) (Figure 1).

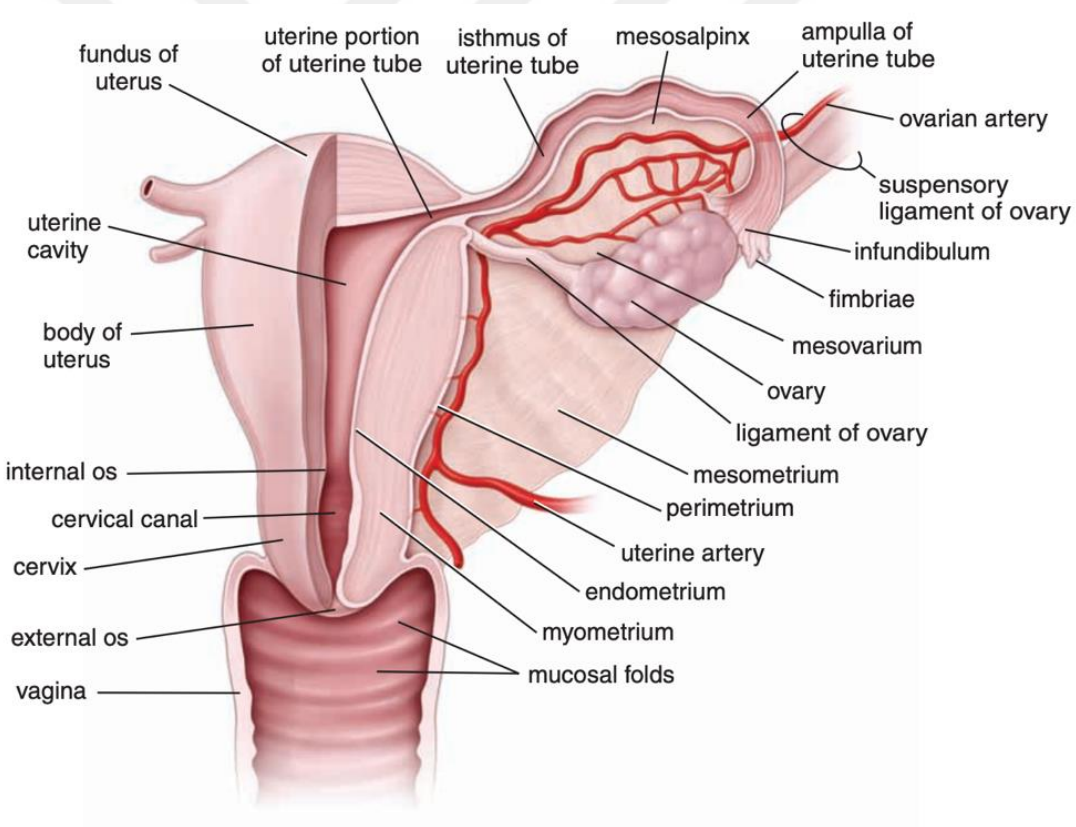

Figure 1. Structures of the female reproductive system (20).

2.2. The Ovaries

The ovary is an essential organ of the female reproductive system. Ovaries are the female gonads that undergo major structural changes during each reproductive cycle. Oocyte production and steroid hormone release are the two main functions of the ovary (19).

Ovaries in the human pelvis are paired, flattened, ovoid structures, approximately the size of an almond-shaped located near the bilaterally lateral pelvic walls of the uterus on either side of the ovarian fossa. Each gonad size is around 2-3 cm long, 1.5-2 cm wide, and 1 cm thick (23) (Figure 1). Gonads are bound with the broad ligament extending on the lateral edges of the uterus by a peritoneal fold called the mesovarium. The fold of the peritoneum transmits the blood vessels in the hilum, where hilus cells, vessels and nerves enter and exit the organ to the ovaries (20,23) (Figure 2).

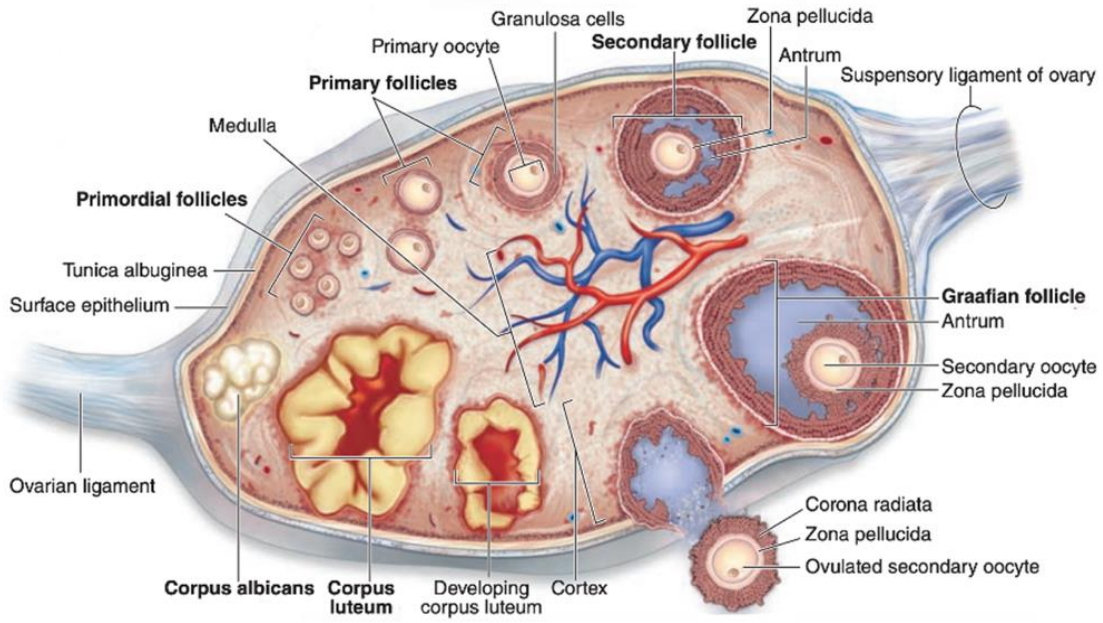

Figure 2. Diagram of a cross-section of the ovary (23).

2.2.1. Embryonic Development of The Ovary

The mammalian embryonic gonads form as called bipotential or indifferent primordium that are morphologically indistinguishable from one another until the seventh week of the development (24). Gonads develop from three different sources; the mesothelium covering the posterior abdominal wall, the mesenchyme, and the primordial germ cells (25).

The development of the genital or gonadal ridges, which are the somatic precursor structures of the ovaries. The gonads appear as a pair of longitudinal gonadal ridges with an increase in the epithelium and underlying mesenchyme during the 5th week of gestation in humans and embryonic day 10 in mice (E10) (26,27). Ovaries develop from the cortical region of the primitive gonads. Germ cells do not appear on the genital ridges until the 6th week of development (26).

The process of gametogenesis involves the formation and development of gametes, which are specialized reproductive cells. In the second week of development, gametes develop from primordial germ cells (PGCs) formed in the epiblast. These germ cells migrate to the yolk sac wall during gastrulation from the primitive streak at the end of the third week of development (25,26) (Figure 3). Afterward, PGCs migrate from the developing gonadal ridges to the hindgut and dorsal mesentery between E9.5 and E11.5 in the mouse and between the 5th and 7th week of gestation in humans (25).

A female's gametes are responsible for supplying the genetic material to the embryo (24). Oogonia, also known as oocytes, start to undergo meiosis around E13.5 in mice and during the 10th week of gestation in humans. At the beginning of puberty, developing oocytes arrest in the diplotene phase of the first meiotic prophase before ovulation occurs (28). Meanwhile, they rapidly multiply through mitosis, increasing the number of oogonia, and undergo a process where they are surrounded by a layer of flattened cells and enter the first stage of meiotic division. These cells are then referred to as primary oocytes. The process of reproduction for oogonia is through mitosis, resulting in a reserve of around 500,000 primordial follicles in each ovary (21,29).

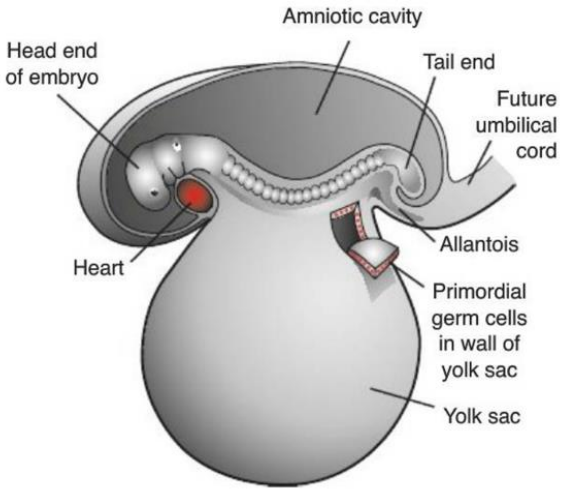

Figure 3. Illustrating an embryo at the end of the third week with primordial germ cells (PGCs) positioned with in the yolk sac wall (29).

2.2.1.1. Follicle Formation

During the reproductive life of the mammalian female, the primordial follicle pool, as known the ovarian reserve, corresponds to the entire germ cell population (30). It is essential for fertility that this supply of oocytes is established. The formation and migration of primordial germ cells during embryogenesis, the development of oogonial clusters (germ cell cysts) in the ovary, and the development of individual primordial follicles are crucial stages required for follicle formation (31). The extraembryonic mesoderm of the mouse ovary is where the PGCs develop 6.5-7.5 days post coitus (dpc) of embryonic development. Oogonial clusters (germ cell cysts) develop from mitosis by the migration of PGCs to the genital ridge at approximately 10-11dpc. At 13,5 dpc, germ cell cysts begin mitosis, and at 17,5 dpc, oocytes begin to arrest in the diplotene stage of meiotic division. The germ line cysts break apart after birth, and a single layer of squamous somatic pre-granulosa cells that will differentiate to form granulosa cells (GC) form primordial follicles, enclosing individual oocytes (32,33). As a result of cyst breakdown, there is a major loss of oocytes (30,31).

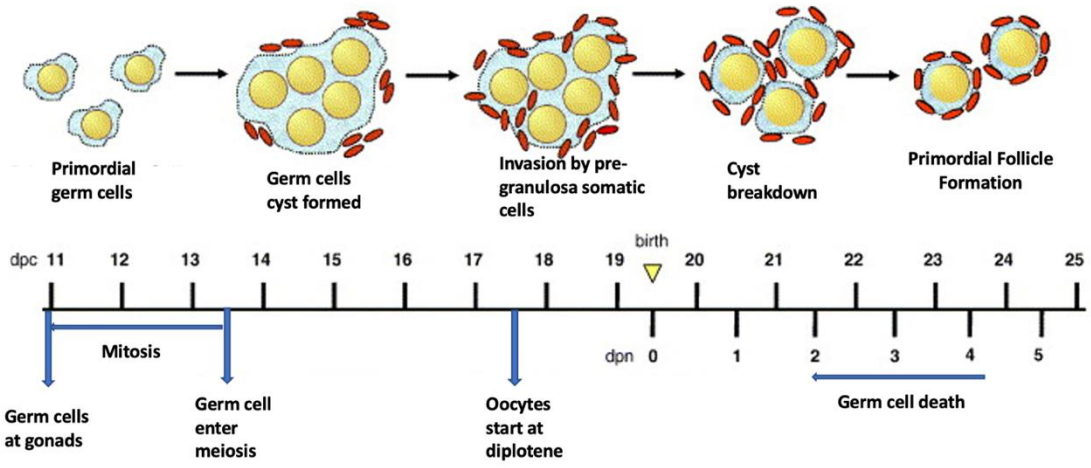

Figure 4. The developmental process of primordial follicles from primordial germ cells in the mouse ovary (31,34) (The figure adapted from the sources).

2.2.2. Histology of The Ovary

The surface of the ovary is covered with a single layer of squamous or cuboidal epithelium called the germinal epithelium, a cellular layer, that is continuous with the mesothelium, which surrounds the mesovarium. This layer continues with the

mesothelium of the visceral peritoneum. Underneath the germinal epithelium, the tunica albuginea is a poorly vascularized, dense irregular tight connective tissue (19).

The ovary is divided into two parts: the cortex and the medulla. The ovarian cortex is the part located just below the tunica albuginea. It contains ovarian follicles at various stages of development embedded in a richly cellular connective tissue (19,20). The ovarian medulla called zona vasculosa, is a well-vascularized irregular loose connective tissue, that consists mostly of smooth muscle fibers, a little amount of elastic and collagen fibers, and interstitial cells, that continues with the mesovarium. Medulla is rich in blood vessels and extends to all parts of the cortex with smaller vessels (19).

The ovarian artery, which comes straight from the abdominal aorta, and the ovarian branch of the uterine arteries provide them with blood (35). Thus, the branches of the ovarian artery enter the ovary through the hilus, the same area where the venous blood exits (24). Also, the medulla has abundant lymphatic vessels and nerve fibers (19). Histologically, the ovarian cortex and medulla do not have a distinct border. Besides, the mesovarium is lined by the germinal epithelium of the ovary and the mesothelium of the peritoneum (23) (Figure 4).

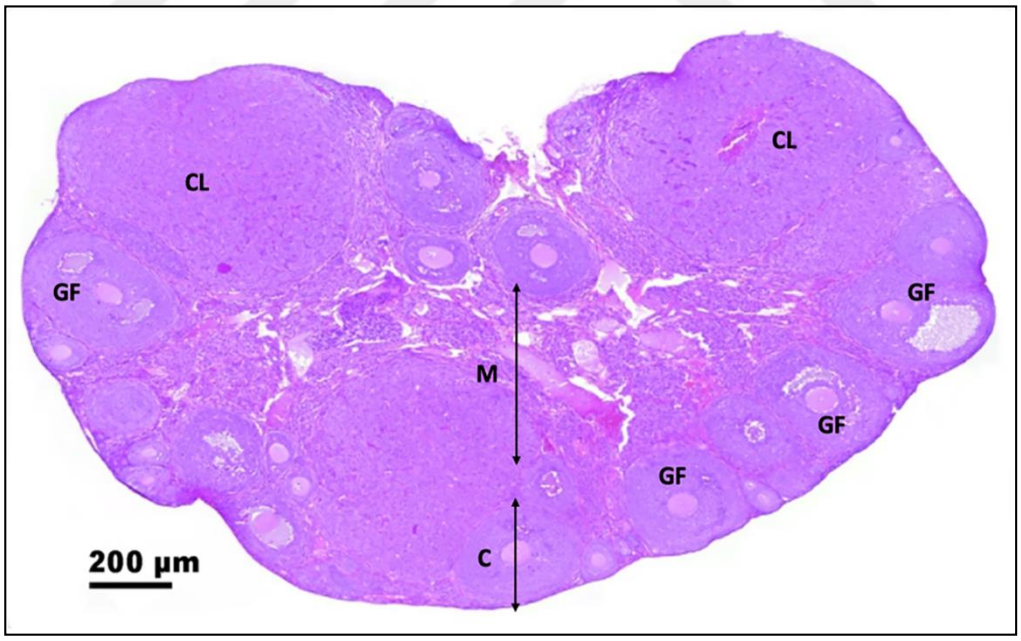

Figure 5. Hematoxylin-eosin (H&E) staining of the histological section of the mouse ovary. The cortex (C) contains numerous growing follicles (GF) and corpus luteum (CL) at various stages of maturation. Medulla (M) contains lymphatic nerves and numerous blood vessels (36).

2.2.3. Ovarian Cycle

Ovarian follicles are the major units of the female reproductive system. Further, ovarian follicles consist of different types and numbers of cells that provide a proper environment for oocyte development. Various follicles are seen in different stages of development in the cortex. The process of follicle development known as folliculogenesis involves the selection of the primordial follicle from the pool of growing follicles and can result in ovulation or atresia. Endocrine hormones and intraovarian regulators are involved in this process. Follicle development is controlled by the anterior pituitary and local factors (19).

The female reproductive system undergoes monthly ovarian and uterine cycles beginning at puberty and is properly controlled by the hypothalamic-pituitary-ovarian (HPO) axis (37). The ovarian cycle consists of three phases; the follicular phase (folliculogenesis), the ovulatory phase (ovulation), and the luteal phase (luteinization) (38).

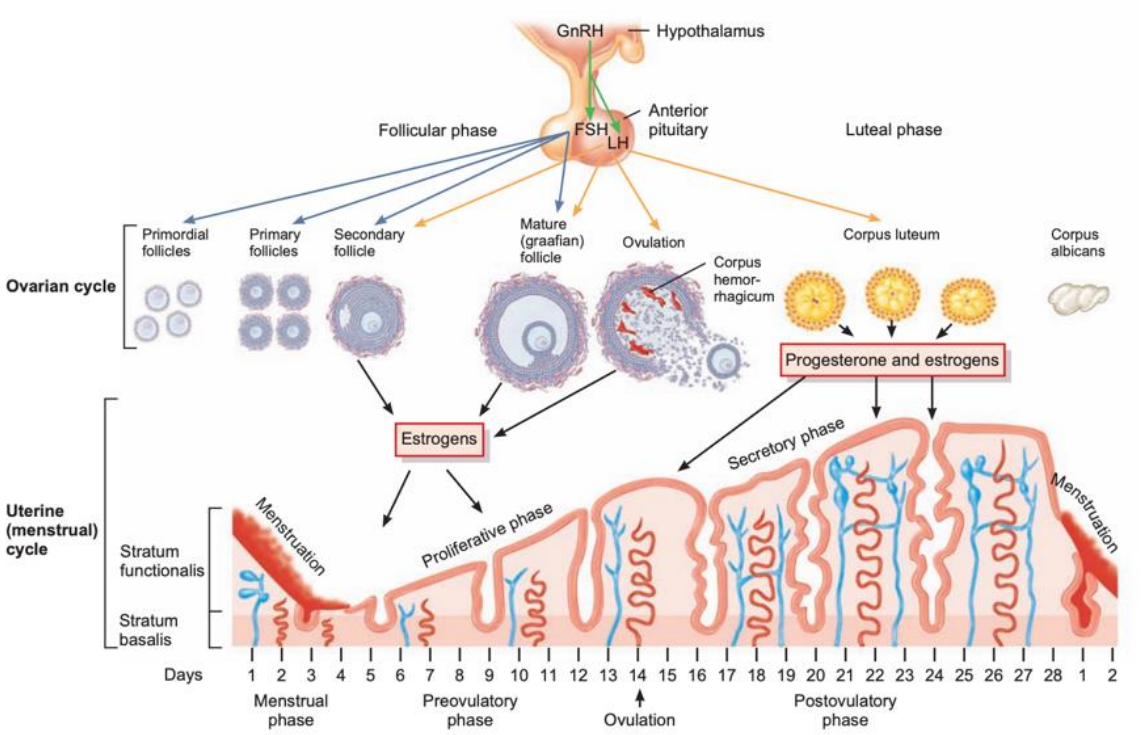

Figure 6. Hormonal regulation changes in ovarian and uterine cycles (39).

Before puberty, all the follicles of the ovarian cortex are in the primordial follicle stage. Beginning at puberty, the release of follicle stimulating hormone (FSH) and luteinizing hormone (LH) from the anterior pituitary gland with gonadotropin releasing

hormone (GnRH) is synthesized from the hypothalamus (Figure 5). FSH modulates the maturation and proliferation for follicular development and LH provides for continued development of follicles to the preovulatory phase (25,29). Thus, the ovarian cycle and uterine cycles occur simultaneously (23). Additionally, cell-cell interaction and apoptosis are the most important factors influencing follicular selection. The follicular dominant selection is influenced by the balance between cellular proliferation and apoptosis (40).

The formation of primary follicles in the first half of the cycle is independent of gonadotropic hormones, but FSH is required for further development. Increased FSH release at the beginning of the follicular phase stimulates the growth of primary follicles and increases the number of FSH receptors in granulosa cells. With this effect, granulosa cells proliferate and aromatase enzyme is synthesized in these cells. High estrogen levels decrease FSH and increase LH. LH receptors are found in theca interna cells. In these cells androgens are synthesized and secreted from cholesterol and diffuse into granulosa cells. Aromatase converts androgens into estrogens. The estrogen passes into the theca interna, where it enters the general circulation via capillaries. Increased estrogens affect the pituitary via negative feedback and indirectly inhibit FSH secretion by suppressing GnRH synthesis. Estrogens increase LH secretion before ovulation and ovulation occurs. Under the influence of FSH and estrogens, LH receptors increase in granulosa and theca cells and the effect of LH is observed. This increases progesterone production and decreases estrogen production in the luteal phase. Progesterone prepares the endometrium for pregnancy, suppresses LH and prevents follicle development. Decreased FSH adversely affects follicles and although dormant follicles continue to develop, others undergo atresia (19,23) (Figure 7).

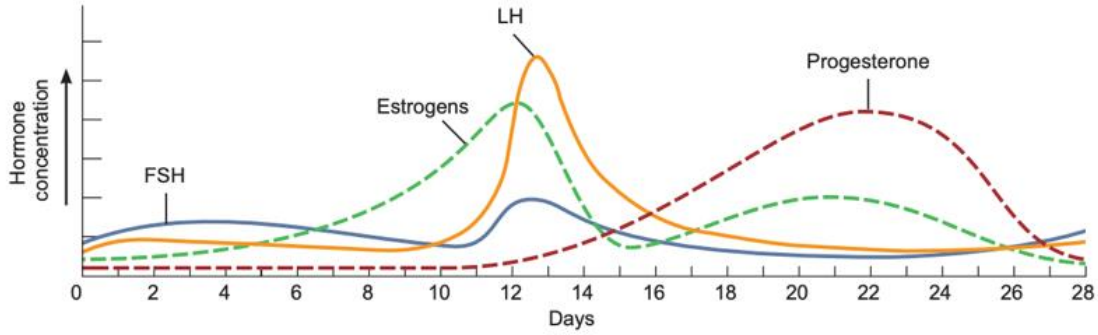

Figure 7. The concentration of ovarian hormones and anterior pituitary hormones changes (39).

2.2.4. Follicular Growth and Development (Folliculogenesis)

The adult ovary is a functional organ that varies physiologically. Folliculogenesis is characterized by the morphological and functional stages of a follicle from primordial to ovulation. Follicles can develop or undergo atresia. Follicles in the growth phase can be divided into two morphologic categories depending on whether an antrum is present in the granulosa. Preantral follicles are primordial, primary, or secondary, whereas antral follicles are either tertiary or ovulatory (also called Graafian follicles). Unlike primordial follicles, which are non-growing, all other types depend on growth, differentiation and ovulation (Figure 8) (41)

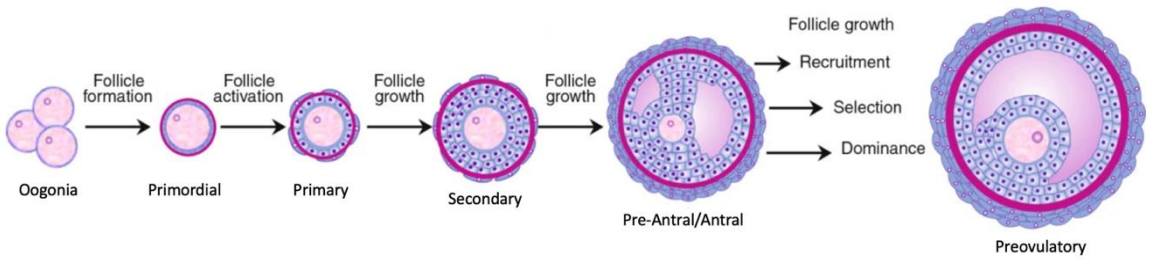

Figure 8. Schematic representation of folliculogenesis (42).

Primordial follicles are located at the surface of the ovarian cortex and the follicle contains the primary oocyte arrested at the diplotene stage of meiosis I surrounded by a single layer of flattened and squamous pre-granulosa cells that are segregated from the basal membrane (43). Pre-granulosa cells will differentiate to form granulosa cells (GC). Primordial follicles receive nutrients and oxygen by passive diffusion from blood vessels (44).

During folliculogenesis, bidirectional communication between the oocyte and its surrounding somatic cells plays an essential role in coordinating the development of both (45). Recent studies confirmed that; growth factor 9 (GDF 9), bone morphogenetic protein 6 (BMP 6), and bone morphogenetic protein 15 (BMP 15) promote activation of primordial follicles for development. Also, GDF 9 and BMP 15 are required in the control of oocyte maturation and granulosa cell activity (46). Additionally, previous studies revealed that the correlation of granulosa cell-derived kit ligand (KL) with oocyte and theca cell-derived c-kit is important for granulosa cell proliferation and primordial follicle activation (47). The stage of the primordial to primary follicle is gonadotropin stimulation is not effective in early follicle development. The primordial follicle transition into

primary follicles, granulosa cells from flat to cuboidal in shape. At this stage, the zona pellucida is formed around the primary oocyte and this glycoprotein polymer capsule separates the oocyte from the granulosa cells (32) (Figure 9).

The primary follicle develops to form a multilayered secondary follicle. With the formation of the secondary follicle, stromal cells surrounded the basal lamina. These cells are called theca cells and differentiate into two layers, theca interna, and theca externa. With the development of the theca layers, many vessel structures also develop through angiogenesis. Additionally, theca interna cells synthesize androstenedione, a steroid hormone that is transported to the granulosa cell layer. Granulosa cells produce the aromatase enzyme, which converts androstenedione to estrogen with the effect of the hormone FSH. Estrogen returns to the stroma surrounding follicle, passes into the blood through the blood vessels and spread throughout the body (23).

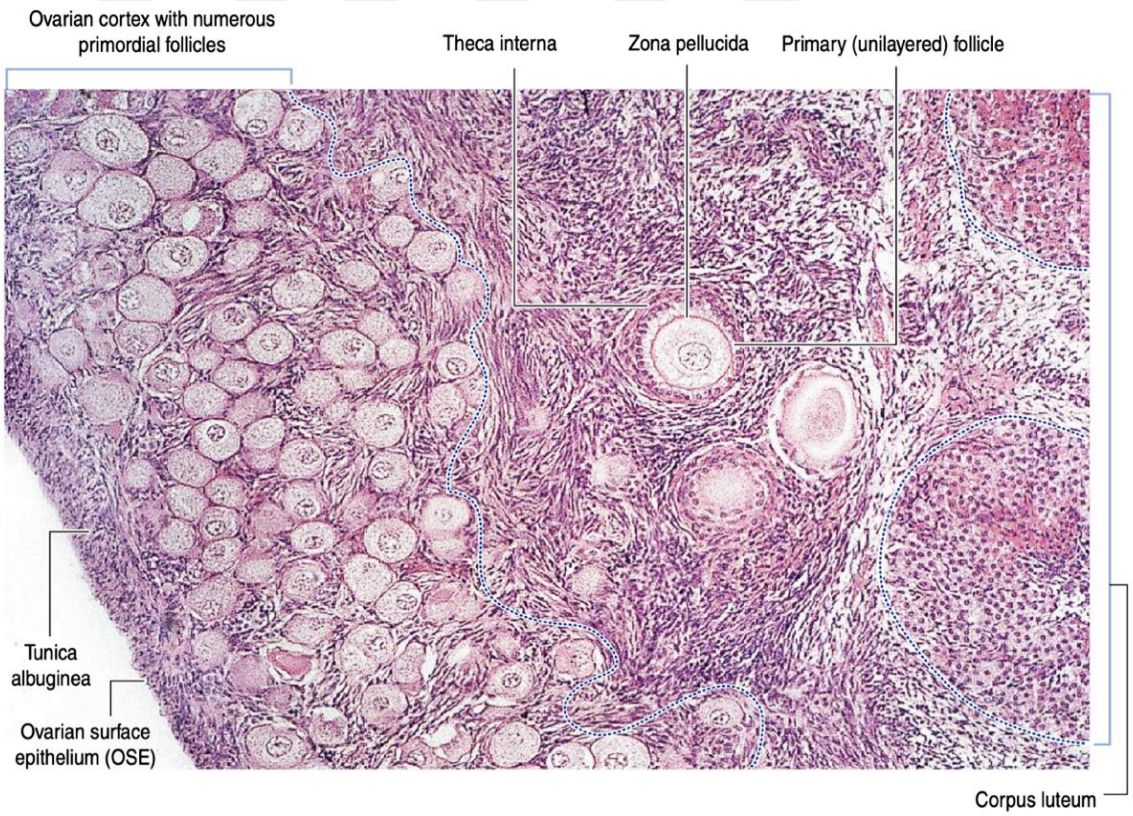

Figure 9. Hematoxylin-Eosin (H&E) staining of the histological section of the ovary (38).

During the proliferation of granulosa cells, at the end of secondary follicle development, a fluid filled cavity begins to form between the granulosa cell layer (32). This follicle is called a preantral follicle. The fluid accumulates and the granulosa cells

reorganize themselves around a larger cavity or gap called the antrum, now this follicle is called an antral follicle (23). The largest ovarian follicle is the Graafian follicle. As the antrum develops, the group of granulosa cells becomes rearranged and surrounded by the oocyte. This structure is called the cumulus oophorus (19). The single layer of granulosa cells surrounds the secondary oocyte, and it is called corona radiata. At this stage, two different types of granulosa cells are the mural granulosa cells and the cumulus granulosa cells. Additionally, Connexin 37 is the gap junction that has an important role in the connection of oocyte and cumulus cells (48). Connexin 43 is also expressed in the interaction between mural layers and cumulus layers (49). The theca interna layer surrounding the Graafian follicle is rich in blood vessels and releases steroids. The theca externa, which acts as a support, is in a relationship with the ovarian stroma (38).

Follicular atresia is a regular and widespread process that affects all stages of follicular development in the ovary, causing degeneration of follicles and oocytes. Atresia is highly prevalent in mammals and is estimated to be responsible for 99% of oocyte loss in humans, from fetal ovarian development to reproductive senescence. The glassy membrane is the term used to describe the folded material of the basement membrane in atretic follicles. Oocytes fragmented by apoptosis often have a folded zona pellucida surrounding them. Apoptosis is a mechanism of follicular atresia in oocyte and granulosa cells. Follicle cells stop mitosis and intercellular hydrolytic enzymes proliferate, cells undergo apoptosis and the follicle shrinks. Atretic follicles are eventually replaced by connective tissue. The exact mechanism of atresia is an unknown process as that why oocytes are eliminated so thoroughly during fetal and adult life (38,50).

At the end of the folliculogenesis, the increase in the amount of estradiol and FSH secreted by the granulosa cells of the dominant follicles continues and reaches its highest level. The Graafian follicle is rich in LH receptors. The resulting increase in FSH levels and estradiol trigger, LH expression from the pituitary gland and a peak in LH levels on days 14-16 of follicle development. After LH release, follicular fluid increases further and the diameter of the follicle increases. This triggers follicle rupture and enlargement of the cumulus cells as a result of high LH receptor levels in the mural granulosa cells. The theca layer and tunica albuginea of the Graafian follicle is ruptured by proteolytic enzymes in the stigma. The secondary oocyte is expelled into the peritoneal cavity together with the zona pellucida, corona radiata, and some follicular fluid. The secondary oocyte completes the prophase stage of the first meiotic division and is arrested at metaphase in the second meiotic division. From this stage onwards, the oocyte is called

the ovum and this process is called ovulation. After ovulation, the ovum is taken into the fallopian tubes and if it is not fertilized within approximately 24 hours, it degenerates and undergoes a process of redifferentiation in the ovary and becomes the corpus luteum (20,23,24).

Following ovulation, the ovary enters the luteal phase then the corpus luteum is formed by reorganization and vascularization of the granulosa cells and theca interna of the ovulated follicle. At this stage, LH secretion leads to the transformation into granulosa lutein cells and theca lutein cells. The function of the corpus luteum is the production and secretion of estrogen and progesterone in response to the release of FSH and LH. Progesterone and estrogen are responsible for the maintenance of the endometrium for a possible pregnancy until approximately the 10th week of gestation. In the absence of fertilization, the corpus luteum begins to regress about two weeks after ovulation, and the corpus albicans forms (20,21,23).

2.3. Overview of Endocrine Disruptors

Endocrine-disrupting compounds (EDs) can have harmful effects on the endocrine systems of both humans and animals (51). Endocrine hormones are affected by exogenous agents that interfere with their synthesis, secretion, transport, and metabolism (52). EDs substances may adversely affect female reproduction, which is a process that is regulated by hormones (51). EDs affect the hypothalamus-pituitary-ovary function and have a damaging effect on other organs, especially oocytes, and ovaries (53). EDs have benzene rings similar to those in the reproductive organs and can easily act and affect reproductive hormones. Exposure to EDs is particularly risky in the early stages of prenatal or postnatal life and exposure during development frequently has permanent effects (51). EDs can be produced naturally (phytoestrogens, contraceptive pills) or synthetically (bisphenol A (BPA), polycyclic aromatic hydrocarbons (PAHs)) (54).

2.3.1. General Properties of Polycyclic Aromatic Hydrocarbons (PAHs)

Polycyclic aromatic hydrocarbons (PAHs), which are endocrine disruptors, are a diverse class of organic compounds with two or more benzene rings that are hydrophobic and widespread pollutants (55–57). PAHs are formed as a result of incomplete combustion or organic compounds of natural or human origin. However, it can occur naturally as a result of volcanic eruptions or forest burns or it can be caused by industrial sources, such as motor vehicle emissions, cigarettes, and tobacco. They are also found in

water, air, soil, and food. Because of these hazards, the amounts found in the environment, food, and beverages have become crucial for human health. In daily life, tobacco smoke, smoke from burning wood, cereals, bread, vegetables, fruit, meat, processed products, contaminated cow's milk, or breast milk are available. Products grown in contaminated soil, air, and water also contain PAHs. Cooking meat or other food on the grill or at high temperatures so that it burns increases the amount of PAHs in food (51,53,55,57,58). Over 100 PAH compounds are present in nature. However, the United States Environmental Protection Agency (US-EPA) has identified 16 of them as priority pollutants (Table 1) (59).

Acenaphthene (Ane)	Chrysene (Chr)
Acenaphthylene (Anp)	Dibenz(a,h)anthracene (DahA)
Anthracene (An)	Fluoranthene (Flu)
Benz(a)anthracene (BaA)	Fluorene (Flr)
Benzo(a)pyrene (BaP)	Indeno (1,2,3-cd)pyrene (IcdP)
Benzo(b)fluoranthene (BbF)	Naphthalene (Np)
Benzo(g,h,i)perylene (BghiPy)	Perylene (Phe)
Benzo(k)fluoranthene (BkF)	Pyrene (Py)

Table 1. The 16 PAH compounds recognized as priority pollutants are shown (59).

The hydrophobic structure of PAHs reduces their solubility in water. Considering the molecular structure, it is possible to define PAHs as light or heavy PAHs. If the PAH compound has less than four benzene rings "light polyaromatic hydrocarbon compound" for such PAHs and "heavy polyaromatic hydrocarbon compound" for PAHs containing more than four benzene rings. Thus, an increase in the molecular weight of a PAH compound means a decrease in its water solubility. And this shows that the toxic, mutagenic, and carcinogenic effects of that compound also increase (60,61).

PAHs enter the body primarily through absorption through respiratory, digestive, skin, and other mucosal barriers. Thus, exposure to PAHs has been found to cause cancer and other diseases, including endocrine and reproductive disorders. Several studies have shown the toxic effects of PAHs on endocrine and developmental functions, including a

decrease in the weight of reproductive organs, damage to embryonic development and ovarian follicles, and defects in the testis and spermatogenesis (51,62).

2.3.1.1. Overview of 7,12-Dimethylbenz(a)anthracene (DMBA)

7,12-dimethylbenz(a) anthracene (DMBA), an environmental polycyclic aromatic hydrocarbon, is a potent carcinogenic compound that initiates, promotes, and progresses tumors (63). DMBA is found in nature as a product of semi-completed combustion reactions of complex hydrocarbons. This toxic and carcinogenic substance comes from the combustion of organic matter such as charred food, fossil fuels, and cigarette smoke (64). As an indirect-acting carcinogen, it requires DMBA to be metabolized by the cytochrome p450 enzyme system to convert to diol epoxide and other reactive oxygen species known to cause increased intracellular oxidation (64). Substances such as DMBA disrupt the structure of DNA and cause lipid peroxidation, leading to the formation of radicals such as hydroxyl and superoxide anion (65).

A metabolic activation by members of the cytochrome P450 (CYP450) superfamily, such as CYP1A1 and CYP1B1, is required for DMBA to exert its carcinogenic effects (63). The formation of the highly reactive metabolite DMBA-3,4-diol-1,2-epoxide, which has an epoxide moiety capable of reacting with nucleophiles present in the cellular environment such as proteins and DNA, is thought to be what gives DMBA its carcinogenic and ovotoxic effects. Bioactivation of DMBA to 3,4-epoxide by CYP 450 isoform 1B1 (CYP1B1) and subsequent hydrolysis of the intermediate 3,4-diol by microsomal epoxide hydrolase (mEH) to produce the highly carcinogenic and ovotoxic DMBA-3,4-diol-1,2-epoxide are the first steps in the metabolic conversion of DMBA to this compound (Figure 10) (66).

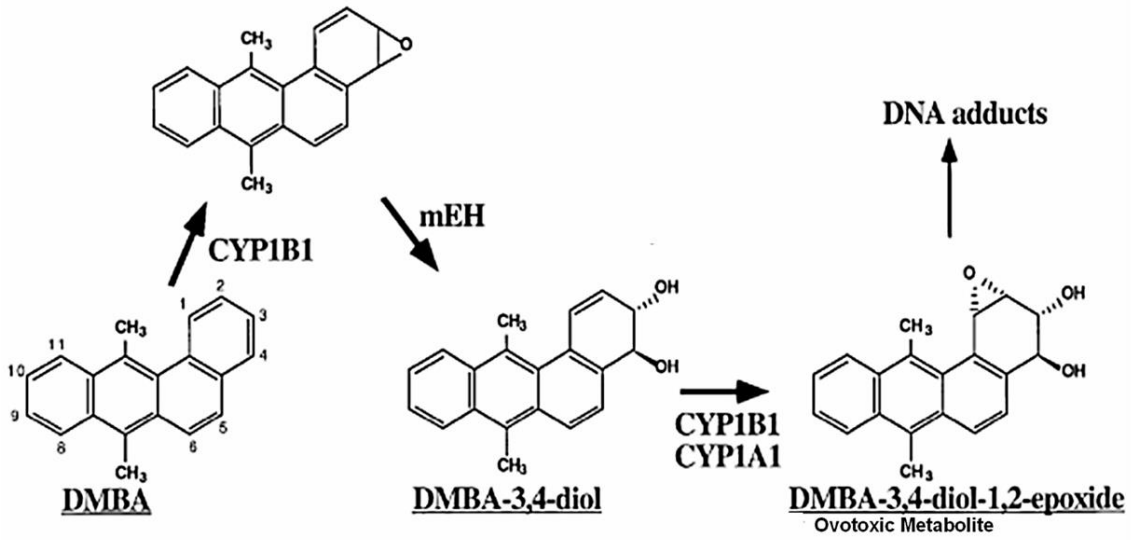

Figure 10. The figure shows the metabolic pathway of DMBA.

2.3.1.2. Role of 7,12-Dimethylbenz(a)anthracene (DMBA) in Ovotoxicity

In recent decades, epidemiology studies have demonstrated declining fertility among women. It has been proven that exposure to a significant number of xenobiotics may be responsible for the decline in fertility. These include environmental polycyclic aromatic hydrocarbons, pharmaceuticals, industrial compounds, xenoestrogenic and chemotherapeutic chemicals that target the follicle population in the ovary (67,68). Ovotoxic chemicals affect the function of the ovary in a variety of ways. The carcinogen has been extensively studied for its ability to induce mammary, skin, and ovarian tumors, especially in rodents (69–72). This compound has also been shown to cause ovotoxicity in mammals (73).

Ovotoxicants have different effects on reproduction depending on the particular stage of development at which they target the follicle. According to the number of follicles, the chemical is targeting as well as the length of exposure to the chemical across a lifetime, different outcomes of follicle loss might occur. Growing follicles can be damaged and causing ovarian steroidogenesis and ovulation to be disrupted. Additionally, chemicals that specifically damage growing follicles may only temporarily disrupt reproduction since these follicles can be replaced by recruitment from the pool of primordial follicles. However, if the number of primordial follicles is chemically reduced, irreversible damage occurs as women are born with a restricted reserve of follicles. Loss

of primordial follicles can be the cause of premature ovarian failure or early menopause in women (67).

Studies have shown that exposure to cigarette smoke causes earlier menopause in women who smoke compared to non-smokers (74). Moreover, maternal exposure to PAHs before pregnancy or during lactation, even if smoking is stopped during pregnancy, leads to decreased ovarian reserve, reduced fertility, and early menopause in female offspring (75).

An important ovotoxic agent DMBA, dose, and time-dependently disrupted follicle development in experimental rodent models and caused the destruction of all follicle types and induces ovarian tumor formation (76–78). In DMBA-induced experiments, follicle destruction starts with oocyte loss followed by somatic cell apoptosis. Through the increase in expression of the pro-apoptotic BAX and the activation of the caspase 3 in granulosa and theca cells of pre-ovulatory follicles, DMBA triggers apoptosis in these cells (79). Thus, a decrease in ovarian volume occurs with the loss of all follicle types and corpus luteum in rats and mice (66,80–82).

As reported by Mattison et al., mice treated with DMBA for 6 days lost 99.4% of their primordial follicles, compared with DBA/2N mice who lost 94.4% (83). Another study showed a significant decrease in primordial follicles and developing follicles in mice after 45 days of DMBA treatment compared to the control group and a decrease in the body weight of mice in the treatment group (84).

Borman et al. conducted an ovotoxic index and showed that in mice and rats, low-dose DMBA exposure (0.35 mg/kg to 7.0 mg/kg intraperitoneal (i.p.) per day for 15 days) caused more follicle loss than a single high dose (80 mg/kg i.p.). With this study, low-dose DMBA exposure is of particular importance in terms of the consequences of chronic low-dose exposures to environmental chemicals in humans (85).

In another study to further investigate the mechanisms by which dose-dependent DMBA exposure causes follicular depletion, rat ovaries were examined using a neonatal ovarian culture system. Two concentrations of DMBA were investigated at which follicle depletion was observed (75 nM) and not observed (12.5 nM). As a result, no concentration affected the number of primordial or unilaminar primary follicles. However, showed that a single dose exposure to DMBA depleted multilaminar primary follicles at concentrations of 12.5 and 75 nM, while secondary follicles were destroyed only at 12.5 nM (86).

According to a study, mice treated with DMBA (80 mg/kg) also showed signs of necrosis in primordial follicles (87). In combination with physical stress, DMBA can damage DNA in non-ovarian tissues (peripheral lymphocytes, liver, and skin cells) in rats (88). All these studies add to the scientific evidence showing that DMBA can adversely affect the function of the ovaries.

2.4. The Hippo Signaling Pathway

The Hippo signaling pathway, also referred to as Salvador/Warts/Hippo signaling pathway was first discovered in Drosophila melanogaster to identify genes involved in growth control and was later found to be highly conserved in mammals through evolution and has been studied for the past 20 years (89). The presence of a kinase cascade, transcription coactivators, and DNA binding members in the core of the Hippo signaling pathway, recent studies have shown that the Hippo pathway is a complex signaling network with at least 30 components (90). Hippo signaling is involved in regulating cell proliferation, differentiation, apoptosis, and cell fate determination to either control organ growth and size, and also early embryonic development, and regeneration (91). Recent studies have recognized more diverse functions of this pathway, including development, tissue homeostasis, stem cell regeneration, immunity, and tumorigenesis. It has also been found to play a role in the regulation of follicle activation, growth and follicle development. The result of a defect in the Hippo signaling pathway leads to tumor formation or organ degeneration (92–97) (Figure 11).

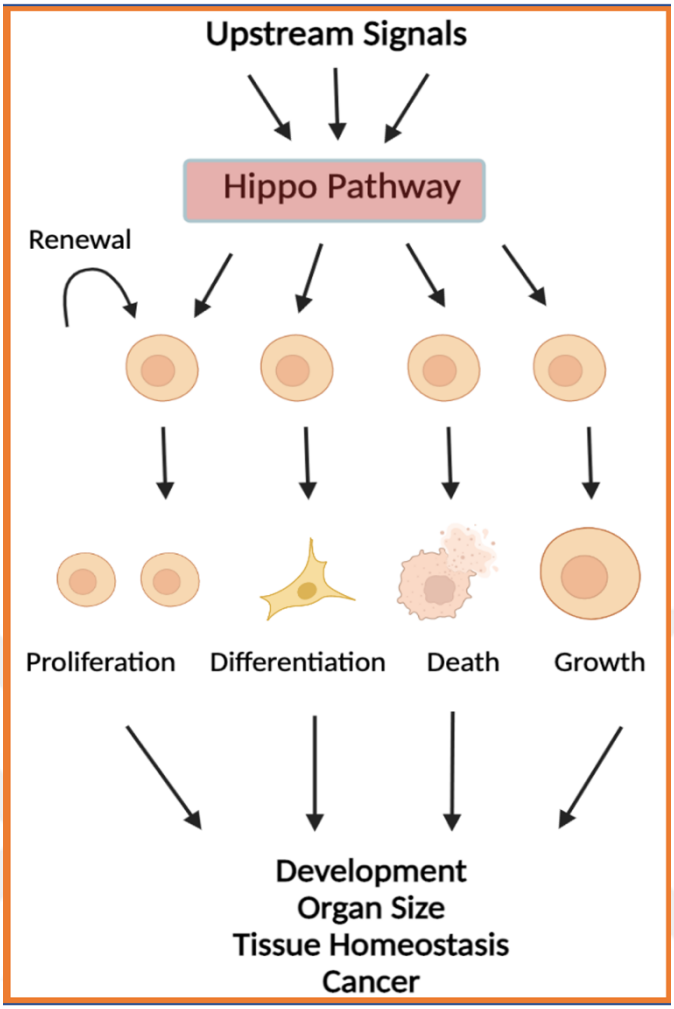

Figure 11. Functions of Hippo signaling pathway in cells. The Hippo signaling pathway controls cell proliferation, differentiation, death, and growth (98) (The figure adapted from the source).

2.4.1. The Hippo Signaling Pathways in Mammals

The Hippo signaling pathway is highly evolutionarily conserved and therefore, most components of the Hippo signaling pathway found in Drosophila have mammalian homologs. The core of this pathway is a protein kinase cascade and phosphorylation of serine/threonine is controlled by a variety of kinases. Hippo (Hpo), Salvador (Sav), Warts (Wts), Mats, Yorkie (Yki), and Scalloped (Sd) mammalian orthologs respectively; Mammalian sterile 20-like 1/2 (MST1/2, also called STK4/3), SAV1, Large tumor suppressor homolog 1/2 (LATS1/2), MOB kinase activator 1A/B (MOB1a/b), transcriptional coactivator with Yes-associated protein (YAP)/PDZ binding motif (TAZ,

also called WWTR1) and TEA domain transcription factor (TEAD) components (99) (Figure 12).

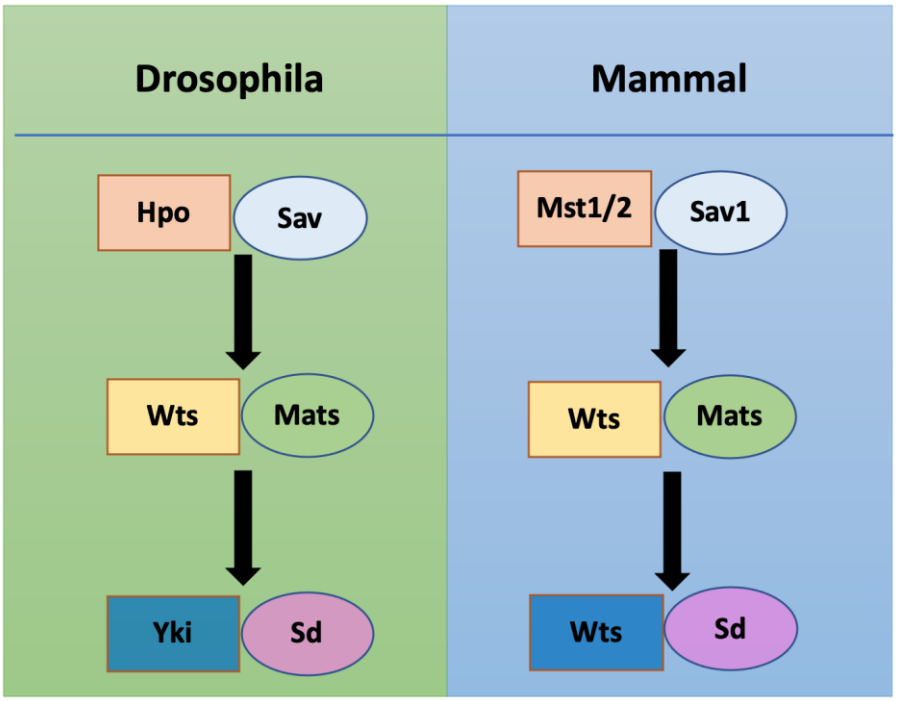

Figure 12. Comparison of Hippo signaling pathway core components between Drosophila and mammals (100) (The figure adapted from the source).

Essentially, the Hippo pathway is composed of two primary components: the core serine/threonine protein kinase cascade is modulated by a variety of upstream signals, and the transcriptional module drives downstream gene expression (101). As the core component of the Hippo pathway, MST1/2, SAV1, LATS1/2, YAP, and TAZ play an important role (102).

After receiving the upstream activation signals, the downstream Mst1/2 kinase phosphorylates Lats1/2 kinases and MOB1 cofactor via SAV1, leading to the activation of these proteins. When the Hippo signal pathway is activated, Lats1/2 kinases promote the cytoplasmic localization and degradation of YAP/TAZ transcription co-activators, phosphorylating and inactivating them. However, when the Hippo pathway is inactivated, dephosphorylated YAP/TAZ translocates into the nucleus, accumulates, and forms complexes, and binds to transcription factors such as TEAD1-4, which is responsible for promoting cell proliferation, migration, and survival genes (92,102,103).

The activation of MST1/2 can be triggered by TAO kinases (TAOK 1/2/3), which phosphorylate the activation loop of the MST dimer (MST1 (Thr183), MST2 (Thr180)) (104,105). Activation loop phosphorylation is increased by MST1/2 dimerization. Therefore, possible that MST1/2 activation can be initiated through dimerization without needing the involvement of upstream kinases (106,107). NF2/Merlin, another important component in this activation, directly associates with LATS 1/2 and facilitates LATS 1/2 phosphorylation by the MST 1/2-SAV1 complex. As a result, LATS 1/2 is activated by autophosphorylation to phosphorylate and inactivate YAP and TAZ (108). Additionally, MAP4Ks (Mitogen-activated protein kinase kinase kinase kinase) can also cause LATS1/2 activation by directly phosphorylating LATS1/2 on their hydrophobic motifs (90,109) (Figure 13).

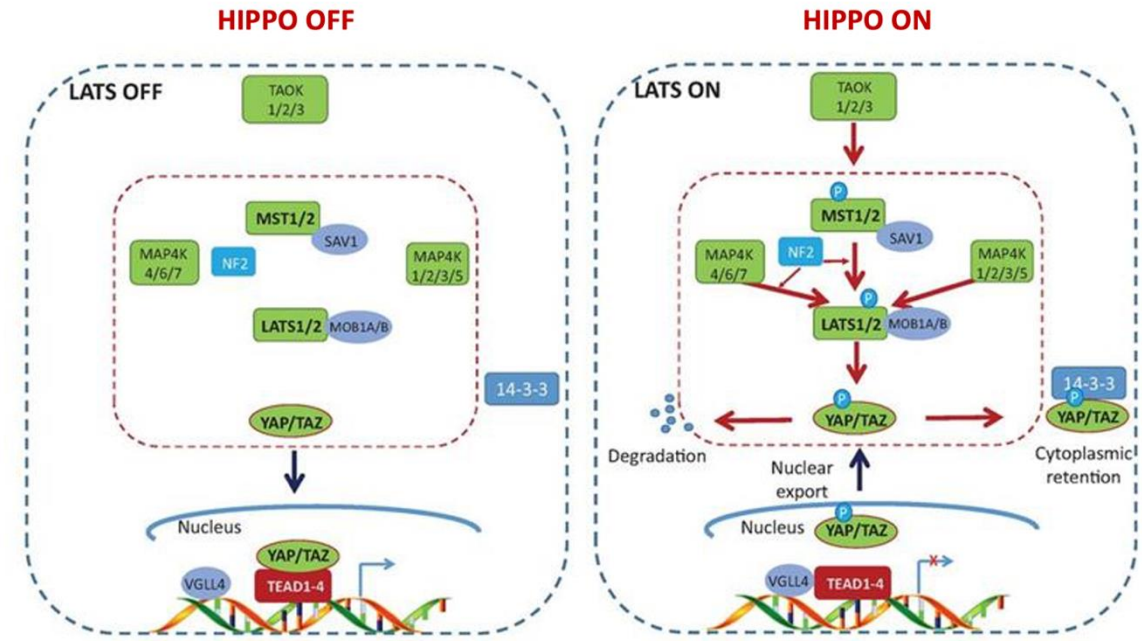

Figure 13. Schematic representation of the Hippo signaling pathway components in mammals (110).

YAP and TAZ are transcriptional coactivators in the signaling pathway and interact with various transcription factors such as TEAD 1-4, RUNX1/2, SMAD, and p73 only when translocated to the nucleus as they do not have DNA binding domains (111–113). TEAD1-4 can also bind to VGLL4 (Vestigial Like Family Member 4) in the nucleus and therefore functions as a transcriptional repressor. In the nucleus, YAP/TAZ binds TEAD and displaces VGLL4, but the interaction between YAP/TAZ and TEAD1-4

dissociates VGLL4 from TEAD1-4, thereby activating TEAD-mediated gene transcription to support normal tissue growth and inhibit ectopic apoptosis (114) (Figure 13).

Studies have shown that the expression of TEAD target genes such as cell proliferation and tissue growth is up-regulated in mouse models generated by deletion of any of the components such as Merlin, MST1/2, LATS1/2, SAV1, YAP, MOB1A/MOB1B. Thus, it provides information about the important roles of each of these components in the Hippo signaling pathway (115–118) (Figure 13).

The Hippo signaling pathway and its effector's control cell physiology by affecting many biological functions in cells. In addition to mechanisms such as differentiation, proliferation, and apoptosis in cells, it has many roles in the control of organ development and size, regeneration and differentiation in stem cells, cell polarity, cell adhesion, extracellular matrix (ECM) contact and energy stress. Especially the relationship between tumour formation in various organs and cancer and the Hippo signaling pathway has been intensively studied in recent years (110,119–121) (Figure 14).

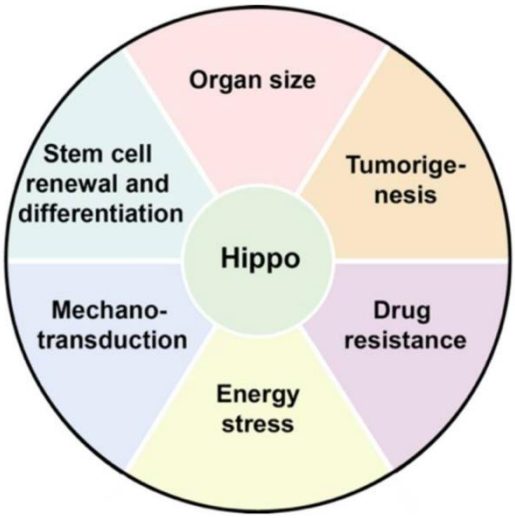

Figure 14. Schematic representation of the major known biological activities regulated by the Hippo signaling pathway (119).

2.4.2. The Hippo Signaling Pathway in Ovary

The Hippo signalling pathway is thought to be essential in regulating the function and activation of follicles in the ovary, which have biological roles in many tissues and organs. In light of the significance of these functions, disruption of the Hippo pathway

plays a role in the loss of follicular development, polycystic ovary syndrome (PCOS), premature ovarian failure (POF), and ovarian cancer (122) (Figure 15).

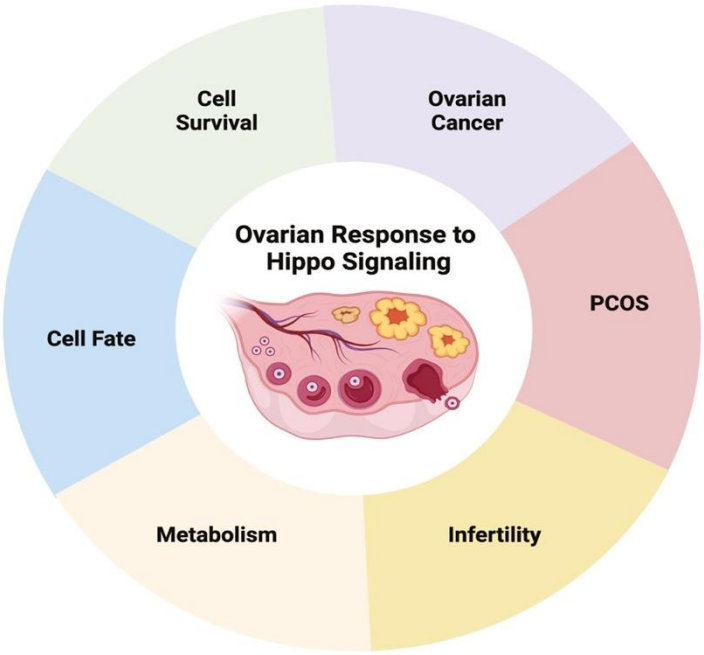

Figure 15. Emerging roles of Hippo signaling in the ovary (122).

Studies have shown that Hippo signaling has important roles in germline differentiation, follicular development, and oogenesis in Drosophila (123,124). However, the mechanisms between ovarian and Hippo signaling in mammalian ovaries are not fully understood so far. Several studies have shown the expression of components of the Hippo signaling pathway at the mRNA level in oocytes, granulosa, and theca cells, some atretic follicles, and corpus luteum at all stages of follicular development and their localiation by immunostaining (125–129). In the literature, there are limited studies on the role of the Hippo pathway component MST1/2 and the adaptor protein SAV1 in the ovary. In a study in mice, ovarian expression of MST1 decreased with age, and YAP1 levels increased before 5 months of age. This increase occurred at the same time as YAP1 levels and follicle number decreased (130). The results of in vitro experiments show that SAV1 alone is unable to phosphorylate the downstream protein kinase LATS1, while the expression of SAV1 in combination with MST1/2 leads to a stimulation of LATS1 phosphorylation (131). Another study analyzed LATS1 as a forkhead box L2 (FOXL2) interacting protein in granulosa cells of small/medium follicles in mouse ovaries and showed that LATS1 can directly phosphorylate FOXL2 (132). In a study using a knockout

mouse model, it was shown that deletion of the LATS1/2 gene in mice disrupted the morphology of granulosa cells and increased YAP1 expression (133). YAP1, a downstream effector of the Hippo signaling pathway, has been examined in most studies. Deletion of YAP1 from granulosa cells disrupted the development of ovarian follicles, and reduced ovary size, resulting in increased follicular atresia and subfertility in transgenic mice (134). Lentiviral knockdown of YAP1 increased primordial follicles and decreased primary follicles in mouse ovaries cultured in vitro, whereas YAP1 overexpression activated follicles (135).

These observations revealed the potential importance of Hippo signaling in ovarian function, but the role of this signaling pathway in follicular development is still poorly understood.

The relationship between follicular development and the Hippo signaling pathway in DMBA-induced mouse ovaries has not been investigated in previous studies. Therefore, in the thesis study, we hypothesized that Hippo signaling pathway proteins may have a role in the ovotoxicity which is induced by DMBA treatment in the mouse ovary. We aim to demonstrate the Hippo signaling pathway in DMBA-treated ovaries by immunohistochemistry and quantitative real-time PCR (qRT-PCR).

3. MATERIALS AND METHODS

3.1. Animal Groups and Experimental Design

All experimental procedures were conducted in the Laboratory of Yeditepe University Faculty of Medicine, Department of Histology and Embryology and Yeditepe University Experimental Research Center (YUDETAM).

A total of 28 day old 18 adult female Balb/C mice were obtained from YUDETAM with the approval of the Yeditepe Ethical Committee. Mice were housed in YUDETAM with 12/12-h light/dark cycles, at 26 °C, with free access to food and water.

These mice were randomly assigned to one of three groups and designed 3 groups (n=6): Control group (No treatment), Experimental group (The injection of DMBA (Sigma-Aldrich, D3254) (1 mg/kg in sesame oil) intraperitoneal for 2 weeks consecutive days according to the manufacturer's instructions), Vehicle group (Daily injection of sesame oil) (Figure 16). Mice were dissected after 1 week from the last treatment day. Right ovaries from each experimental group were used for morphological analysis (Periodic Acid-Schiff (PAS) staining and immunohistochemistry staining) and left ovaries were used for qRT-PCR (n=3). In addition, serum samples were taken from all groups of mice at the end of the experiment and ELISA test was performed.

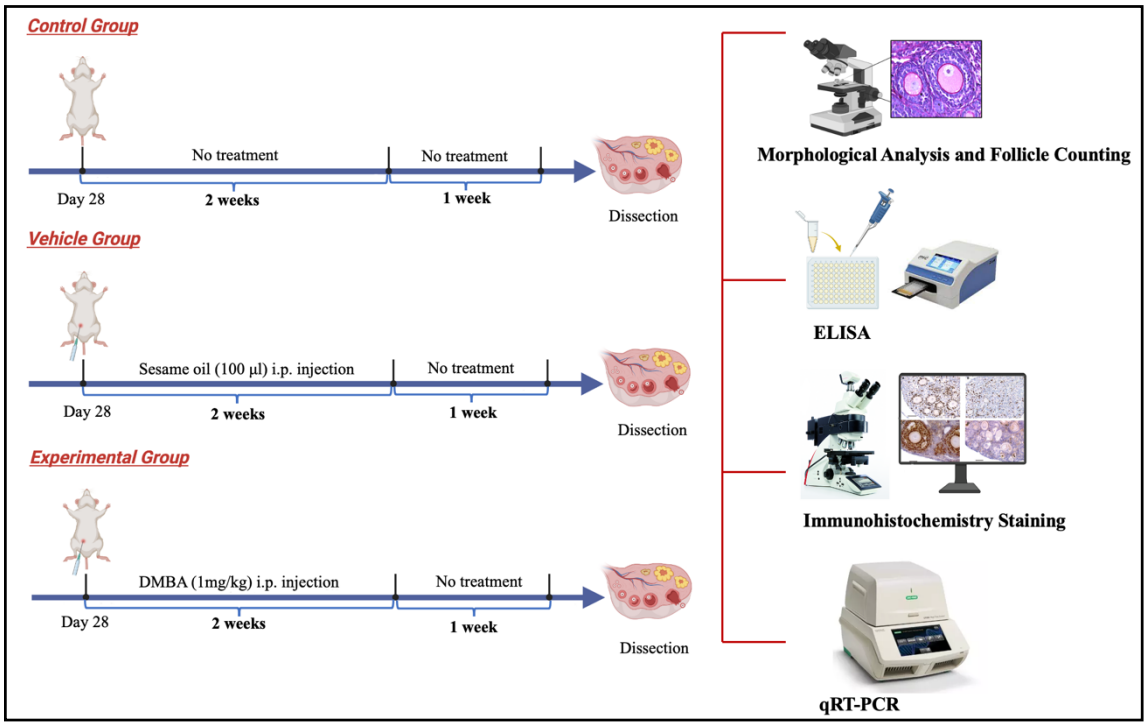

Figure 16. Schematic representation of animal groups and experimental design.

3.2. Tissue Processing

Animals were dissected by cervical dislocations after 3 weeks of experimental protocol. Right ovaries from mice were fixed by neutral formalin solution (Formalin, Buffered, 10% (Phosphate Buffer/Certified), Fisher Scientific, SF100-4) for 12h. After the fixation process, the ovaries were washed 3 times for 10 minutes. Afterward, ovaries were dehydrated in increasing alcohol series (70%, 80%, 90%, and 100%). Then, the ovaries were incubated in xylene. Afterward, ovaries were embedded in paraffin by using a paraffin embedding station (Leica, EG 1160). After then, ovaries were cut into 5 μm histological sections with the aid of using a microtome (Leica, RM 2245 and serial sections were mounted on poly-L-Lysine glass slides.

3.3. Morphological Analysis with Periodic Acid - Schiff (PAS) Staining

For PAS stain sections incubate for 40 min at 60°C to remove paraffin and for 2 times for 20 min left in xylene for complete removal of paraffin. Then sections rehydrate by decreasing the alcohol series for 10 min for each (100%, 96%, 90%, 80%, and 70%). After rehydration, the sections stain with Periodic Acid Schiff Kit (Periodic Acid Schiff, Bio Optica, 04-130802). After washing the sections with water, they pass through increasing alcohol series and clear with xylene. Finally, the sections were covered with a coverslip using a xylene-based mounting medium (Bio Mount HM, Bio-Optica, 05-BMHM500). The examination was done under the light microscope (Leica, DM 500), and images of slides were taken under a microscope (Leica, CTR 6000) with the LASV4.1 computer program.

3.4. Determination of Serum Anti-Müllerian Hormone (AMH) Concentrations by ELISA

When the experimental groups were formed and the experiment was completed, blood samples were taken from the animals to determine the levels of Anti Müllerian Hormone (AMH) before dissection. The blood samples were centrifuged at 4000 rpm for 15 minutes and stored at -80°C for ELISA test.

Serum samples taken at -80°C were brought to room temperature, then centrifuged for 20-30 seconds. Standards were prepared as recommended in the kit (Sunred Bio, Mouse AMH Elisa Kit). The 5 standards specified in the kit, positive control and 9 serum samples of our study were added to the wells to determine AMH levels according to the previously planned order. 50 μL Streptavidin-HRP was added to the standard wells and

10 µL AMH antibody and 40 µL HRP enzyme conjugate were added to the samples and incubated at 37°C for 1 hour. Two blank wells were set aside for blanks. At the end of the incubation, the liquid in all wells was removed. The washing solution at 30X concentration was diluted 30-fold to 1X concentration. All wells were washed 5 times with 350 µl of 1X wash solution. 50 µl of chromogen A followed by 50 µl of chromogen B solution was added to each well, shaken gently and incubated at 37°C for 10 minutes in the dark. This time different shades of blue color formation was observed in the wells. Then 50 µl of stop solution was added to each well. Shaking gently ensured homogeneous distribution of the solution in the wells and a color change from blue to yellow was observed. Immediately afterwards, the absorbance values were recorded by reading the samples on an ELISA reader using the Gen5 program at 450 nm within 15 minutes. Statistical analyses were performed in GraphPad Prism Version 8.0 (GraphPad Software, USA).

3.5. Follicle Counting

During development of the mouse ovary, the follicles are arranged according to the number of granulosa layers surrounding the oocyte. The primary oocyte is surrounded by a single layer of flat follicular cells which is called the primordial follicle (136). A follicle that has one layer of cuboidal shape follicular cells is called a primary follicle. When two or more granulosa cells surround the oocyte, it is called a secondary follicle. Then, the antral cavities fuse to form a large antrum cavity, this follicle is called an antral follicle. In the Graafian follicle, the oocyte is eccentrically positioned and surrounded cumulus cells (137). The number of atretic follicles was determined when only degenerated oocytes and pyknotic granulosa cells were seen (138). The structure of the corpus luteum, which is composed of large granulosa luteal cells and small theca luteal cells, has been determined (139).

Serial 5 µm sections taken from the right ovaries were stained with hematoxylin and eosin (H&E) staining and follicle counting was done under the light microscope (Leica, DM 500). Follicle counting was performed from serial sections through the center of the ovaries in each group. To avoid double counting, only follicles containing an oocyte with a visible nucleus were counted.

3.6. Immunohistochemistry Staining

3.6.1. Immunohistochemistry Staining For MST1/2, LATS1/2, YAP1 and TEAD4 Antibodies

5 µm histological sections cut by microtome and mounted on poly-L-Lysine glass slides (Poly Lysine, Thermo Fisher Scientific, 165014) were deparaffinized in the incubator (60°C) for 1 hour. To be able to remove paraffin from the sections, they were cleared with xylene 2 times for 20 min. Sections were rehydrated with decreasing alcohol series (100%, 90%, 80%, and 70%) to remove xylene. Sections were washed by distilled water for 5 min then by PBS (Phosphate Buffer Saline, pH:7.2-7.4) for 5 min. For antigen retrieval, sections were heated in a microwave (around 600 Watts) in Citrate buffer (10mM, pH 6.0) prepared by dissolving sodium citrate tribasic dihydrate (Sodium Citrate Tribasic Dihydrate, Sigma Aldrich, 6132-04-3) in distilled water, followed by about 5 min low watt (300 Watt). After the sections were heated in a microwave, they were left at room temperature to cool down at the room temperature for 20 min. Then a circle was drawn around the tissues on the slides with a hydrophobic barrier pen and the slides were washed with PBS 3 times for 5 min. For blocking endogenous peroxidase enzymes, sections were incubated with 3% hydrogen peroxide (prepared in methanol) for 10 min. Sections were washed with distilled water 2 times for 5 min. 1.5% Normal Horse Serum (Vector Laboratories, 3002) was used for blocking and the section was incubated with Normal Horse Serum 10 minutes at room temperature. After removal of blocking solution, sections were not washed, and they were incubated with the primary antibodies MST1/2 Polyclonal Antibody in 1:100 (MST1/2 Polyclonal Antibody, İnvitrogen, PA5-36100), LATS1/2 Polyclonal Antibody in 1:200 (LATS1/2 Polyclonal Antibody, Bioss, bs4081R), YAP1 Polyclonal Antibody in 1:200 (YAP1 Polyclonal Antibody, Cell Signaling, 14074), TEAD4 Polyclonal Antibody in 1:200 (TEAD4 Polyclonal Antibody, İnvitrogen, PA5-21977) which were prepared in PBS solution at 4°C for overnight (Table 2). After the incubation with primary antibodies, sections were washed with PBS 3 times 5 min and then incubated with biotinylated pan-specific secondary antibody (Vector Laboratories, 30144) 10 minutes at room temperature (Table 3). Sections were washed with PBS 3 times for 5 min and then incubated with streptavidin/peroxidase complex (Vector Laboratories, 30143) for 5 minutes and incubated at room temperature. After slides were washed with PPS for 3 times for 5 min, slides were incubated with the mix of

DAB and DAB substrate 1:20 (UltraVision Detection System Large Volume DAB Substrate System (RTU), Thermo Fisher Scientific HD16378). Sections were washed with PBS 3 times for 5 minutes. Counterstaining was performed with hematoxylin (Gill's hematoxylin No.3, Bio-Optica, 05-06015/L), and counterstaining slides were washed with tap water. Sections were dehydrated by increasing alcohol series (70%, 80%, 90%, and 100%). Then they were cleared with xylene 2 times for 20 min. The sections were covered with a coverslip using a xylene-based mounting medium (Bio Mount HM, Bio-Optica, 05-BMHM500) and examination was performed by using a light microscope (Leica CTR 6000).

Table 2. List of primary antibodies for immunohistochemistry staining.

Primary Antibody	Isotype	Catalog Number	Dilution
MST1/2	Rabbit Polyclonal	Invitrogen, PA5-36100	1:100
LATS1/2	Rabbit Polyclonal	Bioss, bs4081R	1:200
YAP1	Rabbit Polyclonal	Cell Signaling, #14074	1:200
TEAD4	Rabbit Polyclonal	Invitrogen, PA5-21977	1:200

Table 3. List of secondary antibody for immunohistochemistry staining.

Secondary Antibody	Catalog Number
Prediluted, Biotinylated Universal Pan-Specific (Anti-mouse/rabbit/goat IgG) Secondary Antibody	VECTASTAIN Universal Quick HRP Kit, Peroxidase, R.T.U. – (PK-7800)

3.6.2. Immunohistochemistry Staining For Nitrotyrosine Antibody

Nitrotyrosine (NTY) antibody was used to detect oxidative stress in ovarian tissue. 5 μm histological sections cut by microtome and mounted on poly-L-Lysine glass slides (Poly Lysine, Thermo Fisher Scientific, 165014) were deparaffinized in the incubator (60°C) for 1 hour. To be able to remove paraffin from the sections, they were cleared with xylene 2 times for 20 min. Sections were rehydrated by decreasing alcohol series (100%, 90%, 80%, and 70%) to remove xylene. Sections were washed with distilled water for 5 min then by PBS (Phosphate Buffer Saline, pH:7.2-7.4) for 5 min. For antigen retrieval,

sections were heated in a microwave (around 600 Watts) in Citrate buffer (10mM, pH 6.0) prepared by dissolving sodium citrate tribasic dihydrate (Sodium Citrate Tribasic Dihydrate, Sigma Aldrich, 6132-04-3) in distilled water, followed by about 5 min low watt (300 Watt). After the sections were heated in a microwave, they were left in room temperature to cool down at te room temperature 20 min. Then a circle was drawn around the tissues on the slides with a hydrophobic barrier pen and slides were washed with PBS 3 times 5 min. For blocking endogenous peroxidase enzymes, sections were incubated with 3% hydrogen peroxide (prepared in methanol) for 10 min. Sections were washed with distilled water for 2 times for 5 min, then with Tween-20 PBS for 2 times for 5 min. 5% Normal Goat Serum (prepared in 0.1 % Triton-X-PBS) was used for blocking and the sections were incubated with Normal Goat Serum for 1h at room temperature. After removal of the blocking solution, sections were not washed, and they were incubated with the primary antibodies Nitrotyrosine Polyclonal Antibody in 1:50 (Nitrotyrosine Polyclonal Antibody, Thermo Fisher Scientific, A-21285) which were prepared in blocking solution at +4°C for overnight. After the incubation with primary antibodies, sections were washed with PBS-T (1000µl Tween in 1L PBS) for 3 times for 5 min and then incubated with biotinylated secondary antibody in 1:250 dilution (Goat Anti-Rabbit IgG H&L (Alexa Fluor 488) (ab150077)) for 1,5h at room temperature. Sections were washed with PBS-T for 3 times for 5 min and then incubated with streptavidin for 1,5h at room incubated at room temperature. After slides were washed with PPS-T 3 times for 5 min, slides were incubated with the mix of DAB, and DAB substrate 1:20 (UltraVision Detection System Large Volume DAB Substrate System (RTU), Thermo Fisher Scientific HD16378). Sections were washed with PBS-T for 3 times for 5 minutes. Counterstaining was performed with hematoxylin (Gill's hematoxylin No.3, Bio-Optica, 05-06015/L), and counterstaining slides were washed with tap water. Sections were dehydrated by increasing alcohol series (70%, 80%, 90%, and 100%). Then they were cleared with xylene for 2 times for 20 min. The sections were covered with a coverslip using a xylene-based mounting medium (Bio Mount HM, Bio-Optica, 05-BMHM500) and examination was performed by using a light microscope.

Table 4. List of antibodies for NTY immunohistochemistry staining.

Antibodies	Isotype	Catalog Number	Dilution
Nitrotyrosine (NTY) (Primary antibody)	Rabbit Polyclonal	Thermo Fisher Scientific, A-21285	1:50
Goat Anti-Rabbit IgG H&L (Alexa Fluor 488) (Secondary antibody)	Rabbit Polyclonal	Abcam, (ab150077)	1:250

3.7. Quantitative Real-Time Polymerase Chain Reaction (qRT-PCR)

Hippo signaling proteins MST1, MST2, LATS1, LATS2, YAP1 and TEAD4 mRNA levels were determined by quantitative RT-PCR.

3.7.1. RNA Isolation

qRT-PCR method was applied to show the mRNA levels of Hippo signaling pathway proteins MST1, MST2, LATS1, LATS2, YAP1, and TEAD4. Total RNA was extracted from each group by using the Total RNA Purification Kit-Column Kit (Jena Bioscience, #PP210S).

For the qRT-PCR method, ovarian tissues were cut into small pieces with a scalpel and homogenized with a homogenizer. Then, they were taken into sterile 1.5 ml tubes, and 300 µL of lysis buffer was added to the ovary.

Columns were washed with 100 µL of activation buffer for 30 seconds and centrifuged at 10,000xG. Add 300 µL of isopropanol to the eppendorf containing the sample supernatant and vortex. After the activation buffer settled to the bottom of the colon of eppendorf is emptied (eppendorf under the colon), the samples to which isopropanol is added was transferred to the colon of eppendorf and 30 seconds. It was centrifuged at 10,000 g. Eppendorf remaining under the colon was emptied, sample RNAs were remain in the colon at this stage. Colons containing RNA was washed with 700 µL of primary buffer washing solution, 30 second. It was centrifuged at 10,000xG. The eppendorf located under the colon was emptied. 700 µl of secondary buffer washing solution was added on the colon and wait for 30 seconds. It was centrifuged at 10,000 g. The tube under the colon was emptied. The colon portion was transferred to a new autoclaved tube. 40 µl of elution buffer was transferred to the center of the colon and

placed for 3 minutes. was incubated at room temperature for 2 minutes. It was centrifuged at 10,000 g. RNAs were collected in the lower ependorf and the upper colon was discarded. Sample RNAs were stored at -20°C.

3.7.2. cDNA Synthesis

RNA measurement was made optionally from the separated RNAs, and a determined/calculated amount of RNA-template, 0.5 µLOligo-DT, and water mixture were prepared. 5-10 min at 70°C. were subjected to the heating process (denaturation process). The first stage used in preparation and DNA amplification volumes are indicated in Table 5.

Table 5. cDNA synthesis reaction contents.

Content	Volume (µl)
SCRIPT RT Buffer	4
dNTP Mix	1
DTT Stock Solution	1
RNase inhibitor	1
SCRIPT Reverse Transcriptase	0.5
RNase-free Water	2.5
Total	**10 µl mix**

10 µL of the mix solution obtained as a result of this process was mixed with 10 µL of sample RNA. It was inserted into the PCR device by entering the appropriate program information (45 minutes at 50°C, 10 minutes at 42°C). After the cDNA synthesis process is completed, the samples were stored at -20°C.

3.7.3. qRT-PCR

The qRT-PCR reaction was prepared according to the manufacturer's instructions. qRT-PCRs carried out on a CFX96 TouchTM Real-Time PCR Detection System (Bio-Rad Laboratories). The reaction volumes are given in Table 6. The qRT-PCR reaction

protocol was performed as follows. An initial denaturation of 30 seconds at 95°C continued as a single cycle, followed by 45 cycles of 95°C/15 sec, 53°C/20 sec and 60°C/20 sec for *MST1, MST2, LATS1, LATS2, YAP1* and *TEAD4* genes. All expression data were normalized by dividing the amount of target gene by the amount of *β-actin.* The primer sequences used in the reactions are given in Table 7.

Table 6. qRT-PCR reaction contents.

Maxima SYBR Green qPCR Master Mix (2x)	10 µl
PCR Grade Water	7.8 µl
Forward Primer	0.6 µl
Reverse Primer	0.6 µl
Template DNA	1 µl

The reaction mixture was prepared by adding the reactants specified in the Table 6.

Table 7. Primer sequences used in qRT-PCR.

MST1	F: 5'-GAACACAGACCTGTGGATTG-3' R: 5'-CGCCTTGATATCTCGGTGTA-3'	(Pengi et al., 2013) (140)
MST2	F: 5'-TCTCCTCAATACAGAAGGAC-3' R: 5'-AGAAGTAATGCCAAGGGACC-3'	(Pengi et al., 2013) (140)
LATS1	F: 5'-GAATGAGCCCGTGAAAGCAACACA-3' R: 5'-TTCAGACTTCAGACGCTCCATGCT-3'	(Sun et al., 2019) (141)
LATS2	F: 5'-TGAAGAGGGCCAAGATGGACAAGT-3' R:5'-AGAGCGTGAGTGTCCAGCTTACAA-3'	(Sun et al., 2019) (141)
YAP1	F: 5'-ATCCCTGATGATGTACCACTGCCA-3' R: 5'-CAGGAACGTTCAGTTGCGAAAGCA-3'	(Sun et al., 2019) (141)
TEAD4	F: 5'-AGGCCGGCACCATTACCTC-3' R: 5'-TGGATCTCCCGGGCTTTTC-3'	(Huapeng et al., 2019) (142)
β-ACTIN	F: 5'-ACCAACTGGGACGACATGGAGAA-3' R: 5'-TACGACCAGAGGCATACAGGGAC-3'	(Li et al., 2013) (143)

3.8. Statistical Analysis

ImageJ and FIJI software was used to perform intensity analysis for immunohistochemistry staining.

One way ANOVA and Tukey's multiple comparison test were used for statistical analysis by GraphPad Prism Version 8.0 (GraphPad Software, USA). The p-value which was lower than 0.05 was called significant.

4. RESULTS

4.1. Morphological Evaluation of Experimental Groups by Periodic Acid-Schiff (PAS) Staining

Morphological evaluation with Periodic Acid-Schiff (PAS) staining was performed to control, vehicle and DMBA ovarian tissues. There is no significant difference between the sizes of ovaries from control, vehicle and DMBA groups. We observed normal fibrous structure of the ovarian stroma in all groups. In the ovarian tissue of the control and vehicle groups, follicles at different stages of follicular development and corpus luteum were identified in the cortex of the ovary. When we morphologically evaluated the oocytes in the developing follicles, we determined that their nucleus, cytoplasm and zona pellucida were normal appearance. We determined that the granulosa cells were organized around the oocyte in relation to the oocyte. We also observed atretic follicles in the ovaries from control and vehicle groups that did not complete development as a requirement of the normal follicular process. When we evaluated the ovarian tissues obtained from the vehicle group, we observed the same morphological results as the control group. We observed more corpus luteum structure in the vehicle group compared to the other groups. We evaluated the ovarian tissues of DMBA-treated mice, which we aimed to establish a mouse model of ovotoxicity, we found follicles at different stages of follicular development in the ovarian cortex. When we examined the developing follicles, we observed deterioration in the cytoplasm, nucleus and zona pellucida of the oocytes in the follicle compared to the control group. We did not observe an increase in atretic follicles in the 2 week DMBA-treated group compared to the control and vehicle groups, but we detected atretic follicles at each stage of follicular development. We showed that ovulation occurred in the ovaries of the DMBA-treated group due to the presence of the corpus luteum. Although we observed follicles at all stages of development in the ovaries of the DMBA-treated group, we also evaluated that the structure of the follicles was disrupted. Follicles usually did not have a spherical appearance and there were disruptions

in tissue integrity between granulosa cells. The granulosa cells were not in close cellular contact with each other and were not always organized around the oocyte.

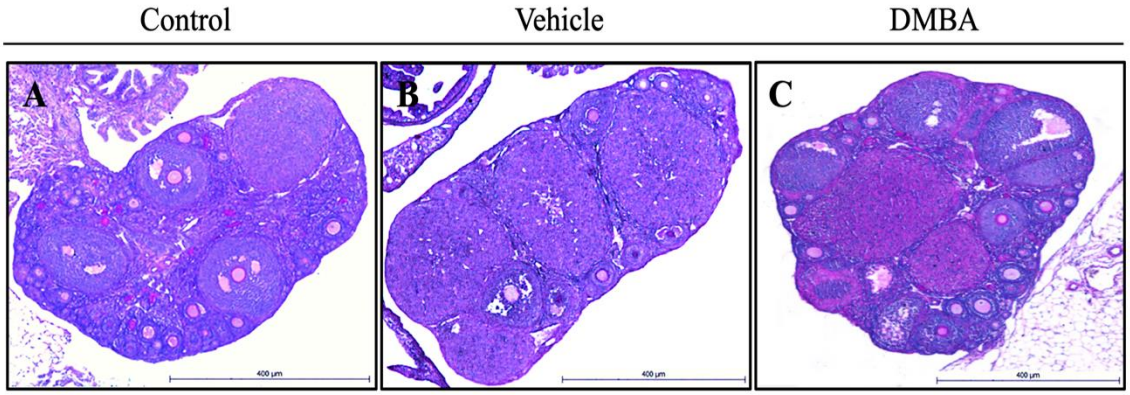

Figure 17. Morphological evaluation of control, vehicle and DMBA groups by Periodic Acid-Schiff (PAS) staining. The structure of cortex and medulla of the ovaries from control (A), vehicle (B), and DMBA (C) groups are shown (Scale bar: 400 µm).

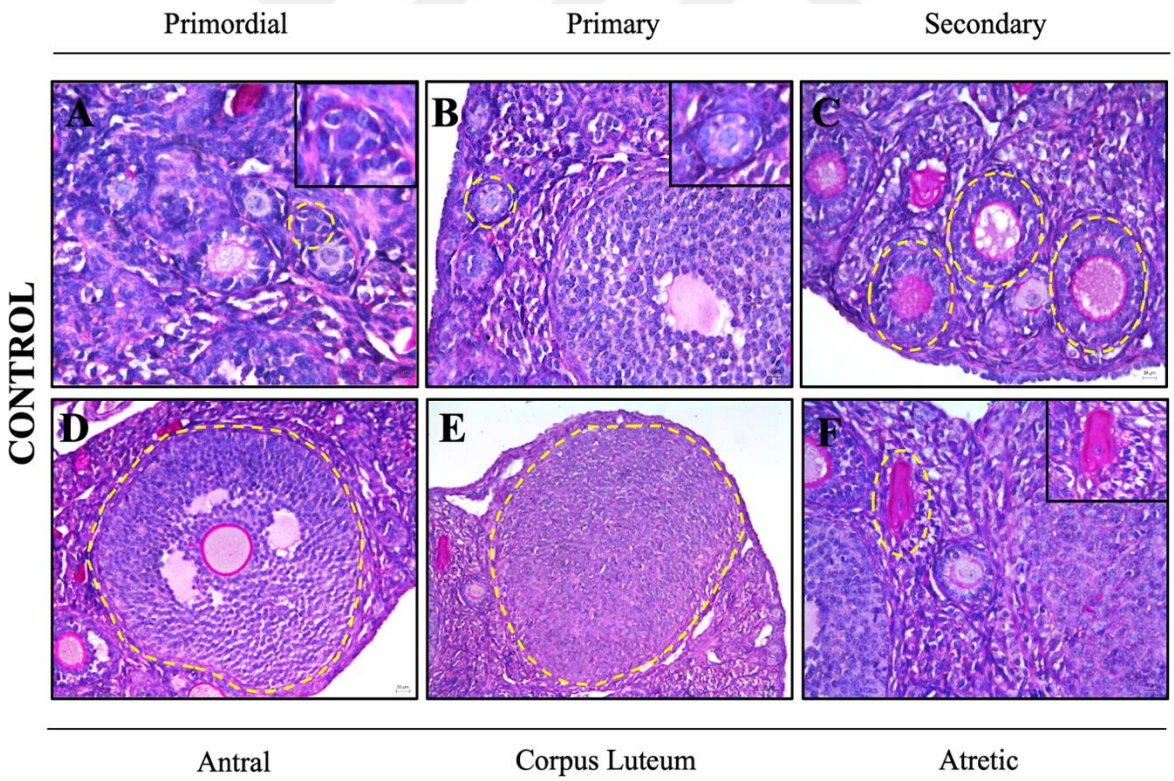

Figure 18. Morphological evaluation of control group by PAS staining. In the control group primordial (A), primary (B), secondary (C), antral (D), corpus luteum (E), and atretic (F) follicle structures are shown (Scale bar: 50 µm and 100 µm). Insert figure in A

is higher magnification of primordial follicle, insert figure in B is higher magnification of primary follicle and insert figure in F is higher magnification of atretic follicle.

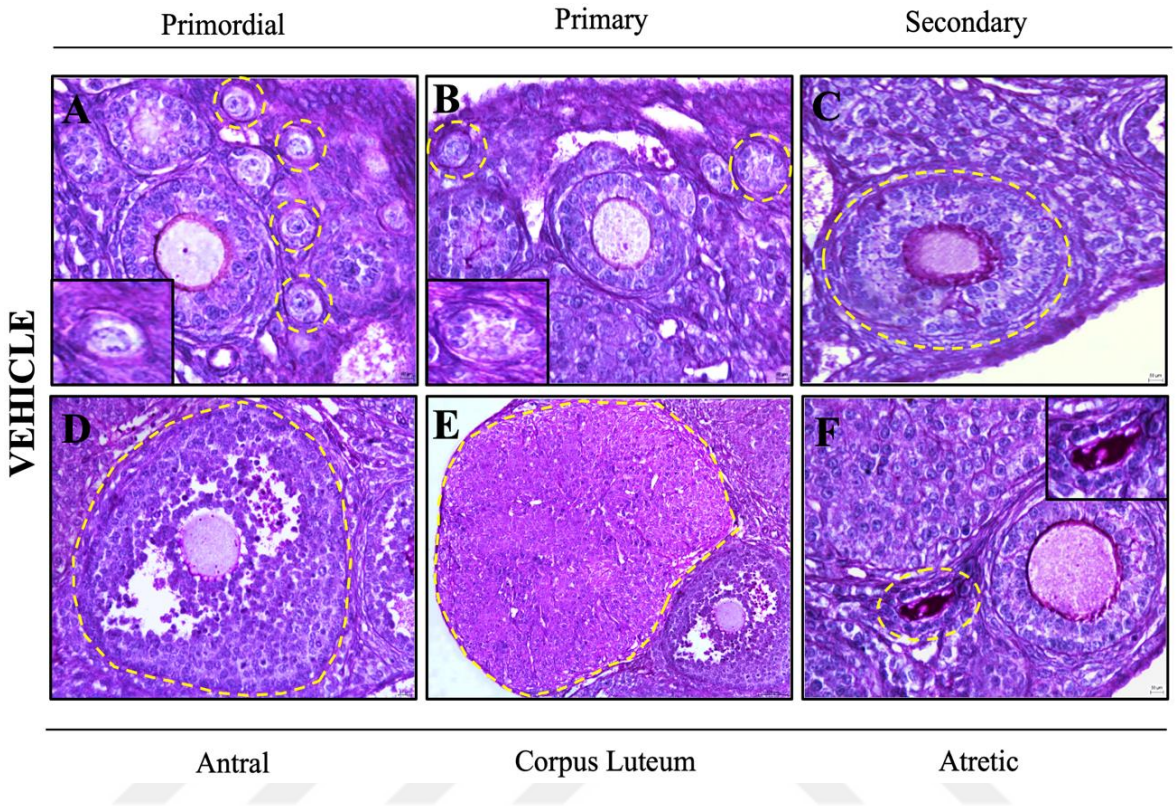

Figure 19. Morphological evaluation of vehicle group by PAS staining. In the vehicle group primordial (A), primary (B), secondary (C), antral (D), corpus luteum (E) and atretic (F) follicle structures are shown (Scale bar: 50 µm and 100 µm). Insert figure in A is higher magnification of primordial follicle, insert figure in B is higher magnification of primary follicle, and insert figure in F is higher magnification of atretic follicle.

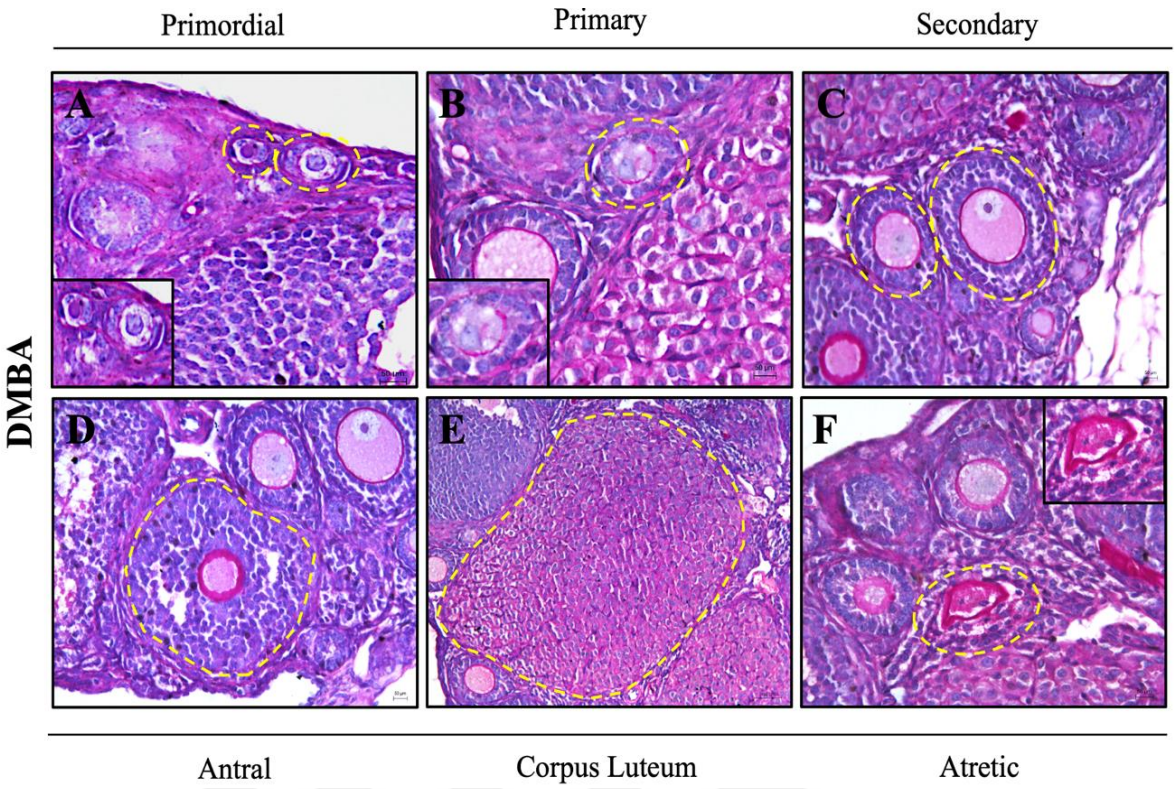

Figure 20. Morphological evaluation of DMBA group by PAS staining. In the DMBA group primordial (A), primary (B), secondary (C), antral (D), corpus luteum (E) and atretic (F) follicle structures are shown (Scale bar: 50 µm and 100 µm). Insert figure in A is higher magnification of primordial follicle, insert figure in B is higher magnification of primary follicle, and insert figure in F is higher magnification of atretic follicle.

4.2. ELISA Results

Serum AMH level was determined by ELISA method to evaluate the size of primordial follicle reserve in all experimental groups. When the concentration measurements of the standards were made, the following standard curve graph was obtained (Figure 21). When we compared the standards with the experimental groups, the AMH concentration in the experimental groups is shown in Figure 22.

The AMH levels in the serum obtained from the DMBA-treated group, the experimental group in which ovotoxicity occurred with DMBA administration for 2 weeks, were compared with the control and vehicle groups, we did not detect statistically difference for AMH levels between all experimental groups. These results showed that 2

weeks DMBA administration is not present stimulative effect on primordial follicles activation in ovarian reserve (Figure 22).

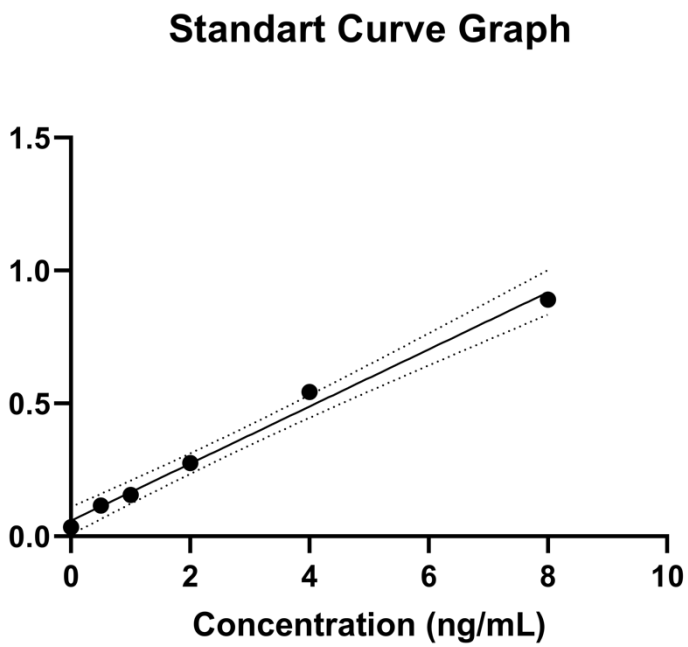

Figure 21. Standard concentration curve for AMH.

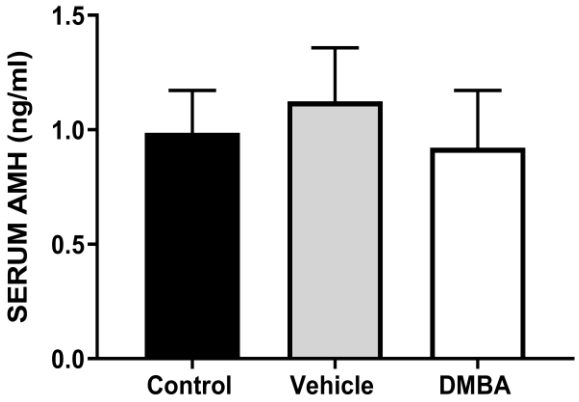

Figure 22. Comparison of serum AMH levels between control, vehicle and DMBA-treated groups.

4.3. Follicle Counting

When the 2 week DMBA-treatment group was compared with the control and vehicle groups, we determined that the number of primordial, primary follicles and corpus luteum signifcantly decreased (*p<0.1, **p<0.01, ***p<0.001, ****p<0.0001). Moreover, we determined that the number of secondary (*p<0.1) and atretic follicles (**p<0.01) increased in the DMBA-treated group compared with the control and vehicle groups. Follicle numbers are given in Figure 23.

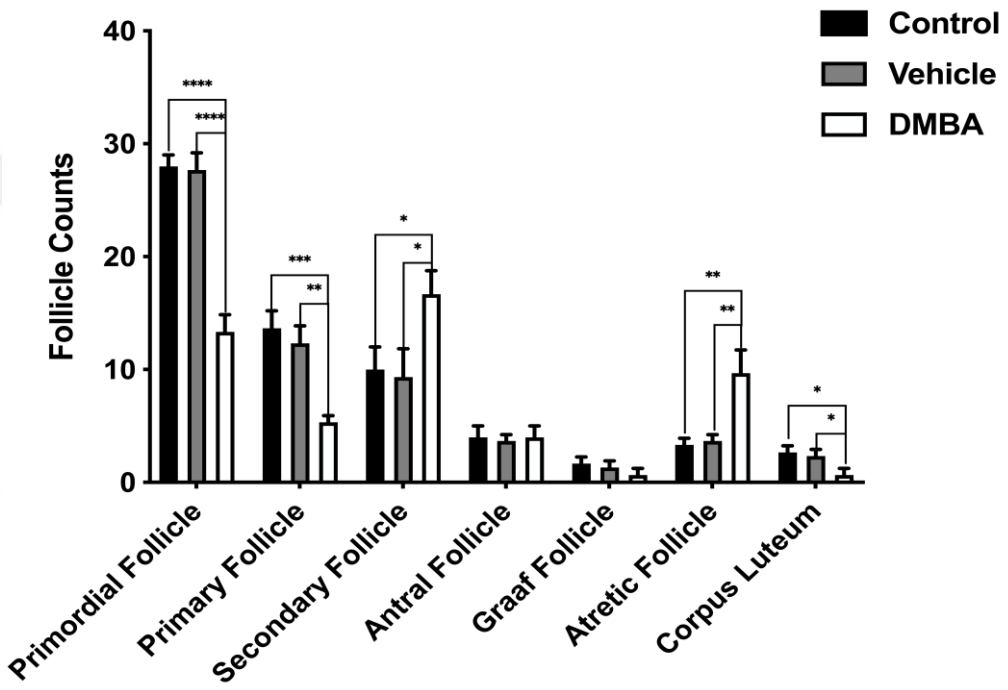

Figure 23. Comparison of the number of primordial, primary, secondary, antral, Graafian, atretic follicles and corpus luteum with control, vehicle and DMBA-treated groups (****p<0,0001, ***p<0,001, **p<0,01, *p<0,1).

4.4. Localization of Hippo Signaling Pathway Proteins by Immunohistochemistry

We performed immunohistochemistry staining on paraffin sections to evaluate Hippo signaling pathway proteins in mice control, vehicle and DMBA-treated ovarian tissues to show localization of Hippo signaling pathway proteins MST1/2, LATS1/2, YAP1, TEAD4.

MST1 and MST2 are essential components of the Hippo signaling pathway that regulates apoptosis and proliferation to maintain organ size and tissue homeostasis in mammals (144). To evaluate MST1 and MST2 localization in ovaries, we observed primordial, primary, secondary, antral and atretic follicles and corpus luteum in sections stained with immunohistochemical staining with MST1/2 antibody.

We determined that MST1/2 localization was stronger in the cytoplasm of granulosa cells in primordial follicle in the DMBA-treated group compared to the control and vehicle groups. MST1/2 expression was weak in oocytes in primordial follicle from all groups (Figure 24A, 24A', 24A''). We found that MST1/2 localization was higher in cells cytoplasm of granulosa cells in primary follicle in the DMBA-treated group. MST1/2 showed weak expression in primary follicle oocytes in all groups (Figure 24B, 24B', 24B''). When MST1/2 expression in granulosa cells of secondary follicles was analyzed, expression was stronger in the cytoplasm of granulosa cells in DMBA-treated group compared to control and vehicle groups (Figure 24C, 24C', 24C''). In addition, the granulosa cell integrity of the secondary follicles in the DMBA-treated group was disrupted and the intercellular space increased (Figure 24C''). We detected weak MST1/2 expression in secondary follicle oocytes in all groups (Figure 24C, 24C', 24C'').

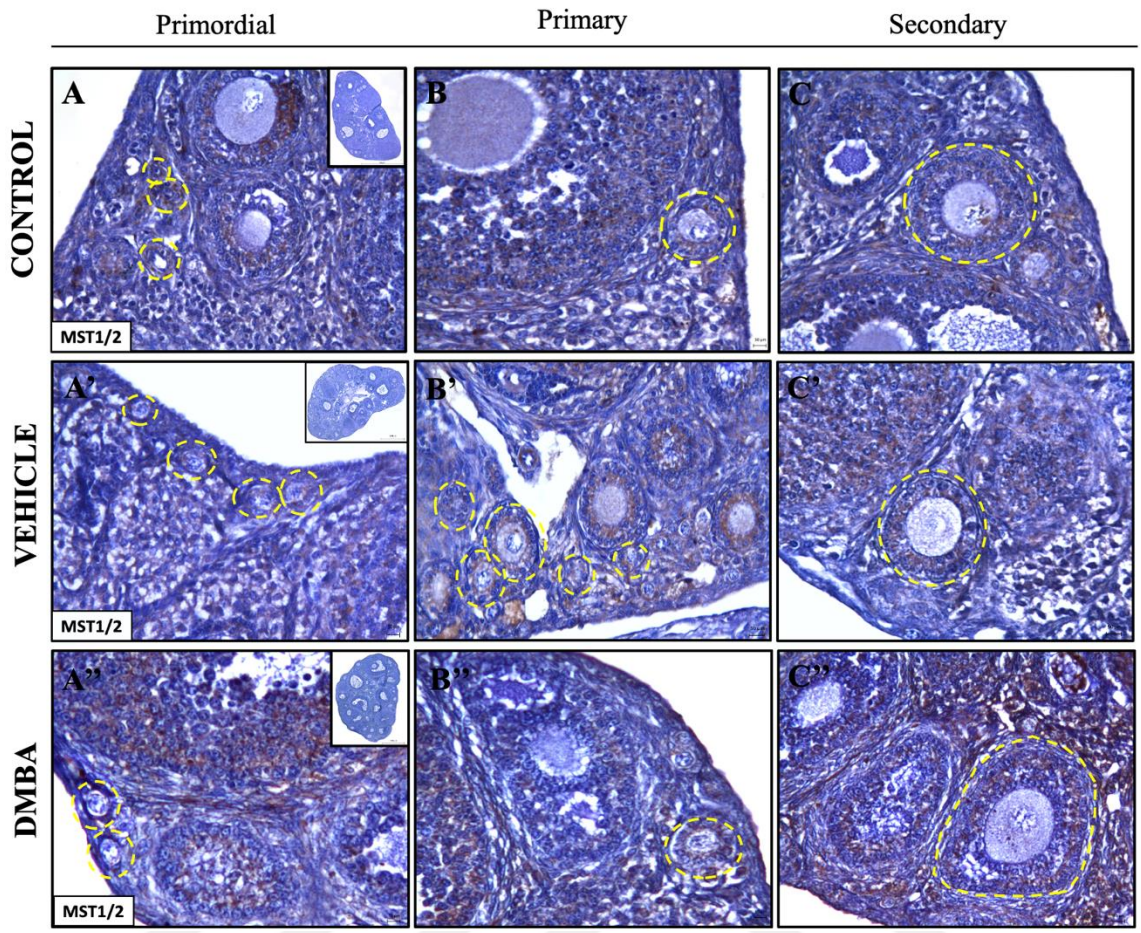

Figure 24. MST1/2 protein localization to primordial, primary and secondary follicles in control, vehicle and DMBA groups demonstrated by immunohistochemistry staining. The yellow circles represent primordial follicles in control (A), vehicle (A') and DMBA (A") groups, primary follicles in control (B), vehicle (B") and DMBA (B") groups and secondary follicles in control (C), vehicle (C') and DMBA (C'') groups. The brown stained areas indicate MST1/2 and blue stained areas indicate the nucleus. The nucleus staining was performed with Hematoxylin. In the additional images shown in the control, vehicle and DMBA group, there is no staining pattern in the negative control (Inserts) (Scale bar: 50 µm).

MST1/2 expression was highest in antral groups to follicles at other developmental stages. MST1/2 expression was higher in granulosa cells of DMBA-treated group compared to vehicle and control groups (Figure 25D''). In all groups, very weak MST1/2 expression was observed in antral follicle oocytes (Figure 25D, 25D', 25D''). MST1/2 localization was observed in luteal cells of the corpus luteum in all

groups (Figure 25E, 25E', 25E''). Also, MST1/2 localization was observed in granulosa cells of atretic follicles in all groups (Figure 25F, 25F',25F'').

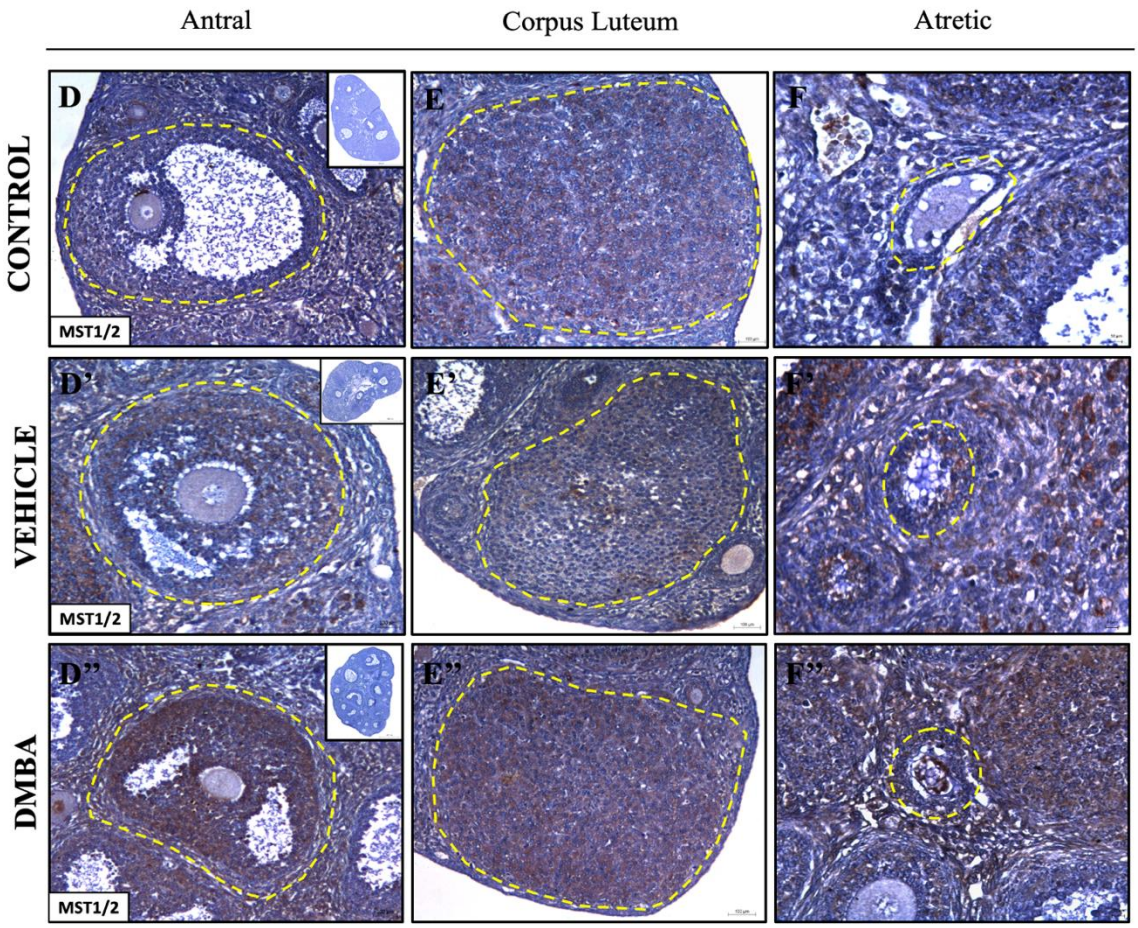

Figure 25. MST1/2 protein localization to antral, atretic follicles and corpus luteum in control, vehicle and DMBA groups demonstrated by immunohistochemistry staining. The yellow circles represent antral follicles in control (D), vehicle (D') and DMBA (D") groups, corpus luteum in control (E), vehicle (E") and DMBA (E") groups and atretic follicles in control (F), vehicle (F') and DMBA (F'') groups. The brown stained areas indicate MST1/2 and blue stained areas indicate the nucleus. The nucleus staining was performed with Hematoxylin. In the additional images shown in the control, vehicle and DMBA group, there is no staining pattern in the negative control (Inserts) (Scale bar: 100 µm and 50 µm).

We analyzed MST1/2 intensity in granulosa cells, oocytes and total ovary for control, vehicle and DMBA groups. In DMBA group, MST1/2 intensity was higher in granulosa cells compared to vehicle and control group, the difference was statistically

significant ($p<0.1$) (Figure 26A). MST1/2 intensity in oocytes was increased in DMBA group compared to control and vehicle groups, but not significantly (Figure 26B). MST1/2 intensity in total ovary was significantly increased in DMBA group compared to control and vehicle groups ($p < 0.0001$). There is no significant difference in MST1/2 intensity between control and vehicle groups (Figure 26C).

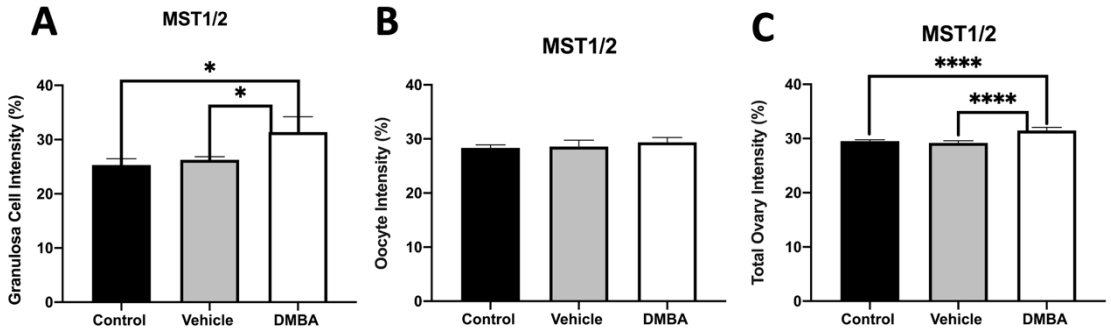

Figure 26. Results of the MST1/2 intensity in granulosa cells, oocytes and total ovary for control, vehicle and DMBA groups. One-way ANOVA and Tukey's multiple comparison test were applied. **A.** Representative granulosa cell intensity (%). **B.** Representative oocyte intensity (%). **C.** Representative total ovary intensity (%) (*$p<0.1$), (****$p<0.0001$).

LATS1/2 is an important Hippo kinase involved in the regulation of cellular processes such as cell proliferation and cell death (145). To evaluate LATS1/2 localization in ovaries, we observed primordial, primary, secondary, antral and atretic follicles and corpus luteum in sections stained with immunohistochemical staining with LATS1/2 antibody. LATS1/2 expression was weak in cytoplasm of granulosa cells in primordial, primary, secondary, antral, atretic follicle stages and corpus luteum in control, vehicle and DMBA groups. We observed slightly localization of LATS1/2 in ovarian tissues from all experimental group (Figure 27 and figure 28).

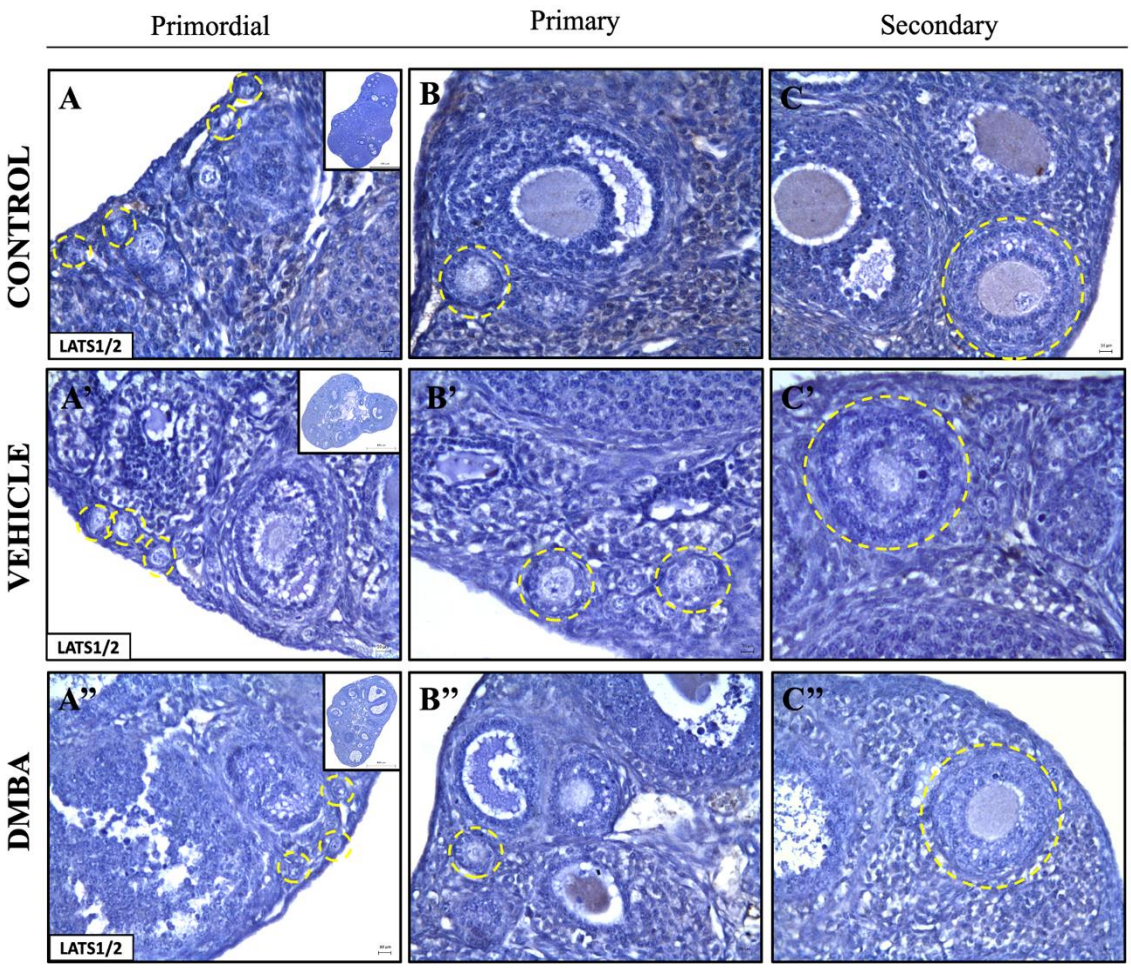

Figure 27. LATS1/2 protein localization to primordial, primary and secondary follicles in control, vehicle and DMBA groups demonstrated by immunohistochemistry staining. The yellow circles represent primordial follicles in control (A), vehicle (A') and DMBA (A") groups, primary follicles in control (B), vehicle (B") and DMBA (B") groups and secondary follicles in control (C), vehicle (C') and DMBA (C'') groups. The brown stained areas indicate LATS1/2 and blue stained areas indicate the nucleus. The nucleus staining was performed with Hematoxylin. In the additional images shown in the control, vehicle and DMBA group, there is no staining pattern in the negative control (Inserts) (Scale bar: 50 µm).

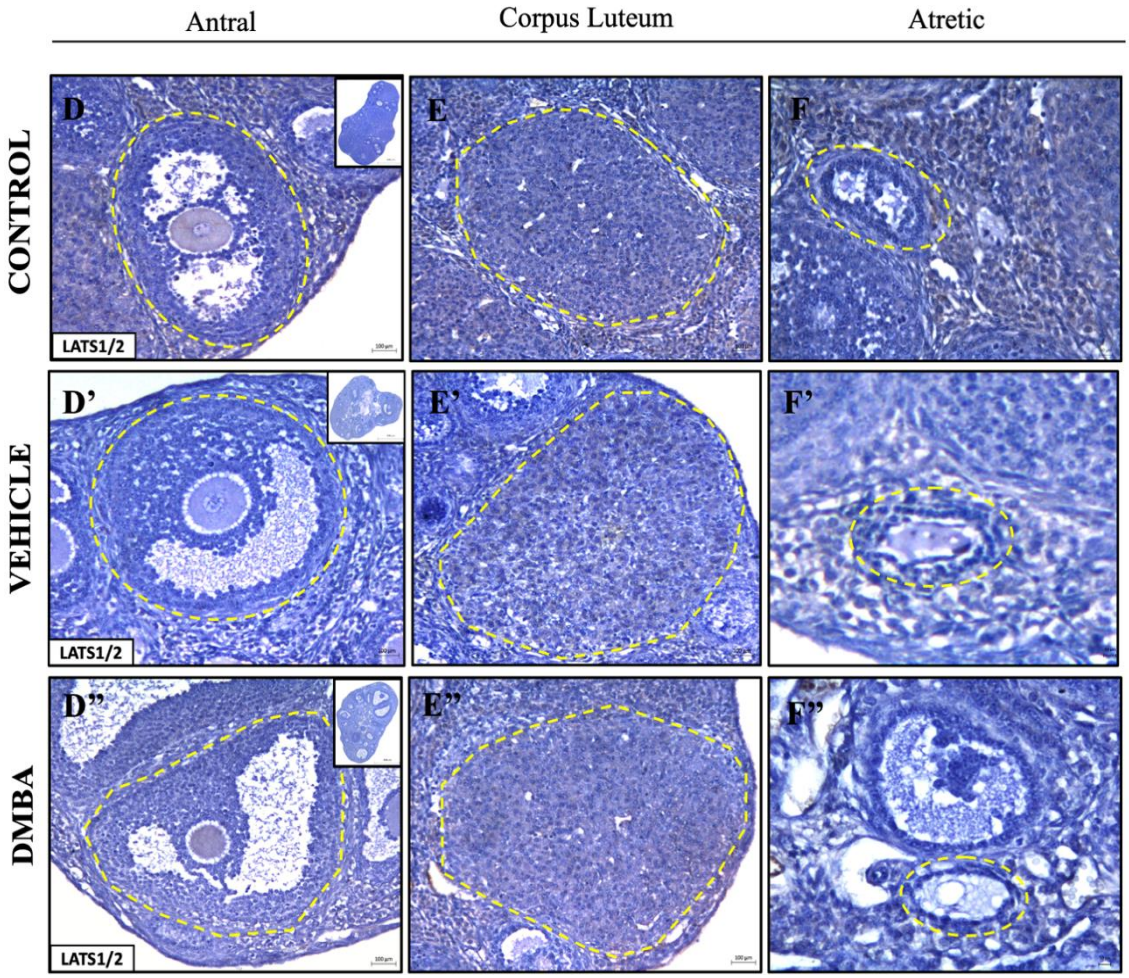

Figure 28. LATS1/2 protein localization to antral, atretic follicles and corpus luteum in control, vehicle and DMBA groups demonstrated by immunohistochemistry staining. The yellow circles represent antral follicles in control (D), vehicle (D') and DMBA (D") groups, corpus luteum in control (E), vehicle (E") and DMBA (E") groups and atretic follicles in control (F), vehicle (F') and DMBA (F'') groups. The brown stained areas indicate LATS1/2 and blue stained areas indicate the nucleus. The nucleus staining was performed with Hematoxylin. In the additional images shown in the control, vehicle and DMBA group, there is no staining pattern in the negative control (Inserts) (Scale bar: 100 µm and 50 µm).

YAP1 is phosphorylated by activation of upstream Hippo pathway kinases. YAP1 has been shown to be a protooncogene that plays important roles in organ development and tumorigenesis by regulating cell proliferation (146). To evaluate YAP1 localization

in ovaries, we observed primordial, primary, secondary, antral and atretic follicles and corpus luteum in sections stained with immunohistochemical staining with YAP1 antibody. YAP1 localization was observed at all stages of follicular development in all groups. YAP1 showed weak expresson in granulosa cells cytoplasm of primordial and primary follicles in control, vehicle and DMBA groups. YAP1 expression was not observed in primordial and primary follicle oocytes in all experimental groups (Figure 29A, 29A', 29A'' and Figure 29B, 29B', 29B''). YAP1 expression was highest in secondary and antral follicles in control, vehicle and DMBA groups. Furthermore, YAP1 expression was strongly expressed in the granulosa cell cytoplasm and nucleus of secondary and antral follicles in DMBA-treated groups compared to control and vehicle groups (Figure 29C, 29C', 29C'' and figure 30D, 30D', 30D''). YAP1 localization was also observed in oocytes of follicles that developed with follicular development in all groups (Figure 29C, 29C', 29C'' and figure 30D, 30D', 30D''). YAP1 localization was detected in luteal cells of the corpus luteum in all groups (Figure 30E, 30E', 30E''). Also, YAP1 localization was observed in granulosa cells of atretic follicles in all groups (Figure 30F, 30F', 30F'').

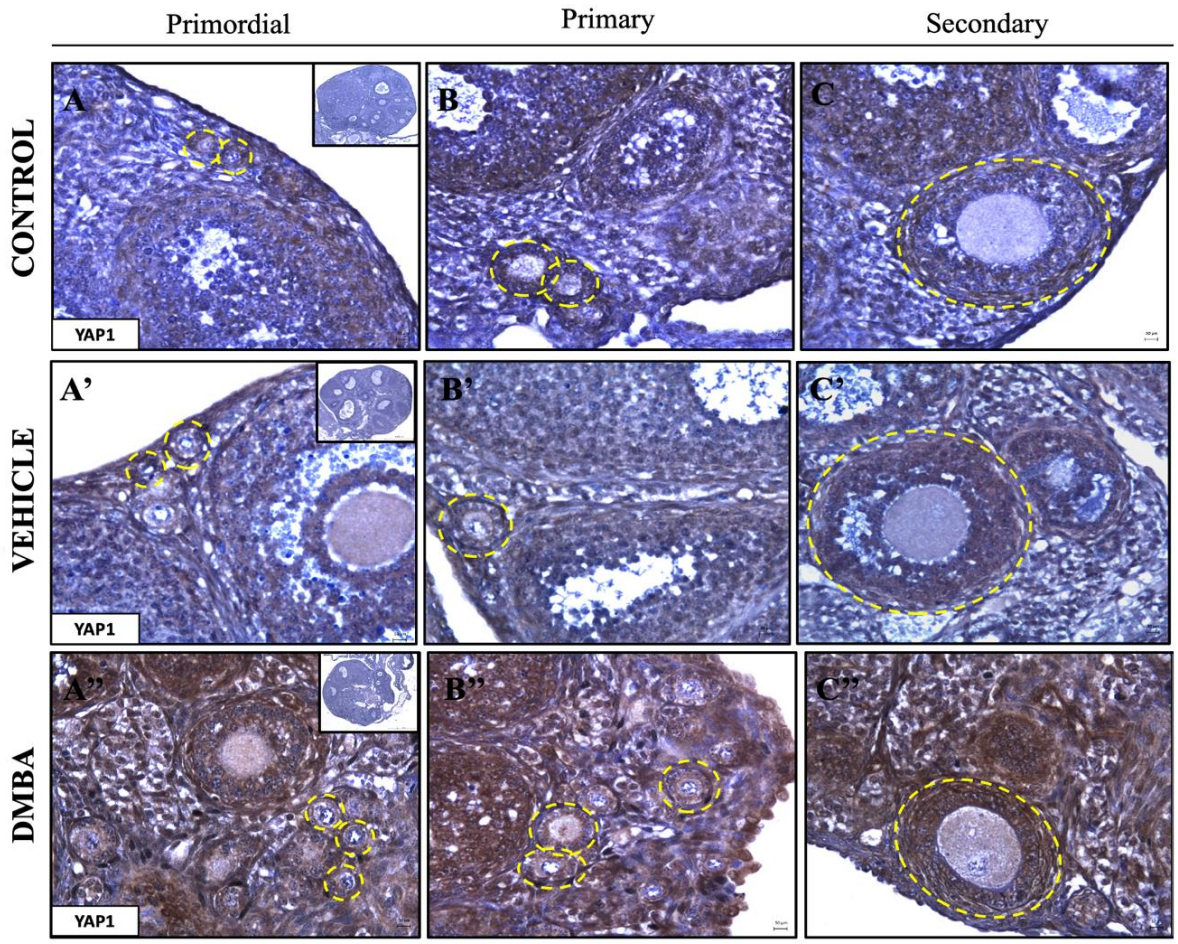

Figure 29. YAP1 protein localization to primordial, primary and secondary follicles in control, vehicle and DMBA groups demonstrated by immunohistochemistry staining. The yellow circles represent primordial follicles in control (A), vehicle (A') and DMBA (A") groups, primary follicles in control (B), vehicle (B") and DMBA (B") groups and secondary follicles in control (C), vehicle (C') and DMBA (C'') groups. The brown stained areas indicate YAP1 and blue stained areas indicate the nucleus. The nucleus staining was performed with Hematoxylin. In the additional images shown in the control,

vehicle and DMBA group, there is no staining pattern in the negative control (Inserts) (Scale bar: 50 µm).

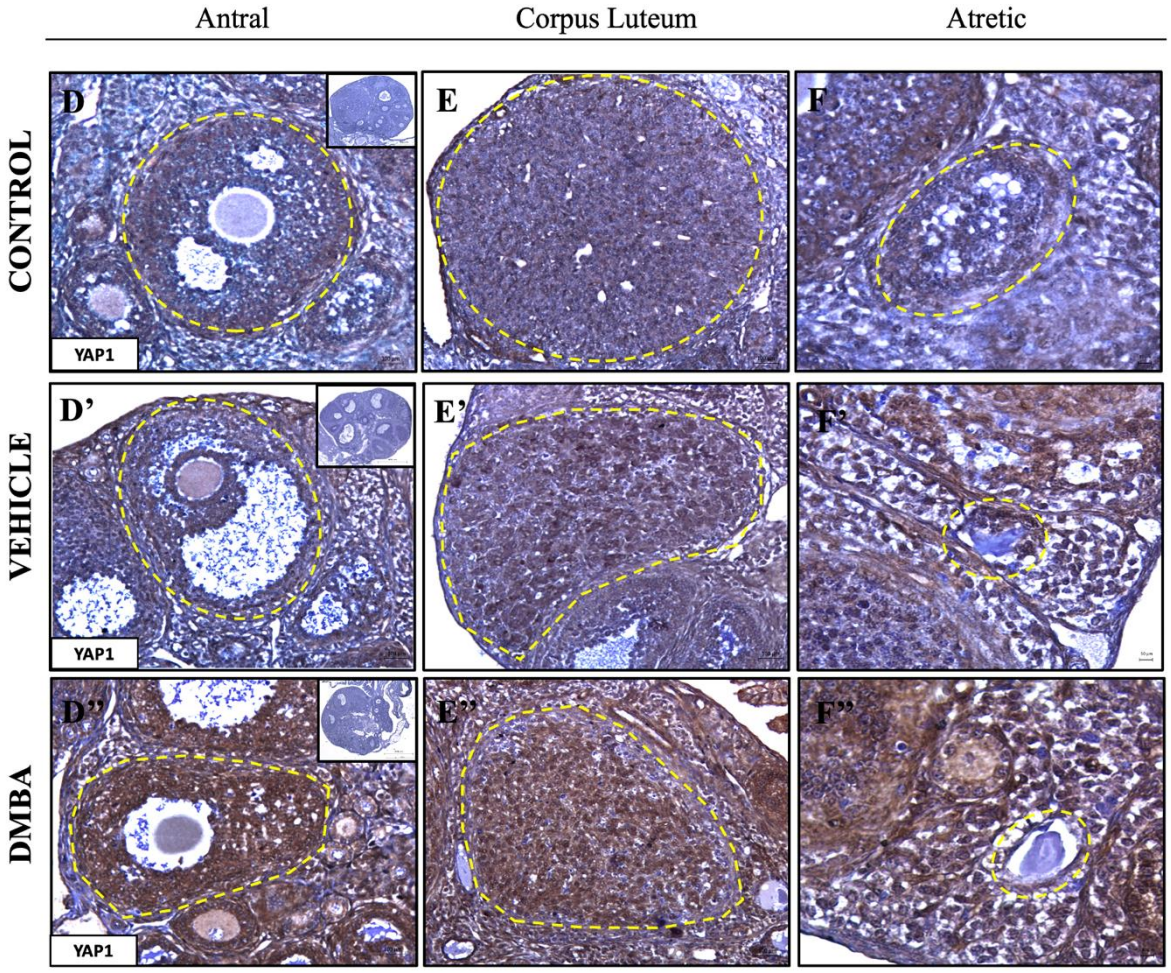

Figure 30. YAP1 protein localization to antral, atretic follicles and corpus luteum in control, vehicle and DMBA groups demonstrated by immunohistochemistry staining. The yellow circles represent antral follicles in control (D), vehicle (D') and DMBA (D") groups, corpus luteum in control (E), vehicle (E") and DMBA (E") groups and atretic follicles in control (F), vehicle (F') and DMBA (F'') groups. The brown stained areas indicate YAP1 and blue stained areas indicate the nucleus. The nucleus staining was performed with Hematoxylin. In the additional images shown in the control, vehicle and DMBA group, there is no staining pattern in the negative control (Inserts) (Scale bar: 100 µm and 50 µm).

We analyzed YAP1 intensity in granulosa cells, oocytes and total ovary from control, vehicle and DMBA groups. YAP1 intensity in granulosa cells were significantly increased in DMBA group compared to control and vehicle groups ($p < 0.001$). There is no significant difference in YAP1 intensity between control and vehicle groups (Figure 31A). YAP1 expression in oocytes was increased in DMBA group compared to control and vehicle groups, but not significantly (Figure 31B). YAP1 intensity in total ovary was significantly increased in DMBA group compared to control ($p < 0.01$) and vehicle groups ($p < 0.1$). There is no significant difference in YAP1 intensity between control and vehicle groups (Figure 31C).

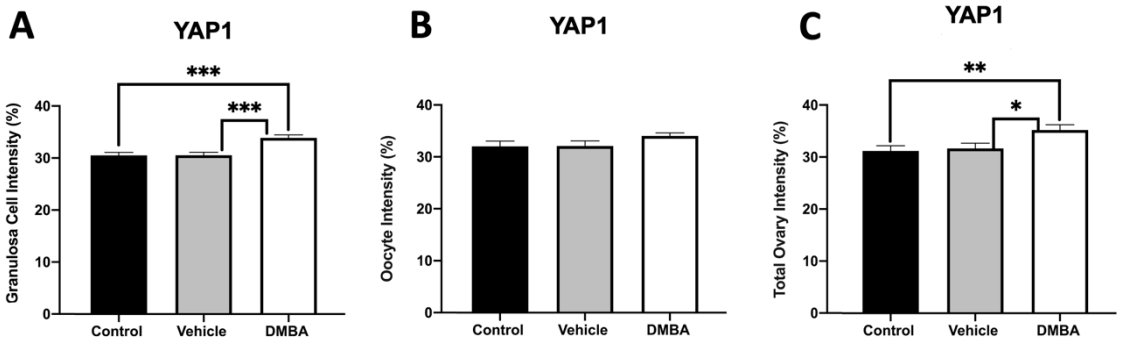

Figure 31. Results of the YAP1 intensity in granulosa cells, oocytes and total ovary for control, vehicle and DMBA groups. One-way ANOVA and Tukey's multiple comparison test were applied. A. Representative granulosa cell intensity (%). B. Representative oocyte intensity (%). C. Representative total ovary intensity (%) (***$p<0.001$, **$p<0.01$, *$p<0.1$).

TEAD4 is a downstream effector of the Hippo pathway and plays an important roles in cell survival, proliferation and tumorogenesis (147). To evaluate TEAD4 localization in ovaries, we observed primordial, primary, secondary, antral and atretic follicles and corpus luteum in sections stained with immunohistochemical staining with TEAD4 antibody. TEAD4 localization was strongly expressed in granulosa cell cytoplasm of primordial and primary follicles in control, vehicle and DMBA-treated groups. TEAD4 expression was not observed in primordial follicle oocytes but TEAD4 expression observed in primary follicles oocytes in all groups (Figure 32A, 32A’, 32A’’ and Figure 32B, 32B’, 32B’’). TEAD4 expression was highest in secondary and antral follicles in control, vehicle and DMBA groups. When TEAD4 expression in cytoplasm

and nucleus of granulosa cells of secondary and antral follicles was analyzed, expression was stronger in DMBA group to control and vehicle groups. Also, TEAD4 was localized in oocytes of secondary and antral follicles in all groups (Figure 32C, 32C', 32C'' and Figure 33D, 33D', 33D''). TEAD4 localization was observed in luteal cells of the corpus luteum in all groups (Figure 33E, 33E', 33E''). Also, TEAD4 localization was observed in granulosa cells of atretic follicles in all experimental groups (Figure 33F, 33F',33F'').

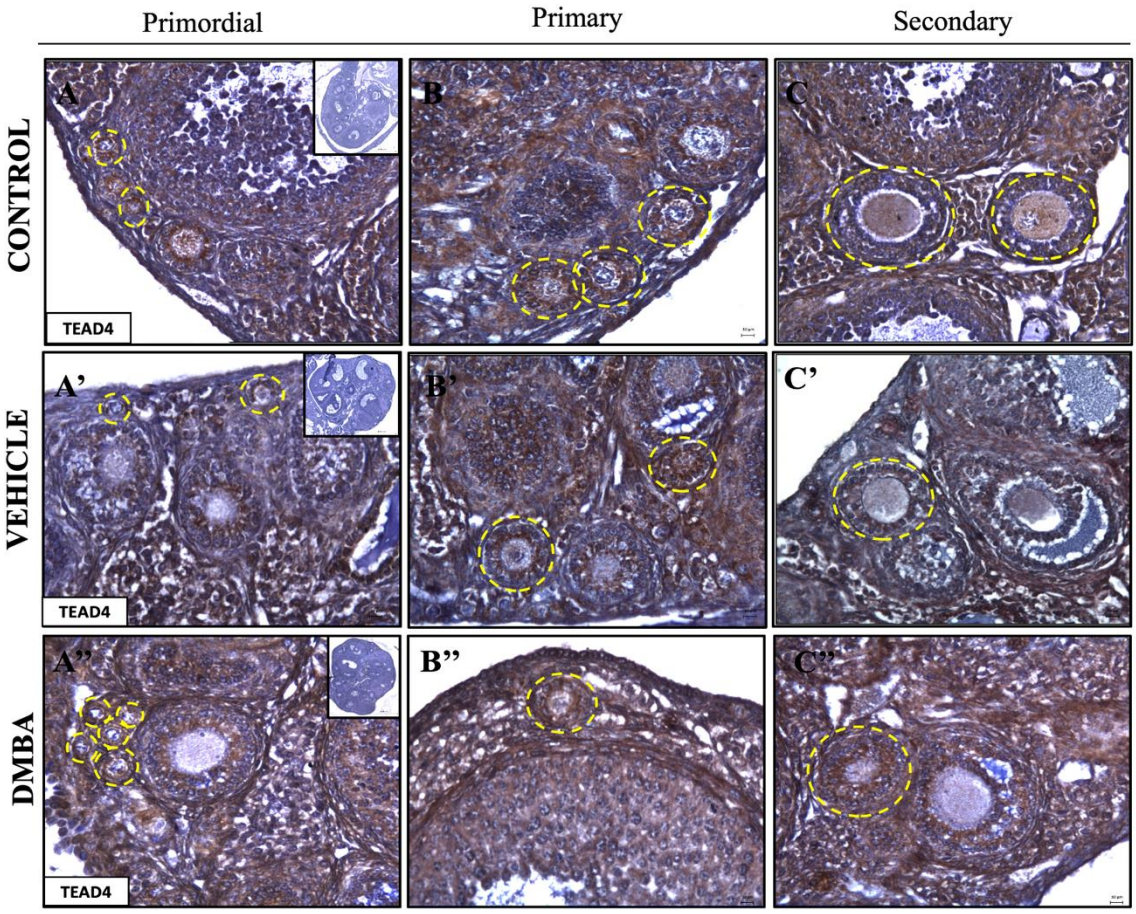

Figure 32. TEAD4 protein localization to primordial, primary and secondary follicles in control, vehicle and DMBA groups demonstrated by immunohistochemistry staining. The yellow circles represent primordial follicles in control (A), vehicle (A') and DMBA (A") groups, primary follicles in control (B), vehicle (B") and DMBA (B") groups and secondary follicles in control (C), vehicle (C') and DMBA (C'') groups. The brown stained areas indicate TEAD4 and blue stained areas indicate the nucleus. The nucleus staining was performed with Hematoxylin. In the additional images shown in the control,

vehicle and DMBA group, there is no staining pattern in the negative control (Inserts) (Scale bar: 50 µm).

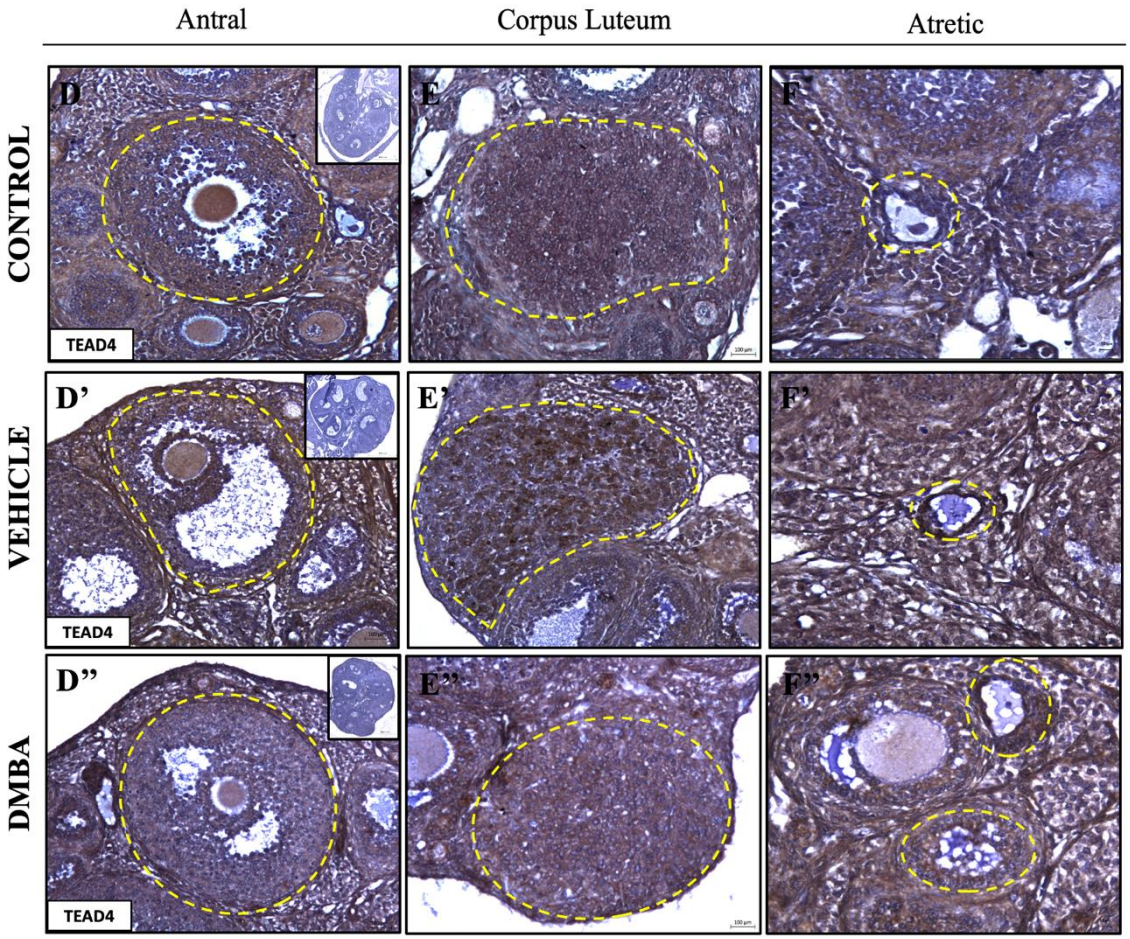

Figure 33. TEAD4 protein localization to antral, atretic follicles and corpus luteum in control, vehicle and DMBA groups demonstrated by immunohistochemistry staining. The yellow circles represent antral follicles in control (D), vehicle (D') and DMBA (D") groups, corpus luteum in control (E), vehicle (E") and DMBA (E") groups and atretic follicles in control (F), vehicle (F') and DMBA (F'') groups. The brown stained areas indicate TEAD4 and blue stained areas indicate the nucleus. The nucleus staining was performed with Hematoxylin. In the additional images shown in the control, vehicle and DMBA group, there is no staining pattern in the negative control (Inserts) (Scale bar: 100 µm and 50 µm).

We analyzed TEAD4 intensity in granulosa cells, oocytes and total ovary for control, vehicle and DMBA groups. In DMBA group, TEAD4 intensity was higher in

granulosa cells compared to vehicle and control group, the difference was statistically significant ($p<0.01$) (Figure 34A). TEAD4 intensity in oocytes was increased in DMBA group compared to control and vehicle groups, but not significantly (Figure 34B). TEAD4 intensity in total ovary was significantly increased in DMBA group compared to control and vehicle groups ($p < 0.01$). There is no significant difference in TEAD4 intensity between control and vehicle groups (Figure 34C).

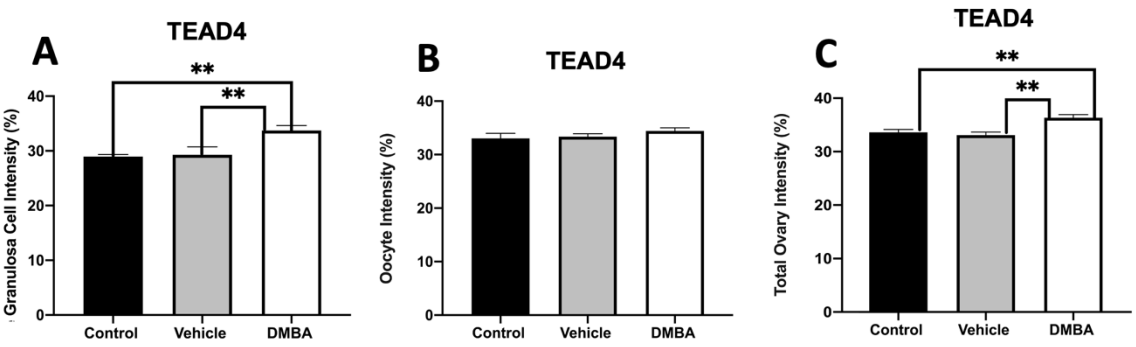

Figure 34. Results of the TEAD4 intensity in granulosa cells, oocytes and total ovary for control, vehicle and DMBA groups. One-way ANOVA and Tukey's multiple comparison test were applied. **A.** Representative granulosa cell intensity (%). **B.** Representative oocyte intensity (%). **C.** Representative total ovary intensity (%) (**$p<0.01$).

4.5. Localization of Nitrotyrosine (NTY) by Immunohistochemistry

We performed immunohistochemistry staining on paraffin sections to detection of oxidative stress protein in mice control, vehicle and DMBA groups. Nitrotyrosine (NTY) was used to detect oxidative stress in primordial, primary, secondary, antral, atretic follicles and corpus luteum, while counterstaining was performed with Hematoxylin and images were evaluated using light microscopy.

NTY was strongly expressed cytoplasm of granulosa cells in primordial follicles from control, vehicle and DMBA groups. NTY expression was not observed in primordial follicle oocytes in all groups (Figure 35A, 35A', 35A''). NTY expression was strongly expressed from DMBA-treated group in primary follicle cytoplasm of granulosa cells and oocytes in primary follicle compared to vehicle and control groups (Figure 35B, 35B', 35B'').

NTY expression was highest in secondary and antral follicles in control, vehicle and DMBA groups. When NTY expression cytoplasm of granulosa cells and oocytes in secondary follicles was analyzed, expression was stronger in DMBA group to control and vehicle groups. Also, NTY was localized in oocytes of secondary follicles in all groups (Figure 35C, 35C', 35C''). We observed strong expression in cytoplasm of granulosa cells and oocytes of antral follicles in all groups, however we found the strongest expression in the DMBA group (Figure 36D, 36D', 36D'').

NTY localization was observed in luteal cells of the corpus luteum in control and vehicle groups (Figure 36E, 36E', 36E'). Also, NTY localization was observed in granulosa cells of atretic follicles in all groups (Figure 36F, 36F',35F'').

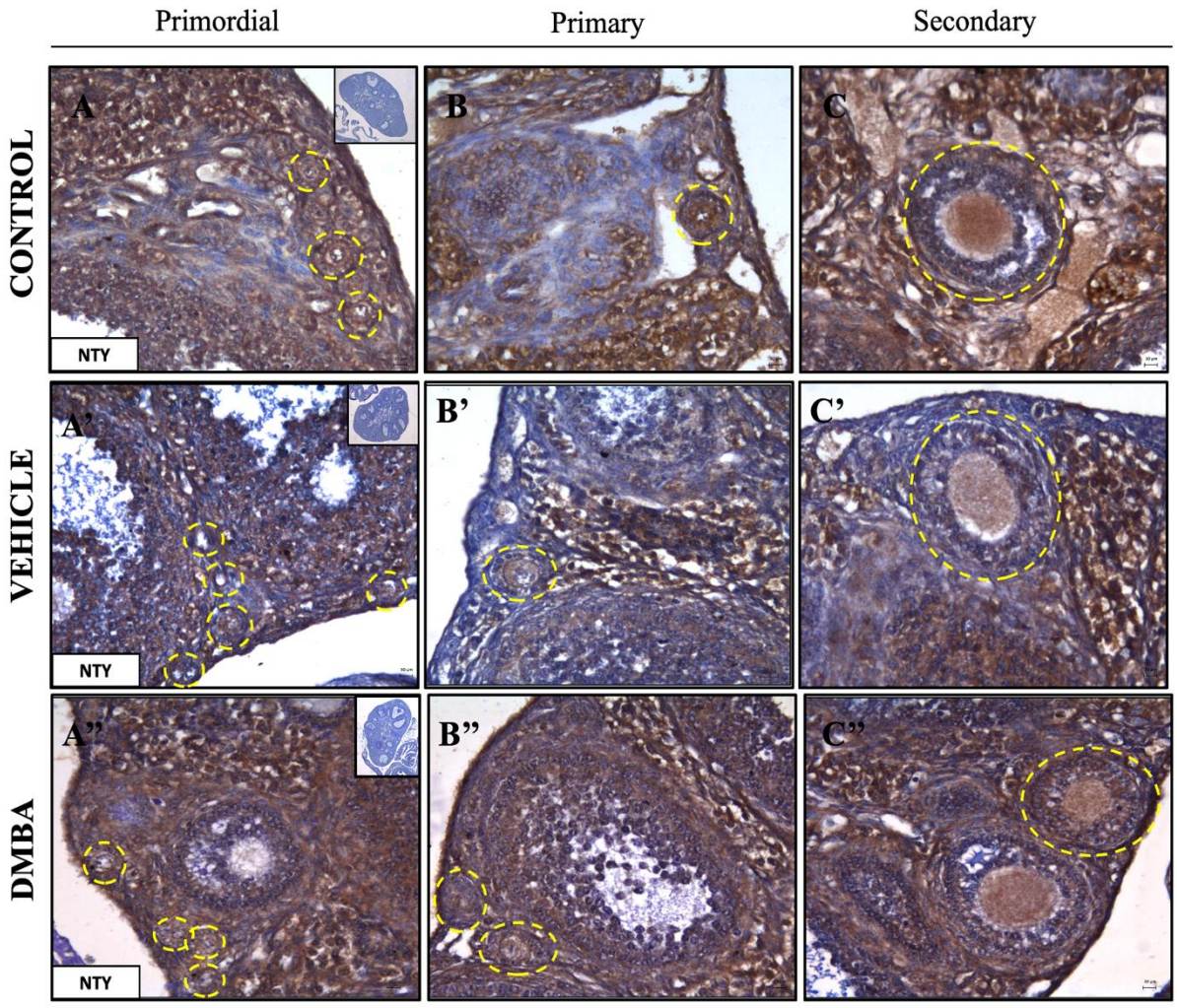

Figure 35. NTY protein localization to primordial, primary and secondary follicles in control, vehicle and DMBA groups demonstrated by immunohistochemistry staining. The yellow circles represent primordial follicles in control (A), vehicle (A') and DMBA (A'') groups, primary follicles in control (B), vehicle (B'') and DMBA (B'') groups, secondary

follicles in control (C), vehicle (C') and DMBA (C'') groups. The brown stained areas indicate NTY and blue stained areas indicate the nucleus. The nucleus staining was performed with Hematoxylin. In the additional images shown in the control, vehicle and DMBA group, there is no staining pattern in the negative control (Inserts) (Scale bar: 50 μm).

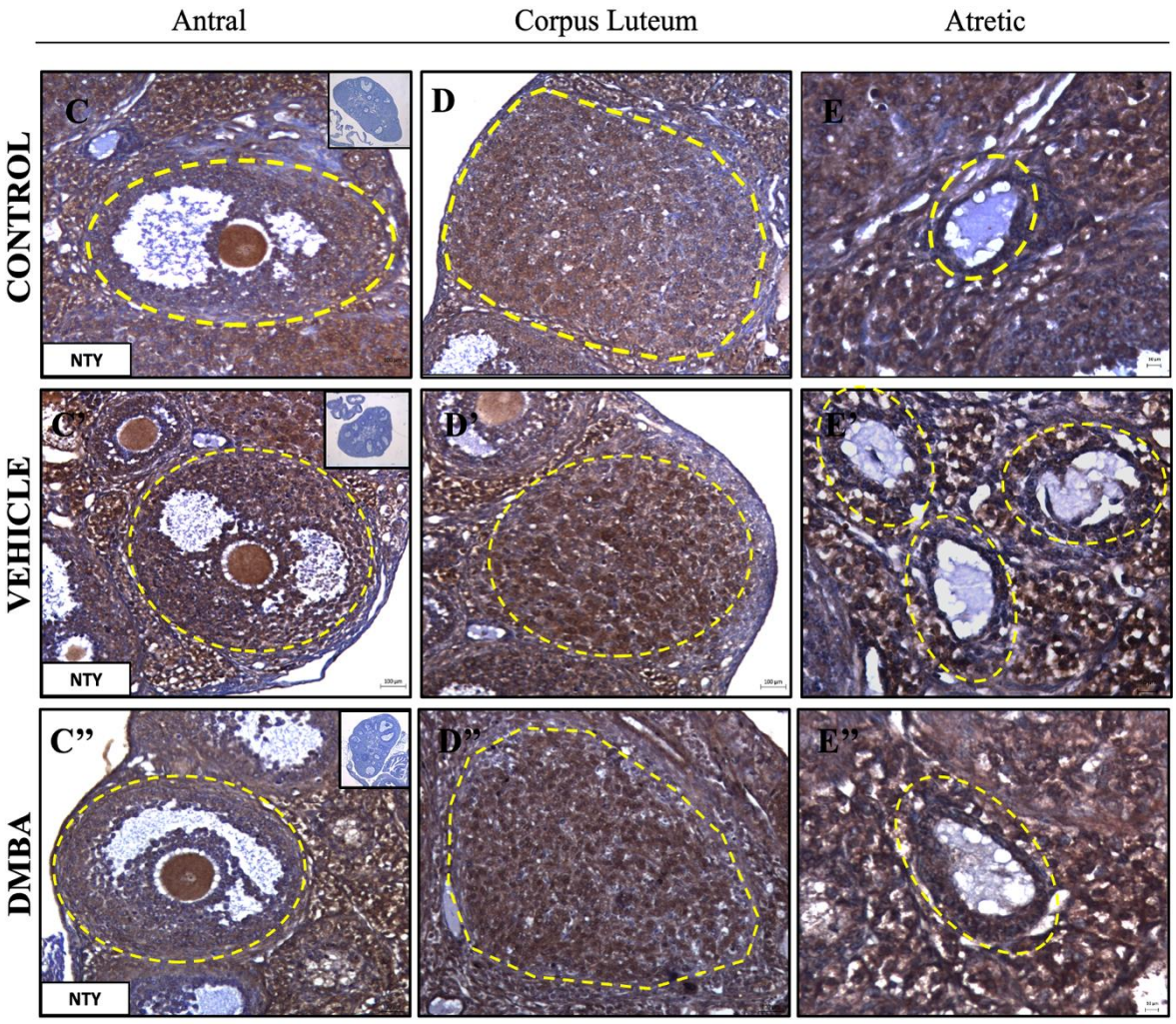

Figure 36. NTY protein localization to antral, atretic follicles and corpus luteum in control, vehicle and DMBA groups demonstrated by immunohistochemistry staining. The yellow circles represent antral follicles in control (D), vehicle (D') and DMBA (D") groups, corpus luteum in control (E), vehicle (E") and DMBA (E") groups and atretic follicles in control (F), vehicle (F') and DMBA (F'') groups. The brown stained areas indicate NTY and blue stained areas indicate the nucleus. The nucleus staining was performed with Hematoxylin. In the additional images shown in the control, vehicle and

DMBA group, there is no staining pattern in the negative control (Inserts) (Scale bar: 100 μm and 50 μm).

We analyzed NTY intensity in granulosa cells, oocytes and total ovary for control, vehicle and DMBA groups. In DMBA group, NTY intensity was increased in granulosa cells compared to vehicle and control group, the difference was statistically significant ($p<0.1$) (Figure 37A). NTY intensity in oocytes was increased in DMBA group compared to control and vehicle groups, the difference was statistically significant ($p<0.1$) (Figure 37B). NTY intensity in total ovary in oocytes was increased in DMBA group compared to control and vehicle groups, the difference was statistically significant ($p<0.1$) (Figure 37C).

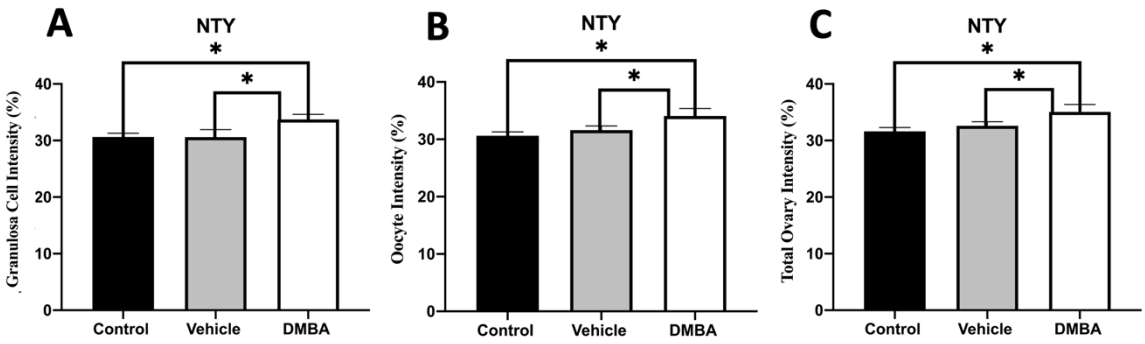

Figure 37. Results of the NTY intensity in granulosa cells, oocytes and total ovary for control, vehicle and DMBA groups. One-way ANOVA and Tukey's multiple comparison test were applied. **A.** Representative granulosa cell intensity (%). **B.** Representative oocyte intensity (%). **C.** Representative total ovary intensity (%). (*$p<0.1$).

4.5. qRT-PCR Results

The mRNAs obtained from ovaries were translated into cDNA and amplified by RT-PCR. Expression of Hippo signaling pathway genes was determined in ovaries from control, vehicle and DMBA-treated groups.

MST1, MST2, LATS1, LATS2, YAP1 and *TEAD4* expressions in ovarian tissues obtained from the experimental groups are shown. In general, when we evaluated the effect of DMBA treatment on *MST1, MST2, LATS1, LATS2, YAP1* and *TEAD4*

expressions in mouse ovary, no significant difference was detected at mRNA level between the experimental groups (Figure 38).

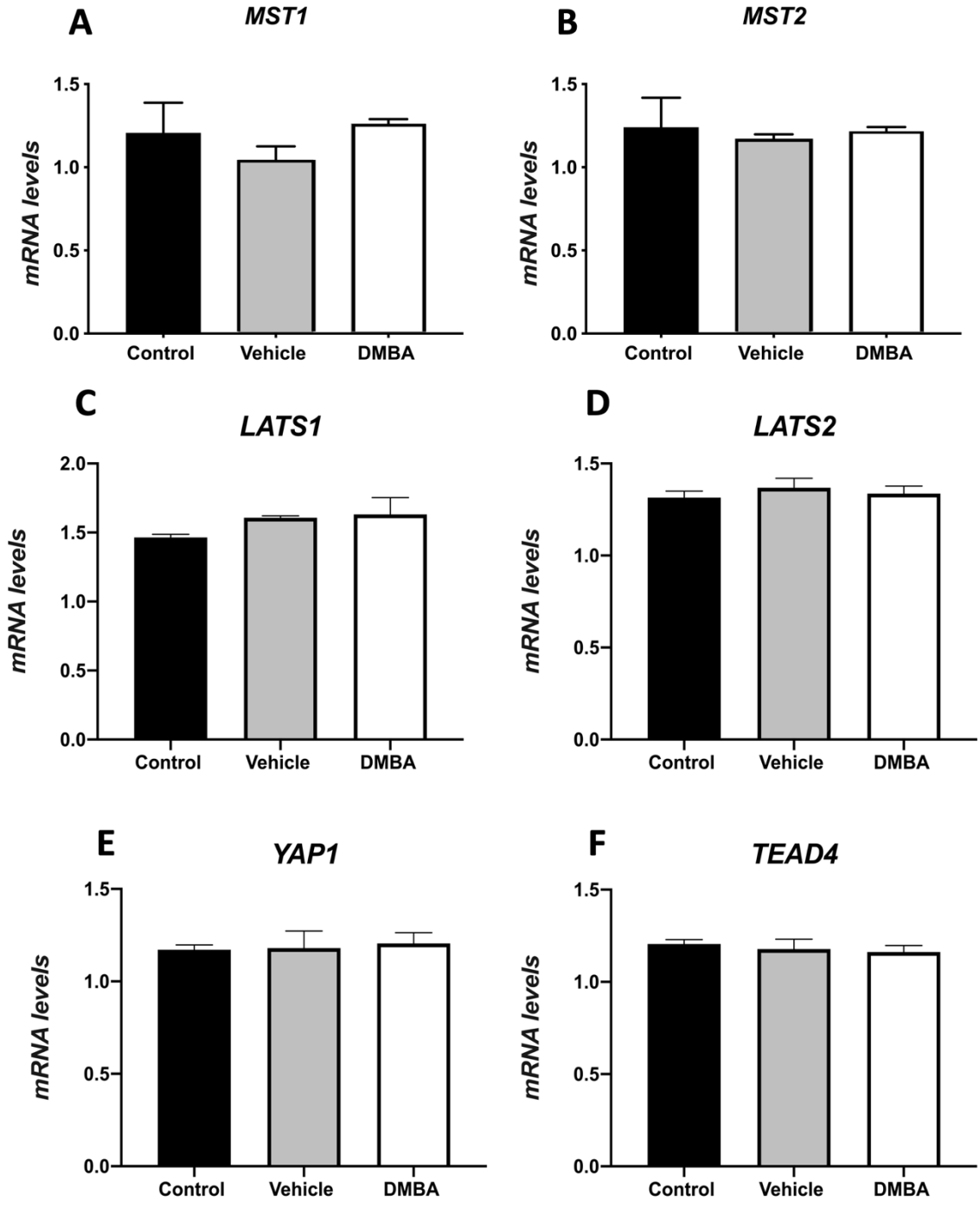

Figure 38. Results of the qRT-PCR experiment. A. *MST1*, B. *MST2*, C. *LATS1*, D. *LATS2*, E. *YAP1* and F. *TEAD4* mRNA expression levels.

5. DISCUSSION AND CONCLUSION

The contamination of the environment with organic pollutants has long lasting negative effects on the female reproductive system, especially by exposing the ovaries to toxic substances (148,149). Females are born with a limited reserve of nonrenewable primordial follicles and ovotoxic substances that rapidly deplete the ovarian reserve will reduce their reproductive lifespan (150). Experiments in rodents have shown the effects of toxic substances on follicles at all stages of development in the ovary (151,152).

7,12-DMBA, a polycyclic aromatic hydrocarbon, is an environmental carcinogen that acts on numerous tissues, including ovarian tissue, through the combustion of organic substances (148,153). DMBA is a carcinogenic and ovotoxic agent that disrupts follicle development and causes follicle depletion (149,154). Exposure to DMBA affects the reproductive system adversely and increases the risk of early menopause and infertility in women (155).

The Hippo signaling pathway, as an evolutionarily conserved pathway contributes to the understanding of many molecular mechanisms, including cell proliferation, differentiation, apoptosis, organ size regulation and tumorigenesis (11–15). Dysregulation of the Hippo signaling pathway contributes to impaired follicular development due to reproductive disorders such as loss of follicular homeostasis and depletion of follicular reserve. Furthermore, activation of YAP1, a major effector of the Hippo signaling pathway, plays an crucial role in cellular processes such as follicular development, follicle activation and ovarian steroidogenesis (17).

We evaluated the histomorphological evaluation of control, vehicle and DMBA ovary groups by Periodic Acid-Schiff (PAS) staining. Sobinoff et al. showed that follicular atresia was caused by DMBA in their study (156). In our study, we observed that the number of atretic follicles was increased in the DMBA-induced treatment group compared to the control and vehicle groups in histological sections. Based on these results, our study and Sobinoff et al. showed parallel results.

The presence of DMBA causes follicles to decrease at various stages of development (157). Studies have shown that DMBA induces primordial follicle activation and atresia of developing follicles and consequently causes rapid depletion of follicles (157,158). In the study by Sobinoff et al., neonatal mice were exposed to 1mg/kg intraperitoneal DMBA for 1 week, there was a significant loss of primordial follicles and an increase in the number of secondary follicles in DMBA-treated ovaries compared to

control groups (158). In line with the literature, in our study, we administered 1mg/kg intraperitoneal DMBA to the experimental group mice for 2 weeks to create a DMBA-treatment model in the ovaries. We also found a significant decrease in primordial follicles and increase in secondary follicles in DMBA-treated ovaries. This outcome subsequently established a viable model for examining the loss of follicles prior to ovulation. Beside this, we also demonstrated that DMBA-treated group showed increased number of atretic follicle and decreased number of corpus luteum.

Oxidative stress and DNA damage are intricately linked in scientific research. Oxidative stress refers to an imbalance in cellular redox homeostasis, leading to excessive production of reactive oxygen species (ROS) (159). DNA damage in ovarian tissues is caused either directly or indirectly by DMBA. Although the DNA damage caused by DMBA has been extensively studied in numerous cell types (160,161). The ovarian response to oxidative stress is also critical for follicular development. *In vitro* studies have demonstrated that ROS increase before DMBA-induced follicle loss, suggesting oxidative stress may be induced by DMBA exposure (0.1-100mM) (162). Ganesan et al. observed that γH2AX protein localization within the nucleus and granulosa cells of primary and secondary follicles increased significantly following both DMBA exposures (163). However, there was minimal staining observed in the oocyte nucleus of ovaries treated as controls. Based on the provided data, it can be inferred that DNA damage is taking place in DMBA-exposed ovaries. In our study, we performed immunohistochemistry analysis to show the localization of NTY protein, which is a marker of oxidative stress. In total ovary, oocyte and granulosa cells, NTY intensity was significantly higher in the DMBA-treated group than in the control and vehicle groups. When our results are evaluated together, exposure to DMBA increases NTY-induced oxidative stress in the ovary. According to Ganesan et al. there is an indirect relationship between our results and their study. In our study, for the first time in the literature, the expression pattern of oxidative stress caused by DMBA in the ovary, oocyte, and granulosa cells of the follicles was demonstrated immunohistochemically, and the degree of expression was demonstrated by immunohistochemical intensity measurement. Our findings suggest that DMBA induces ROS production in the ovary and that oxidative stress contributes to DMBA-induced follicle degeneration. We demonstrated that NTY signals were more stronger in the developing follicles from DMBA-treated group compared to control and vehicle groups.

We performed immunohistochemistry staining to determine the localization of Hippo signaling pathway components in the ovaries of control, vehicle and DMBA groups. MST1/2, which are components of the Hippo signaling pathway, play a crucial role in regulating cell proliferation in various processes within the tissues (164). We demonstrated for the first time the immunohistochemical localization of MST1/2 induced by DMBA in the ovary. Based on the obtained intensity results, we detected that MST1/2 expression in the cytoplasm of granulosa cells of primordial, primary, secondary, and antral follicles was higher in the DMBA-treated group compared to the control and vehicle groups, and this elevation was statistically significant. In contrast, the expression of MST1/2 in the oocytes of primordial, primary, secondary, and antral follicles was found to be low in the control, vehicle, and DMBA groups, and the difference in this low expression was not statistically significant. However, the overall expression of MST1/2 in the entire ovary was significantly higher in the DMBA group compared to the control and vehicle groups. When considering these results collectively, it can be concluded that MST1/2 expression in the follicular granulosa cells, excluding oocytes, and consequently in the total ovary, is elevated in the DMBA group.

Clark et al. demonstrated the expression levels of genes in the Hippo pathway in a mouse model induced by Perfluorooctanoic acid (PFOA). According to their findings, the mRNA expression levels of MST1 and MST2 showed no significant difference in the experimental group receiving ovotoxic 50 µl doses compared to the control group (165). In our study, we assessed the mRNA expression levels of MST1 and MST2 in the DMBA-induced mouse model using q-PCR analysis. Consistent with these results, we also did not observe a significant increase in the expression levels of MST1 and MST2 in the total ovary following administration of the ovotoxic dose of 1 mg/kg DMBA for 2 weeks treatment.

LATS1/2 are members of the Hippo signaling pathway, which plays a crucial role in regulating tissue growth, organ size, and tumorigenesis (166). Like MST1/2, the localization of LATS1/2 has not been demonstrated in ovarian tissues. In our study, we reported that LATS1/2 expression was weakly expressed at all stages of follicular development in control, vehicle and DMBA groups. Tsoi et al. showed cytoplasmic localization of Lats1 and Last2 in granulosa cells from primordial, primary and secondary follicles in ovarian tissue (167). In our study, we reported that LATS1/2 was weakly expressed at all stages of follicular development in control, vehicle and DMBA groups.

Besides, we found that the gene expression levels of Lats1 and Last2 were not different significantly between the groups. These results are in line with Tsoi et al.

YAP/TAZ-TEAD represents a new type of transcriptional regulator that controls the expression of genes responsible for producing steroidogenic enzymes in granulosa cells of rats (168). YAP/TAZ act as transcriptional co-factors in the nucleus, working alongside TEAD 1-4, to regulate the expression of target genes (169). Mizutani et al. showed that increased mRNA expression of YAP/TAZ and decreased mRNA expression of TEAD in granulosa cells (168). The expression and activation of YAP is crucial for the proper progression of ovarian follicular development and allows granulosa cells to reach the late stage and undergo final differentiation in response to LH surge (170). FSH acts rapidly and transiently on granulosa cells to promote proliferation via cyclin D2, followed by the translocation of YAP/TAZ into the cytoplasm, which in turn induces follicular differentiation, including steroid hormone production (170). Verteporfin functions as a small molecule inhibitor of the YAP-TEAD interaction, directly preventing the binding of YAP1 and TEAD (171). Sun et al. showed that verteporfin on oocyte-induced cell proliferation, 200 nM highly ovotoxic dose caused a decrease in cell number compared to untreated cells. 200 nM Verteporfin completely blocked the ability of oocytes to stimulate cell proliferation. In line with the activation of YAP1 induced by oocytes, YAP1 was found in both the nucleus and cytoplasm of granulosa cells when cultured alone. However, in the co-culture group, YAP1 predominantly localized to the nucleus (172). In our study, weak YAP expression was observed in the granulosa cell cytoplasm of primordial and primary follicles, YAP expression was increased in both granulosa cell cytoplasm and granulosa cell nucles of secondary and antral follicles at late stages of development. When we measured positive granulosa cell intensity, it was significantly higher in the DMBA group compared to the control and vehicle groups. In addition, YAP1 expression in total ovarium was significantly higher in DMBA group compared to control and vehicle groups. When the results were evaluated together, YAP1 expression was expressed in the granulosa cell cytoplasm and nucleus of secondary and antral follicles and oocytes at late stages of development. Sun et al. showed that parallel results with our results and we reported that verteporfin, like DMBA, significantly increased YAP1 expression in the experimental group compared to control and vehicle groups and decreased cell proliferation. These findings are one of the results of histomorphological that granulosa cell proliferation and cell integrity were impaired in DMBA group.

YAP1 localizes to the nucleus in the outer cells, which coactivates TEAD4 and the transcription of trophectoderm-specific genes, whereas YAP1 localizes to the cytoplasm in the inner cells (18). TEAD4, a transcription factor of the Hippo signaling pathway, has been shown to play a role in ovarian cancer in studies, but there are no studies in the mouse ovary. Xia et. al found that TEAD4 gives immunolabeling in human ovarian cancer tissues an immune positive reaction in correlation with YAP (173). In our study, we showed that TEAD4 expression was observed in granulosa cell cytoplasm of primordial and primary follicles however TEAD4 expression was observed in granulosa cell cytoplasm and nucleus of secondary and antral follicles. This result suggests that YAP1 and TEAD4 colocalized as a result of translocalization of YAP1 to the nucleus in the late stages of follicular development and may be the reason for the localization of TEAD4 in granulosa cell cytoplasm and nucleus.

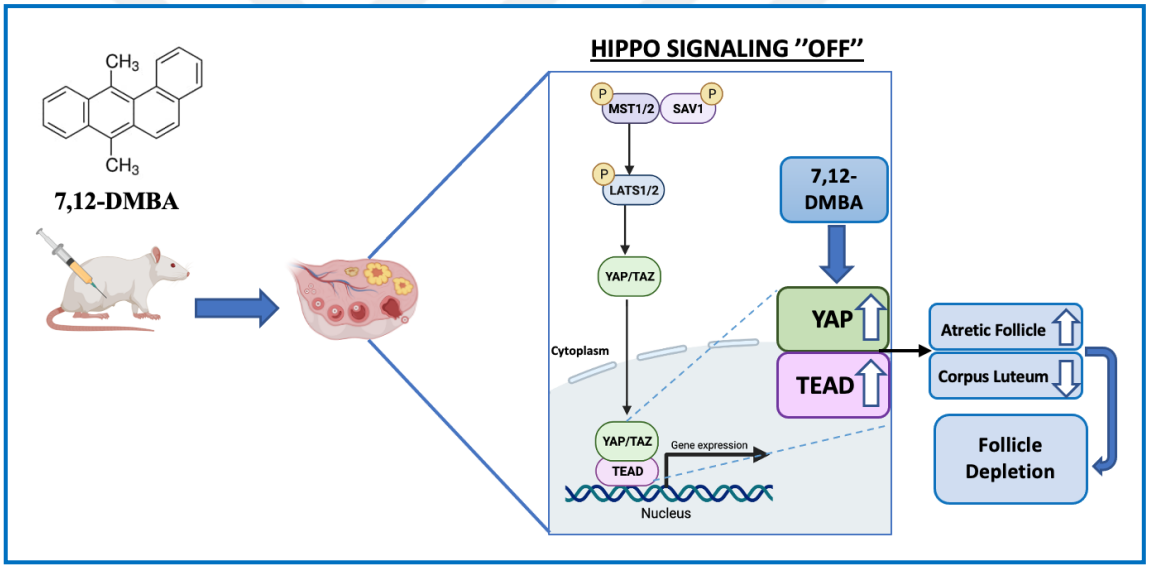

Figure 39. The association of DMBA-induced mouse ovotoxicity model with the Hippo signaling pathway has been demonstrated. In conclusion, we demonstrated that DMBA-induced increase in YAP1 and TEAD4 expression may play a role in the mechanisms underlying the rapid depletion of follicles through the Hippo signaling pathway by causing an increase in the number of atretic follicles and a decrease in the number of corpus luteum.

In this thesis, we provide the first evidence of the relationship between follicular development and the Hippo signaling pathway in DMBA-treated mouse ovaries. YAP1

and TEAD4 expressions are increased due to translocation of YAP1, a transcriptional regulator of the Hippo signaling pathway, and we evaluated the mechanisms underlying the rapid depletion of follicles in the 2-week DMBA treatment group.

As a result, we demonstrated that oxidative stress increased in granulosa cells and oocytes of follicles, granulosa cell integrity was impaired in secondary and antral follicles, primordial and primary follicle number decreased, follicular development was not completed successfully and follicular atresia increased accordingly, and ovulation was not achieved with a decrease in corpus luteum number (Figure 39).

The signaling pathway mechanisms involved in the effects of DMBA on follicular development have not yet been fully elucidated. In this study, we demonstrated that the expression of Hippo signaling pathway proteins may play a role in DMBA treatment-induced ovotoxicity in mouse ovary. Furthermore, this study revealed for the first time the relationship between DMBA-induced follicular development and Hippo signaling pathway in mouse ovaries. This study may contribute to further investigation of problems related to DMBA-induced ovotoxicity and the development of new strategies.

6. REFERENCES

1) Gartner LP. Color Atlas and Text of Histology. *Seventh ed. Philadelphia: Wolters Kluwer*; 2018.

2) Hirshfield AN. Development of follicles in the mammalian ovary. *Int Rev Cytol.* 991;124:43-101.

3) Borman SM, Christian PJ, Sipes IG, Hoyer PB. Ovotoxicity in Female Fischer Rats and B6 Mice Induced by Low-Dose Exposure to Three Polycyclic Aromatic Hydrocarbons: Comparison through Calculation of an Ovotoxic Index. *Toxicol Appl Pharmacol*. 2000;167(3):191-198.

4) Igawa Y, Keating AF, Rajapaksa KS, Sipes IG, Hoyer PB. Evaluation of ovotoxicity induced by 7, 12-dimethylbenz[a]anthracene and its 3,4-diol metabolite utilizing a rat in vitro ovarian culture system. *Toxicol Appl Pharmacol*. 2009;234(3):361-369.

5) Hoyer PB, Davis JR, Bedrnicek JB, et al. Ovarian neoplasm development by 7,12-dimethylbenz[a]anthracene (DMBA) in a chemically-induced rat model of ovarian failure. *Gynecol Oncol*. 2009;112(3):610-615.

6) Shimada T. Xenobiotic-metabolizing enzymes involved in activation and detoxification of carcinogenic polycyclic aromatic hydrocarbons. *Drug Metab Pharmacokinet*. 2006;21(4):257-276.

7) Gelboin H V. Benzo[alpha]pyrene metabolism, activation and carcinogenesis: role and regulation of mixed-function oxidases and related enzymes. *Physiol Rev*. 1980;60(4):1107-1166.

8) Jick H, Porter J, Morrison AS. Relation between smoking and age of natural menopause. Report from the Boston Collaborative Drug Surveillance Program, Boston University Medical Center. *Lancet*. 1977;1(8026):1354-1355.

9) Miyata M, Kudo G, Lee YH, et al. Targeted Disruption of the Microsomal Epoxide Hydrolase Gene. *Journal of Biological Chemistry*. 1999;274(34):23963-23968.

10) Vericat JA, Cheng SC, Dipple A. Absolute stereochemistry of the major 7,12-dimethylbenz(a)anthracene-DNA adducts formed in mouse cells. *Carcinogenesis*. 1989;10(3):567-570.

11) Kawashima I, Kawamura K. Regulation of follicle growth through hormonal factors and mechanical cues mediated by Hippo signaling pathway. *Syst Biol Reprod Med*. 2018;64(1):3-11.

12) Dong J, Feldmann G, Huang J, et al. Elucidation of a universal size-control mechanism in Drosophila and mammals. *Cell*. 2007;130(6):1120-1133.

13) Halder G, Johnson RL. Hippo signaling: growth control and beyond. *Development*. 2011;138(1):9-22.

14) Fallahi E, O'Driscoll NA, Matallanas D. The MST/Hippo Pathway and Cell Death: A Non-Canonical Affair. *Genes (Basel).* 2016;7(6):28.

15) Plouffe SW, Hong AW, Guan KL. Disease implications of the Hippo/YAP pathway. *Trends Mol Med.* 2015;21(4):212-222.

16) Clark KL, George JW, Przygrodzka E, et al. Hippo Signaling in the Ovary: Emerging Roles in Development, Fertility, and Disease. *Endocr Rev.* 2022;43(6):1074-1096.

17) Hsueh AJW, Kawamura K. Hippo signaling disruption and ovarian follicle activation in infertile patients. *Fertil Steril.* 2020;114(3):458-464.

18) Nishioka N, Inoue K ichi, Adachi K, et al. The Hippo signaling pathway components Lats and Yap pattern Tead4 activity to distinguish mouse trophectoderm from inner cell mass. *Dev Cell*. 2009;16(3):398-410.

19) Gartner LP. *Textbook of Histology*. 5th ed.: Elsevier; 2020.

20) Ross MH, Pawlina W. *Histology : A Text and Atlas : With Correlated Cell and Molecular Biology*. Eighth ed. Philadelphia: Wolters Kluwer Health; 2020.

21) Eroschenko VP. *Difiores Atlas of Histology with Functional Correlations*. Thirteenth ed. Philadelphia: Wolters Kluwer; 2017.

22) Magro-Lopez E, Muñoz-Fernández MÁ. The role of bmp signaling in female reproductive system development and function. *Int J Mol Sci*. 2021;22(21).

23) Mescher AL. *Junqueira's Basic Histology : Text and Atlas 15e*. 15th ed., McGraw-Hill Education LLC; 2018.

24) Skinner MK. *Encyclopedia of Reproduction.* Second Edition. Elsevier, 2018.

25) Moore K, Persaud T, Torchia M. The Developing Human-e-Book: Clinically Oriented Embryology.; 2018.

26) Sadler TW. *Langman's Medical Embryology*. Fifteenth ed. Philadelphia: Wolters Kluwer; 2024.

27) Satoh M. Histogenesis and organogenesis of the gonad in human embryos. *Journal of anatomy*. 1991:85-107.

28) Childs AJ, Cowan G, Kinnell HL, Anderson RA, Saunders PTK. Retinoic acid signalling and the control of meiotic entry in the human fetal gonad. *PLoS One*. 2011;6(6).

29) Zhu M, Xu M, Zhang J, Zheng C. The role of Hippo pathway in ovarian development. *Front Physiol*. 2023;14:1198873.

30) Kezele P, Nilsson E, Skinner MK. Cell-cell interactions in primordial follicle assembly and development. *Front Biosci*. 2002;7.

31) Wear HM, McPike MJ, Watanabe KH. From primordial germ cells to primordial follicles: a review and visual representation of early ovarian development in mice. *J Ovarian Res*. 2016;9(1):36.

32) Dahari N, Heinemann L, Alyagor L, Dekel N. Ovarian folliculogenesis. *Results Probl Cell Differ*. 2016;58:167-190.

33) Eppig JJ. Oocyte control of ovarian follicular development and function in mammals. *Reproduction*. 2001;122(6):829-838.

34) Bristol-Gould SK, Kreeger PK, Selkirk CG, et al. Postnatal regulation of germ cells by activin: The establishment of the initial follicle pool. *Dev Biol*. 2006;298(1):132-148.

35) Begley DJ, Firth JA, Hoult JRS. *Human Reproduction and Developmental Biology*. Macmillan Education UK; 1980.

36) Sonigo C, Jankowski S, Yoo O, et al. High-throughput ovarian follicle counting by an innovative deep learning approach. *Sci Rep*. 2018;8(1):13499.

37) Mikhael S, Punjala-Patel A, Gavrilova-Jordan L. Hypothalamic-Pituitary-Ovarian Axis Disorders Impacting Female Fertility. *Biomedicines*. 2019.

38) Kierszenbaum A, Tres L. Histology and Cell Biology: An Introduction to Phatology. Elsevier, ed..; 2020.

39) Tortora Gerard. Principles of Anatomy and Physiology, 3rd Asia-Pacific Edition. John Wiley & Sons, 2021.

40) Liu YX, Zhang Y, Li YY, et al. Regulation of follicular development and differentiation by intra-ovarian factors and endocrine hormones. *Frontiers in Bioscience - Landmark*. 2019;24(5):983-993.

41) Robert C, Gilbert I. Cell-to-Cell Communication in the Ovarian Follicle. *Encyclopedia of Reproduction*. 2018.

42) Araújo VR, Gastal MO, Figueiredo JR, Gastal EL. In vitro culture of bovine preantral follicles: a review. *Reproductive Biology and Endocrinology 2014 12:1*. 2014;12(1):1-14.

43) Borum K. Oogenesis in the mouse: A study of the meiotic prophase. *Exp Cell Res*. 1961;24(3):495-507.

44) Chen YY, Russo DD, Drake RS, et al. Single-cell transcriptomics of staged oocytes and somatic cells reveal novel regulators of follicle activation. *Reproduction*. 2022;164(2):55-70.

45) Senbon S, Hirao Y, Miyano T. Interactions between the oocyte and surrounding somatic cells in follicular development: lessons from in vitro culture. *J Reprod Dev*. 2003;49(4):259-269.

46) Kedem A, Fisch B, Garor R, et al. Growth Differentiating Factor 9 (GDF9) and Bone Morphogenetic Protein 15 both Activate Development of Human Primordial Follicles in vitro, with Seemingly More Beneficial Effects of GDF9. *J Clin Endocrinol Metab*. 2011;96(8):E1246-E1254.

47) Hutt KJ, McLaughlin EA, Holland MK. Kit ligand and c-Kit have diverse roles during mammalian oogenesis and folliculogenesis. *Mol Hum Reprod*. 2006;12(2):61-69.

48) Simon AM, Goodenough DA, Li E, Paul DL. Female infertility in mice lacking connexin 37. *Nature*. 1997;385(6616):525-529.

49) Winterhager E, Kidder GM. Gap junction connexins in female reproductive organs: implications for women's reproductive health. *Hum Reprod Update*. 2015;21(3):340-352.

50) Townson DH, Combelles CMH. Ovarian Follicular Atresia. 2023.

51) Jo YS, Ko HS, Kim AY, Jo HG, Kim WJ, Choi SK. Effects of polycyclic aromatic hydrocarbons on the proliferation and differentiation of placental cells. *Reproductive Biology and Endocrinology*. 2022;20(1):1-7.

52) Diamanti-Kandarakis E, Bourguignon JP, Giudice LC, et al. Endocrine-Disrupting Chemicals: An Endocrine Society Scientific Statement. *Endocr Rev*. 2009;30(4):293.

53) Kummer V, Mašková J, Zralý Z, Faldyna M. Ovarian disorders in immature rats after postnatal exposure to environmental polycyclic aromatic hydrocarbons. *J Appl Toxicol*. 2013;33(2):90-99.

54) Kabir ER, Rahman MS, Rahman I. A review on endocrine disruptors and their possible impacts on human health. *Environ Toxicol Pharmacol*. 2015;40(1):241-258.

55) Zhang H, Yang L, Zhang X, et al. Characteristics and Health Risks of Polycyclic Aromatic Hydrocarbons and Nitro-PAHs in Xinxiang, China in 2015 and 2017. *Int J Environ Res Public Health*. 2021;18(6):1-14.

56) Mesquita SR, van Drooge B, Barata C, Vieira N, Guimarães L, Piña B. Toxicity of atmospheric particle-bound PAHs: an environmental perspective. *Environmental Science and Pollution Research*. 2014;21(20):11623-11633.

57) Li J, Zhang G, Li XD, Qi SH, Liu GQ, Peng XZ. Source seasonality of polycyclic aromatic hydrocarbons (PAHs) in a subtropical city, Guangzhou, South China. *Sci Total Environ*. 2006;355(1-3):145-155.

58) Bolden AL, Rochester JR, Schultz K, Kwiatkowski CF. Polycyclic aromatic hydrocarbons and female reproductive health: A scoping review. *Reprod Toxicol*. 2017;73:61-74.

59) EPA, US Environmental Protection Agency (EPA), (1999). Compendium Method TO-13A, Cincinnati, OH, USA. 2023.

60) Ferrarese E, Andreottola G, Oprea IA. Remediation of PAH-contaminated sediments by chemical oxidation. *J Hazard Mater*. 2008;152(1):128-139.

61) Wenzl T, Simon R, Kleiner J, Anklam E. Analytical methods for polycyclic aromatic hydrocarbons (PAHs) in food and the environment needed for new food legislation in the European Union, *TrAC Trends in Analytical Chemistry*, 2006.

62) Kummer V, Mašková J, Zralý Z, et al. Estrogenic activity of environmental polycyclic aromatic hydrocarbons in uterus of immature Wistar rats. *Toxicol Lett*. 2008;180(3):212-221.

63) Ledet MM, Oswald M, Anderson R, et al. Differential signaling pathway activation in 7,12-dimethylbenz[a] anthracene (DMBA)-treated mammary stem/progenitor cells from species with varying mammary cancer incidence. *Oncotarget*. 2018;9(67):32761-32774.

64) Lim V, Korourian S, Todorova VK, Kaufmann Y, Klimberg VS. Glutamine prevents DMBA-induced squamous cell cancer. *Oral Oncol*. 2009;45(2):148-155.

65) Kavas G. Ö. Reaktif Oksijen Metabolitlerine Fizyopatolojik Yaklaşim. *Ankara Üniversitesi Tıp Fakültesi Mecmuası*. 1994; 47(4).

66) Igawa Y, Keating AF, Rajapaksa KS, Sipes IG, Hoyer PB. Evaluation of ovotoxicity induced by 7, 12-dimethylbenz[a]anthracene and its 3,4-diol metabolite utilizing a rat in vitro ovarian culture system. *Toxicol Appl Pharmacol*. 2009;234(3):361.

67) Hoyer PB, Sipes IG. Assessment of follicle destruction in chemical-induced ovarian toxicity. *Annu Rev Pharmacol Toxicol*. 1996;36:307-331.

68) Mlynarcikova A, Fickova M, Scsukova S. Ovarian intrafollicular processes as a target for cigarette smoke components and selected environmental reproductive disruptors. *Endocr Regul*. 2005;39(1):21-32.

69) Rajapaksa KS. Ovarian Metabolism of Xenobiotics. *Comprehensive Toxicology, Second Edition*. 2010;11:457-467.

70) Kanter EM, Walker RM, Marion SL, Brewer M, Hoyer PB, Barton JK. Dual modality imaging of a novel rat model of ovarian carcinogenesis. *J Biomed Opt*. 2006;11(4):041123.

71) Diagaradjane P, Yaseen MA, Yu J, Wong MS, Anvari B. Synchronous fluorescence spectroscopic characterization of DMBA-TPA-induced squamous cell carcinoma in mice. *J Biomed Opt*. 2006;11(1):014012.

72) Russo J, Russo IH. Experimentally induced mammary tumors in rats. *Breast Cancer Res Treat*. 1996;39(1):7-20.

73) Mattison DR. Difference in sensitivity of rat and mouse primordial oocytes to destruction by polycyclic aromatic hydrocarbons. *Chem Biol Interact*. 1979;28(1):133-137.

74) Harlow BL, Signorello LB. Factors associated with early menopause. *Maturitas*. 2000;35(1):3-9.

75) Jurisicova A, Taniuchi A, Li H, et al. Maternal exposure to polycyclic aromatic hydrocarbons diminishes murine ovarian reserve via induction of Harakiri. *J Clin Invest*. 2007;117(12):3971-3978.

76) Rajapaksa KS, Cannady EA, Sipes IG, Hoyer PB. Involvement of CYP 2E1 Enzyme in Ovotoxicity Caused by 4-Vinylcyclohexene and its Metabolites. *Toxicol Appl Pharmacol*. 2007;221(2):215.

77) Igawa Y, Keating AF, Rajapaksa KS, Sipes IG, Hoyer PB. Evaluation of ovotoxicity induced by 7, 12-dimethylbenz[a]anthracene and its 3,4-diol metabolite utilizing a rat in vitro ovarian culture system. *Toxicol Appl Pharmacol*. 2009;234(3):361.

78) Krarup T. Oocyte destruction and ovarian tumorigenesis after direct application of a chemical carcinogen (9:10-dimethyl-1:2-benzanthrene) to the mouse ovary. *Int J Cancer*. 1969;4(1):61-75.

79) Tsai-Turton M, Nakamura BN, Luderer U. Induction of apoptosis by 9,10-dimethyl-1,2-benzanthracene in cultured preovulatory rat follicles is preceded by a rise in reactive oxygen species and is prevented by glutathione. *Biol Reprod*. 2007;77(3):442-451.

80) Matikainen T, Perez GI, Jurisicova A, et al. Aromatic hydrocarbon receptor-driven Bax gene expression is required for premature ovarian failure caused by biohazardous environmental chemicals. *Nature Genetics 2001 28:4*. 2001;28(4):355-360.

81) Rajapaksa KS, Sipes IG, Hoyer PB. Involvement of Microsomal Epoxide Hydrolase Enzyme in Ovotoxicity Caused by 7,12-Dimethylbenz[a]anthracene. *Toxicological Sciences*. 2007;96(2):327-334.

82) Bengtsson M, Montelius J, Mankowitz L, Rydström J. Metabolism of polycyclic aromatic hydrocarbons in the rat ovary comparison with metabolism in adrenal and liver tissues. *Biochem Pharmacol*. 1983;32(1):129-136.

83) Mattison Donald R., Thorgeirsson Snorri S. Ovarian Aryl Hydrocarbon Hydroxylase Activity and Primordial Oocyte Toxicity of Polycyclic Aromatic Hydrocarbons in Mice. *American Association for Cancer Research*, 2023.

84) Manorahan K and Rao A.Ramesha. Influence of exogenous estrogen on oocytic depletion induced by 7,12-Dimethylbenz[a]anthracene in mice. Cancer Letters, 1980. 10(4), 359–363.

85) Borman SM, Christian PJ, Sipes IG, Hoyer PB. Ovotoxicity in Female Fischer Rats and B6 Mice Induced by Low-Dose Exposure to Three Polycyclic Aromatic Hydrocarbons: Comparison through Calculation of an Ovotoxic Index. *Toxicol Appl Pharmacol*. 2000;167(3):191-198.

86) Ganesan S, Bhattacharya P, Keating AF. 7,12-Dimethylbenz[a]anthracene exposure induces the DNA repair response in neonatal rat ovaries. *Toxicol Appl Pharmacol*. 2013;272(3):690-696.

87) Mattison DR, Nightingale MR. The biochemical and genetic characteristics of murine ovarian aryl hydrocarbon (Benzo[a]pyrene) hydroxylase activity and its relationship to primordial oocyte destruction by polycyclic aromatic hydrocarbons. *Toxicol Appl Pharmacol*. 1980;56(3):399-408.

88) Muqbil I, Azmi AS, Banu N. Prior exposure to restraint stress enhances 7,12-dimethylbenz(a)anthracene (DMBA) induced DNA damage in rats. *FEBS Lett*. 2006;580(16):3995-3999.

89) Udan RS, Kango-Singh M, Nolo R, Tao C, Halder G. Hippo promotes proliferation arrest and apoptosis in the Salvador/Warts pathway. *Nature Cell Biology*, *2003*.:914-920.

90) Meng Z, Moroishi T, Mottier-Pavie V, et al. MAP4K family kinases act in parallel to MST1/2 to activate LATS1/2 in the Hippo pathway. *Nat Commun*. 2015;6.

91) Yildirim E, Bora G, Onel T, Talas N, Yaba A. Cell fate determination and Hippo signaling pathway in preimplantation mouse embryo. *Cell Tissue Res*. 2021;386(3):423-444.

92) Misra JR, Irvine KD. The Hippo signaling network and its biological functions. *Annu Rev Genet*. 2018;52:65.

93) Wu Z, Guan KL. Hippo signaling in embryogenesis and development. *Trends Biochem Sci*. 2021;46(1):51.

94) Fu M, Hu Y, Lan T, Guan KL, Luo T, Luo M. The Hippo signalling pathway and its implications in human health and diseases. *Signal Transduct Target Ther*. 2022;7(1).

95) Dey A, Varelas X, Guan KL. Targeting the Hippo pathway in cancer, fibrosis, wound healing and regenerative medicine. *Nat Rev Drug Discov*. 2020;19(7):480-494.

96) Ma S, Meng Z, Chen R, Guan KL. The Hippo Pathway: Biology and Pathophysiology. *Annual Review of Biochemistry*, 2019. 88:1, 577-604.

97) Dey A, Varelas X, Guan KL. Targeting the Hippo pathway in cancer, fibrosis, wound healing and regenerative medicine. *Nat Rev Drug Discov*., 2020;19(7):480.

98) Yu FX, Guan KL. The Hippo pathway: regulators and regulations. *Genes Dev*. 2013;27(4):355.

99) Yu FX, Zhao B, Guan KL. Hippo Pathway in Organ Size Control, Tissue Homeostasis, and Cancer. *Cell*. 2015;163(4):811-828.

100) Zheng Y, Wang W, Liu B, Deng H, Uster E, Pan D. Identification of Happyhour/MAP4K as Alternative Hpo/Mst-like Kinases in the Hippo Kinase Cascade. *Dev Cell*. 2015;34(6):642-655.

101) Cunningham R, Hansen CG. The Hippo pathway in cancer: YAP/TAZ and TEAD as therapeutic targets in cancer. *Clin Sci (Lond)*. 2022;136(3):197.

102) Wu Z, Guan KL. Hippo signaling in embryogenesis and development. *Trends Biochem Sci*. 2021;46(1):51.

103) Fu M, Hu Y, Lan T, Guan KL, Luo T, Luo M. The Hippo signalling pathway and its implications in human health and diseases. *Signal Transduct Target Ther*. 2022;7(1).

104) Praskova M, Khoklatchev A, Ortiz-Vega S, Avruch J. Regulation of the MST1 kinase by autophosphorylation, by the growth inhibitory proteins, RASSF1 and NORE1, and by Ras. *Biochemical Journal*. 2004;381(2):453-462.

105) Deng Y, Pang A, Chemistry JWJ of B, 2003 undefined. Regulation of mammalian STE20-like kinase 2 (MST2) by protein phosphorylation/dephosphorylation and proteolysis. *ASBMB*, 2023.

106) Meng Z, Moroishi T, Guan KL. Mechanisms of Hippo pathway regulation. *Genes Dev*. 2016;30(1):1.

107) Glantschnig H, Rodan G, Chemistry ARJ of B, 2002 undefined. Mapping of MST1 kinase sites of phosphorylation: activation and autophosphorylation. *ASBMB*, 2023.

108) Chan EHY, Nousiainen M, Chalamalasetty RB, Schäfer A, Nigg EA, Sillje HHW. The Ste20-like kinase Mst2 activates the human large tumor suppressor kinase Lats1. *Oncogene*. 2005;24(12):2076-2086.

109) Hergovich A, Schmitz D, Hemmings BA. The human tumour suppressor LATS1 is activated by human MOB1 at the membrane. *Biochem Biophys Res Commun*. 2006;345(1):50-58.

110) Meng Z, Moroishi T, Guan KL. Mechanisms of Hippo pathway regulation. *Genes Dev*. 2016;30(1):1-17.

111) Zhao B, Ye X, Yu J, et al. TEAD mediates YAP-dependent gene induction and growth control. *Genes Dev*. 2008;22(14):1962-1971.

112) Strano S, Munarriz E, Rossi M, et al. Physical interaction with Yes-associated protein enhances p73 transcriptional activity. *J Biol Chem*. 2001;276(18):15164-15173.

113) Yagi R, Chen LF, Shigesada K, Murakami Y, Ito Y. A WW domain-containing Yes-associated protein (YAP) is a novel transcriptional co-activator. *EMBO Journal*. 1999;18(9):2551-2562.

114) Koontz LM, Liu-Chittenden Y, Yin F, et al. The Hippo effector Yorkie controls normal tissue growth by antagonizing scalloped-mediated default repression. *Dev Cell*. 2013;25(4):388-401.

115) Camargo FD, Gokhale S, Johnnidis JB, et al. YAP1 increases organ size and expands undifferentiated progenitor cells. *Curr Biol*. 2007;17(23):2054-2060.

116) Nishio M, Hamada K, Kawahara K, et al. Cancer susceptibility and embryonic lethality in Mob1a/1b double-mutant mice. *J Clin Invest*. 2012;122(12):4505-4518.

117) Dong J, Feldmann G, Huang J, Wu S, Cell NZ, 2007 undefined. Elucidation of a universal size-control mechanism in Drosophila and mammals. *Elsevier*, 2023.

118) Meng Z, Moroishi T, Guan KL. Mechanisms of Hippo pathway regulation. *Genes Dev*. 2016;30(1):1.

119) Azad T, Rezaei R, Surendran A, et al. Hippo Signaling Pathway as a Central Mediator of Receptors Tyrosine Kinases (RTKs) in Tumorigenesis. *Cancers (Basel)*. 2020;12(8):1-22.

120) Clark KL, George JW, Przygrodzka E, et al. Hippo Signaling in the Ovary: Emerging Roles in Development, Fertility, and Disease. *Endocr Rev*. 2022;43(6):1074-1096.

121) Wang C, Sun H, Davis JS, et al. FHL2 deficiency impairs follicular development and fertility by attenuating EGF/EGFR/YAP signaling in ovarian granulosa cells. *Cell Death Dis*. 2023;14(4):239.

122) Xia L, Shen Y, Liu S, Du J. Iron overload triggering ECM-mediated Hippo/YAP pathway in follicle development: a hypothetical model endowed with therapeutic implications. *Front Endocrinol (Lausanne)*. 2023;14:1174817.

123) Polesello C, Tapon N. Salvador-Warts-Hippo Signaling Promotes Drosophila Posterior Follicle Cell Maturation Downstream of Notch. *Current Biology*. 2007;17(21):1864-1870.

124) Huang J, Reilein A, Kalderon D. Yorkie and Hedgehog independently restrict BMP production in escort cells to permit germline differentiation in the Drosophila ovary. *Development*. 2017;144(14):2584-2594.

125) Xiang C, Li J, Hu L, et al. Hippo signaling pathway reveals a spatio-temporal correlation with the size of primordial follicle pool in mice. *Cell Physiol Biochem*. 2015;35(3):957-968.

126) Masciangelo R, Hossay C, Chiti MC, et al. Role of the PI3K and Hippo pathways in follicle activation after grafting of human ovarian tissue. *J Assist Reprod Genet*. 2020;37(1):101-108.

127) Dos Santos EC, Lalonde-Larue A, Antoniazzi AQ, et al. YAP signaling in preovulatory granulosa cells is critical for the functioning of the EGF network during ovulation. *Mol Cell Endocrinol*. 2022;541.

128) Plewes MR, Hou X, Zhang P, et al. Yes-associated protein 1 is required for proliferation and function of bovine granulosa cells in vitro†. *Biol Reprod*. 2019;101(5):1001-1017.

129) Sun X, Niu X, Qin N, et al. Novel insights into the regulation of LATS2 kinase in prehierarchical follicle development via the Hippo pathway in hen ovary. *Poult Sci*. 2021;100(12).

130) Xiang C, Li J, Hu L, et al. Hippo signaling pathway reveals a spatio-temporal correlation with the size of primordial follicle pool in mice. *Cell Physiol Biochem*. 2015;35(3):957-968.

131) Lyu Z, Qin N, Tyasi TL, et al. The Hippo/MST Pathway Member SAV1 Plays a Suppressive Role in Development of the Prehierarchical Follicles in Hen Ovary. *PLoS One*. 2016;11(8).

132) Pisarska MD, Kuo FT, Bentsi-Barnes IK, Khan S, Barlow GM. LATS1 phosphorylates forkhead L2 and regulates its transcriptional activity. *Am J Physiol Endocrinol Metab*. 2010;299(1).

133) Tsoi M, Morin M, Rico C, et al. Lats1 and Lats2 are required for ovarian granulosa cell fate maintenance. *FASEB J*. 2019;33(10):10819-10832.

134) Lv X, He C, Huang C, et al. Timely expression and activation of YAP1 in granulosa cells is essential for ovarian follicle development. *FASEB J*. 2019;33(9):10049-10064.

135) Hu LL, Su T, Luo RC, et al. Hippo pathway functions as a downstream effector of AKT signaling to regulate the activation of primordial follicles in mice. *J Cell Physiol*. 2019;234(2):1578-1587.

136) Yu J, Yaba A, Kasiman C, Thomson T, Johnson J. mTOR controls ovarian follicle growth by regulating granulosa cell proliferation. *PLoS One*. 2011;6(7).

137) Myers M, Britt KL, Wreford NGM, Ebling FJP, Kerr JB. Methods for quantifying follicular numbers within the mouse ovary. *Reproduction*. 2004;127(5):569-580.

138) Wang W, Liu HL, Tian W, et al. Morphologic observation and classification criteria of atretic follicles in guinea pigs. *J Zhejiang Univ Sci B*. 2010;11(5):307-314.

139) Stocco C, Telleria C, Gibori G. The molecular control of corpus luteum formation, function, and regression. *Endocr Rev*. 2007;28(1):117-149.

140) Li P, Chen Y, Mak KK, Wong CK, Wang CC, Yuan P. Functional Role of Mst1/Mst2 in Embryonic Stem Cell Differentiation. *PLoS One*. 2013;8(11):e79867.

141) Sun T, Diaz FJ. Ovulatory signals alter granulosa cell behavior through YAP1 signaling. *Reproductive Biology and Endocrinology*. 2019;17(1):1-14.

142) Li H, Li Q, Dang K, Wu X, Punzo C, Mao J. YAP/TAZ Activation Drives Uveal Melanoma Initiation and Progression. *Cell Reports*. 2019;29:3200-3211.

143) Li P, Chen Y, Mak KK, Wong CK, Wang CC, Yuan P. Functional Role of Mst1/Mst2 in Embryonic Stem Cell Differentiation. *PLoS One*. 2013;8(11):79867.

144) Lyu Z, Qin N, Tyasi TL, et al. The Hippo/MST Pathway Member SAV1 Plays a Suppressive Role in Development of the Prehierarchical Follicles in Hen Ovary. *PLoS One*. 2016;11(8):160896.

145) Furth N, Aylon Y. The LATS1 and LATS2 tumor suppressors: beyond the Hippo pathway. *Cell Death & Differentiation 2017 24:9*. 2017;24(9):1488-1501.

146) Moroishi T, Hansen CG, Guan KL. The emerging roles of YAP and TAZ in cancer. *Nat Rev Cancer*. 2015;15(2):73.

147) Wu Y, Li M, Lin J, Hu C. Hippo/TEAD4 signaling pathway as a potential target for the treatment of breast cancer. *Oncol Lett*. 2021;21(4).

148) Hoyer PB, Davis JR, Bedrnicek JB, et al. Ovarian neoplasm development by 7,12-dimethylbenz[a]anthracene (DMBA) in a chemically-induced rat model of ovarian failure. *Gynecol Oncol*. 2009;112(3):610.

149) Bhattacharya P, Keating AF. Ovarian metabolism of xenobiotics. *Exp Biol Med* 2011;236(7):765-771.

150) Hirshfield AN. Development of Follicles in the Mammalian Ovary. *Int Rev Cytol*. 1991;124(C):43-101.

151) Hoyer PB, Keating AF. Xenobiotic effects in the ovary: temporary versus permanent infertility. *Expert Opin Drug Metab Toxicol*. 2014;10(4):511-523.

152) Bhattacharya P, Keating AF. Impact of environmental exposures on ovarian function and role of xenobiotic metabolism during ovotoxicity. *Toxicol Appl Pharmacol*. 2012;261(3):227-235.

153) Lawther PJ, Waller RE. Coal fires, industrial emissions and motor vehicles as sources of environmental carcinogens. *IARC Sci Publ*. 1976;Vol. 13(13):27-40.

154) Igawa Y, Keating AF, Rajapaksa KS, Sipes IG, Hoyer PB. Evaluation of ovotoxicity induced by 7, 12-dimethylbenz[a]anthracene and its 3,4-diol metabolite utilizing a rat in vitro ovarian culture system. *Toxicol Appl Pharmacol*. 2009;234(3):361.

155) Mattison DR, Nightingale MR. The biochemical and genetic characteristics of murine ovarian aryl hydrocarbon (Benzo[a]pyrene) hydroxylase activity and its

relationship to primordial oocyte destruction by polycyclic aromatic hydrocarbons. *Toxicol Appl Pharmacol*. 1980;56(3):399-408.

156) Sobinoff AP, Mahony M, Nixon B, Roman SD, McLaughlin EA. Understanding the Villain: DMBA-induced preantral ovotoxicity involves selective follicular destruction and primordial follicle activation through PI3K/Akt and mTOR signaling. *Toxicol Sci*. 2011;123(2):563-575.

157) Sobinoff AP, Pye V, Nixon B, Roman SD, McLaughlin EA. Adding insult to injury: effects of xenobiotic-induced preantral ovotoxicity on ovarian development and oocyte fusibility. *Toxicol Sci*. 2010;118(2):653-666.

158) Sobinoff AP, Pye V, Nixon B, Roman SD, McLaughlin EA. Jumping the gun: smoking constituent BaP causes premature primordial follicle activation and impairs oocyte fusibility through oxidative stress. *Toxicol Appl Pharmacol*. 2012;260(1):70-80.

159) Bolognesi C, Parrini M, Aiello C, Rossi L. DNA damage induced by 7,12-dimethylbenz[a]anthracene in the liver and the mammary gland of rats exposed to polycyclic aromatic hydrocarbon enzyme inducers during perinatal life. *Mutagenesis*. 1991;6(2):113-116.

160) Baskaran, Nagarethinam; Rajasekaran, Duraisamy; Manoharan, Shanmugam. Coumarin protects 7,12-dimethylbenz(a)anthracene-induced genotoxicity in the bone marrow cells of golden Syrian hamsters. *International Journal of Nutrition, Pharmacology, Neurological Diseases* 1(2):p 167-173, Jul–Dec 2011.

161) Muqbil I, Fatima S, Azmi AS, et al. Restraint stress abates the antioxidant potential of melatonin on dimethyl benz (a) anthracene (DMBA) induced carcinogenesis. *Med Oncol*. 2020;37(10):96.

162) Tsai-Turton M, Nakamura BN, Luderer U. Induction of apoptosis by 9,10-dimethyl-1,2-benzanthracene in cultured preovulatory rat follicles is preceded by a rise in reactive oxygen species and is prevented by glutathione. *Biol Reprod*. 2007;77(3):442-451.

163) Ganesan S, Bhattacharya P, Keating AF. 7,12-Dimethylbenz[a]anthracene exposure induces the DNA repair response in neonatal rat ovaries. *Toxicol Appl Pharmacol*. 2013;272(3):690-696.

164) Singh A, Ramesh S, Cibi DM, et al. Hippo Signaling Mediators Yap and Taz Are Required in the Epicardium for Coronary Vasculature Development. *Cell Rep*. 2016;15(7):1384-1393.

165) Clark KL, Davis JS. Perfluorooctanoic acid (PFOA) promotes follicular growth and alters expression of genes that regulate the cell cycle and the Hippo pathway in cultured neonatal mouse ovaries. *Toxicol Appl Pharmacol*. 2022;454.

166) Pan WW, Moroishi T, Koo JH, Guan KL. Cell type-dependent function of LATS1/2 in cancer cell growth. *Oncogene*. 2019;38(14):2595.

167) Tsoi M, Morin M, Rico C, et al. Lats1 and Lats2 are required for ovarian granulosa cell fate maintenance. *FASEB J*. 2019;33(10):10819-10832.

168) Mizutani T, Orisaka M, Kawabe S, Morichika R, Uesaka M, Yoshida Y. YAP/TAZ-TEAD is a novel transcriptional regulator of genes encoding steroidogenic enzymes in rat granulosa cells and KGN cells. *Mol Cell Endocrinol*. 2023;559.

169) Hansen CG, Moroishi T, Guan KL. YAP and TAZ: a nexus for Hippo signaling and beyond. *Trends Cell Biol*. 2015;25(9):499-513.

170) Mizutani T, Orisaka M, Miyazaki Y, et al. Inhibition of YAP/TAZ-TEAD activity induces cytotrophoblast differentiation into syncytiotrophoblast in human trophoblast. *Mol Hum Reprod*. 2022;28(10).

171) Liu-Chittenden Y, Huang B, Shim JS, et al. Genetic and pharmacological disruption of the TEAD-YAP complex suppresses the oncogenic activity of YAP. *Genes Dev*. 2012;26(12):1300-1305.

172) Sun T, Diaz FJ. Ovulatory signals alter granulosa cell behavior through YAP1 signaling. *Reproductive Biology and Endocrinology*. 2019;17(1):1-14.

173) Xia Y, Chang T, Wang Y, et al. YAP Promotes Ovarian Cancer Cell Tumorigenesis and Is Indicative of a Poor Prognosis for Ovarian Cancer Patients. *PLoS One*. 2014;9(3):e91770.

7. APPENDICES

7.1. Ethical Approval

YEDİTEPE ÜNİVERSİTESİ HAYVAN DENEYLERİ YEREL ETİK KURULU	HAYVAN DENEYLERİ YEREL ETİK KURULU KARAR FORMU	Doküman No : FR83 Yayın Tarihi : 06.12.2022 Revizyon No : 00 Revizyon Tarihi : 00.00.0000 Sayfa : 1 / 1

ETİK KURUL KARARI				
Protokol No	**Toplantı Tarihi**	**Toplantı Sayısı**	**Karar No**	**Proje Yürütücüsü**
2023-28	18.05.2023	2023/05	2023/05-07	Prof.Dr.Aylin Yaba Uçar
'7,12-dimethylbenz(a)anthracene (DMBA) ile İndüklenen Fare Ovaryumunda Hippo Sinyal Yolağının Belirlenmesi'isimli proje oy birliğiyle etik açıdan uygun görülmüştür.				
Hayvan Türü / Irkı		**Toplam Hayvan Sayısı**		**Hayvan Cinsiyeti**

Görevi	Adı Soyadı	Onay/Ret Durumu	Katılım Durumu
Başkan	Prof. Dr. Bayram YILMAZ	☐ Onay ☐ Ret	
Başkan Vekili	Prof. Dr. Erdem YEŞİLADA	☐ Onay ☐ Ret	KATILMADI
Üye	Dr. Engin SÜMER	☑ Onay ☐ Ret	
Üye	Prof. Dr. M. Ece GENÇ	☑ Onay ☐ Ret	
Üye	Prof. Dr. Rukset ATTAR	☑ Onay ☐ Ret	
Üye	Prof. Dr. Gamze TORUN KÖSE	☐ Onay ☐ Ret	
Üye	Prof. Dr. Özlem MALKONDU	☑ Onay ☐ Ret	
Üye	Prof. Dr. Aylin YABA UÇAR	☐ Onay ☐ Ret	KATILMADI
Üye	Prof. Dr. Burcu GEMİCİ BAŞOL	☐ Onay ☐ Ret	
Üye	Atakan Mücahit YAVUZ	☐ Onay ☐ Ret	
Üye	Ahmet ŞENKARDEŞLER	☐ Onay ☐ Ret	

Hazırlayan YÜDETAM SORUMLU YÖNETİCİ	Sistem Onayı YÜDETAM MÜDÜRÜ	Yürürlük Onayı YÜDETAM MÜDÜRÜ

7.2. CURRICULUM VITAE

Personal Information

Name	Serra Nur	**Surname**	Ersoy

Education

Degree	Department	The name of the Institution Graduated From	Graduation Year
University	Faculty of Science/ Biology	Hacettepe University	2021

Languages	**Grades**
English	

Computer Skills

Program	**Level**
Microsoft Office Programs	Good
Graphad	Good
Image J	Good
FIJI	Good
Adobe Photoshop	Good
Mendeley	Good
Endnote	Good

****Excellent, good, average or basic**